INVESTIGATING THE EARLY CHANGES IN INTRINSIC PROPERTIES AND SYNAPTIC INPUTS IN THE VULNERABLE FAST-TYPE MOTONEURONS OF SOD1 ^{G93A} MOUSE MODEL OF AMYOTROPHIC LATERAL SCLEROSIS

Arauthy Gina Gnanasampanthan

A Thesis Submitted for the Degree of PhD
at the
University of St Andrews

2023

Investigating the early changes in intrinsic properties and synaptic inputs in the vulnerable fast-type motoneurons of SOD1^{G93A} mouse model of Amyotrophic Lateral Sclerosis

Arauthy Gina Gnanasampanthan

University of St Andrews

This thesis is submitted in partial fulfilment for the degree of

Doctor of Philosophy (PhD)

at the University of St Andrews

March 2023

Candidate's declaration

I, Arauthy Gina Gnanasampanthan, do hereby certify that this thesis, submitted for the degree of PhD, which is approximately 32,000 words in length, has been written by me, and that it is the record of work carried out by me, or principally by myself in collaboration with others as acknowledged, and that it has not been submitted in any previous application for any degree. I confirm that any appendices included in my thesis contain only material permitted by the 'Assessment of Postgraduate Research Students' policy.

I was admitted as a research student at the University of St Andrews in September 2019.

I received funding from an organisation or institution and have acknowledged the funder(s) in the full text of my thesis.

Date 27/3/23 Signature of candidate

Supervisor's declaration

I hereby certify that the candidate has fulfilled the conditions of the Resolution and Regulations appropriate for the degree of PhD in the University of St Andrews and that the candidate is qualified to submit this thesis in application for that degree. I confirm that any appendices included in the thesis contain only material permitted by the 'Assessment of Postgraduate Research Students' policy.

Date 27/3/23 Signature of supervisor

Permission for publication

In submitting this thesis to the University of St Andrews we understand that we are giving permission for it to be made available for use in accordance with the regulations of the University Library for the time being in force, subject to any copyright vested in the work not being affected thereby. We also understand, unless exempt by an award of an embargo as requested below, that the title and the abstract will be published, and that a copy of the work may be made and supplied to any bona fide library or research worker, that this thesis will be electronically accessible for personal or research use and that the library has the right to migrate this thesis into new electronic forms as required to ensure continued access to the thesis.

I, Arauthy Gina Gnanasampanthan, confirm that my thesis does not contain any third-party material that requires copyright clearance.

The following is an agreed request by candidate and supervisor regarding the publication of this thesis:

Printed copy

No embargo on print copy.

Electronic copy

No embargo on electronic copy.

Date 27/3/23 Signature of candidate

Date 27/3/23 Signature of supervisor

Underpinning Research Data or Digital Outputs

Candidate's declaration

I, Arauthy Gina Gnanasampanthan, understand that by declaring that I have original research data or digital outputs, I should make every effort in meeting the University's and research funders' requirements on the deposit and sharing of research data or research digital outputs.

Date 27/3/23 Signature of candidate

Permission for publication of underpinning research data or digital outputs

We understand that for any original research data or digital outputs which are deposited, we are giving permission for them to be made available for use in accordance with the requirements of the University and research funders, for the time being in force.

We also understand that the title and the description will be published, and that the underpinning research data or digital outputs will be electronically accessible for use in accordance with the license specified at the point of deposit, unless exempt by award of an embargo as requested below.

The following is an agreed request by candidate and supervisor regarding the publication of underpinning research data or digital outputs:

No embargo on underpinning research data or digital outputs.

Date 27/3/23 Signature of candidate

Date 27/3/23 Signature of supervisor

Abstract

Amyotrophic lateral sclerosis (ALS) is a progressive neurodegenerative disease characterised by the deterioration of upper and lower motoneurons (MNs), which leads to paralysis and death. Pathophysiological alterations in MN output have been shown at early postnatal stages in ALS model mice; however, it is unclear whether these changes are due to alterations in synaptic inputs or intrinsic MN properties. Here, we investigated the mechanisms contributing to altered MN output by using whole-cell patch clamp electrophysiology to study MN properties and synaptic inputs to MNs during the first two postnatal weeks in the $SOD1^{G93A}$ mouse model of ALS. Our study targeted delayed firing, fast-type lumbar MNs that are vulnerable and degenerate in ALS. We observed increases in the frequency of mixed postsynaptic currents (PSCs) received by $SOD1^{G93A}$ MNs and application of tetrodotoxin also showed increased frequency of action-potential independent miniature PSCs (mPSCs). When pharmacologically characterising the origin of mPSC, we observed a decrease in excitatory mPSC frequency and increases in both frequency and amplitude of inhibitory mPSC in fast-type $SOD1^{G93A}$ MN.

Analysis of MN intrinsic properties, including capacitance, rheobase, persistent inward currents and post-discharge activity, revealed no significant changes in fast-type MNs of $SOD1^{G93A}$ mice. However, a significant increase in the hyperpolarisation-activated inward current (Ih), an important factor driving recruitment and rebound depolarisation, was observed in two-week-old $SOD1^{G93A}$ mice. Next, we investigated the distribution of excitatory and inhibitory post-synaptic density (PSDs) and their subsynaptic nanoclusters (NCs) in motoneuron rich area of lamina IX of $SOD1^{G93A}$ mice. Super-resolution microscopy revealed decreases in both excitatory and inhibitory NCs size in $SOD1^{G93A}$. We found that although the density of inhibitory PSD is lower in the $SOD1^{G93A}$, there was no difference in the excitatory: inhibitory ratio (E:I) in the second postnatal week of $SOD1^{G93A}$ mice.

Overall, early postnatal changes observed in synaptic inputs demonstrate an early role for synaptic dysfunction in SOD1 ALS. Changes in Ih and synaptic inputs may both contribute to improper MN output as the disease progresses. These early changes together could set up the neuronal network for failure which could lead to progressive degeneration of spinal MNs in $SOD1^{G93A}$ ALS.

Acknowledgements

I would like to first thank the organisers of the SPRINT MND/MS programme, the Euan MacDonald Centre, and the Chief Scientist Office for providing funding and support during my PhD. I would also like to thank my supervisor Prof Gareth Miles who provided me guidance and mentorship throughout my PhD journey. Thank you to the members of the NCM lab, as well as the SMAU team for the training and support they have given me. Many thanks to Dr Jessica Valli for providing me training during my time at the microscopy facility at Heriot Watt University.

I am ever so grateful to my friends who have quickly become family during this journey. Carolina and Giulia, I could not have completed this journey without your immense support and encouragements. Thank you for your support during the difficult times and for the wonderful times we had spent together, growing as researchers.

I would like to offer my sincere gratitude to Dr Ganesan Parandhaman. Uncle, thank you for your continued blessings and advice from the first day I've met you.

Thank you, Martin, for standing beside me during the hard times and providing me both moral and emotional support throughout my PhD. You have been my rock and thank you for believing in me with everything I do.

Thanks to my sisters, Suba and Ashwinie for the support they have given me throughout this process. It is interesting to see how the same upbringing can lead to different paths and I am proud of the women you both have become.

Finally, I would like to offer my deepest gratitude to my parents who have dedicated and sacrificed their lives to provide my sisters and I the opportunities that they have been deprived of. From a young age they have taught me the importance of education and its value that is unparallel to anything else. Amma and Appa, we made it.

Arauthy Gina

Chapter 1: Introduction

Amyotrophic lateral sclerosis

Definition

First described by Jean-Martin Charcot, amyotrophic lateral sclerosis (ALS) is a devastating adult-onset neurodegenerative disease that primarily affects motoneurons in the motor cortex, brainstem, and spinal cord. These include the upper motoneurons, found in the motor cortex, that coordinate transmission at the supraspinal level; and the lower motoneurons found in the brainstem and spinal cord, which transmit signals from upper motoneurons to the effector muscles (Zayia & Tadi, 2022). It is characterised by the scarring of the descending axons in the lateral spinal cord (lateral sclerosis) and the denervation of muscle leading to muscle wastage (amyotrophy) because of degenerating motoneurons (Cleveland and Rothstein, 2001; Taylor, Brown and Cleveland, 2016). Motoneurons are highly susceptible to vulnerabilities due to their large cell body, long axonal projection and high metabolic demands (Cleveland and Rothstein, 2001). Although ALS is associated with the loss of motoneurons, there are growing evidence that other neuronal cell types including glial cells such as astrocytes and microglia, and both cortical and spinal cord interneurons have been implicated in the disease (Hardiman *et al.*, 2017)

ALS has a prevalence of approximately 3 per 100,000 people and beyond the age of 60 the risk multiplies. The most common form of ALS is sporadic (sALS) where there is no familial history of the disease. This form of ALS accounts for approximately 90% of all cases. The remaining 10% of cases are termed familial ALS (fALS) and arise from mutations that are inherited in an autosomal manner (Taylor, Brown and Cleveland, 2016). Although sALS and fALS cases are indistinguishable, the aetiology of sALS cases remains largely unknown and it is thought to involve a combination of genetic and environmental factors. sALS and fALS share common clinical manifestations, therefore exploring the mechanisms underlying the progression of fALS can also provide insights into the mechanisms involved in sALS, as models of fALS are more commonly used.

Clinical manifestations of ALS

It is important to pinpoint that ALS is a heterogenous disease, therefore the clinical symptoms presented by all ALS patients varies greatly. A lack of available biomarkers and a wide criterion for ALS diagnosis makes it rather difficult to detect whether the upper or/and lower motoneurons start to degenerate first in the disease. Therefore, the disease phenotype is often classified by the site of onset, in other words, it is manifested by which motoneurons are degenerating. Thus, this heterogenous presentation of the disease makes it difficult to understand the disease mechanisms.

Since motoneurons connect the CNS and the musculoskeletal systems, degeneration of these neurons results in most patients experiencing symptoms that are of limb-onset; whereby the symptoms are presented in the form of muscle weakness in upper and lower limbs as well as fasciculations, hypertonia and hyperreflexia. Approximately two thirds of patients present-spinal onset symptoms, also known as the classical 'Charcot ALS'. Patients with spinal onset ALS present symptoms that are related to muscle weakness where the symptoms can appear distally or proximally in upper and lower limbs. A third of the patients present bulbar-onset symptoms which include dysarthria (speech difficulties) and dysphagia (difficulties in swallowing). On the other hand, approximately 5% of patients experience respiratory-onset symptoms without presenting spinal or bulbar onset symptoms (Wijesekera and Leigh, 2009; Hardiman *et al.*, 2017).

The age of onset of most sALS cases is between 55 and 65 years old, with the age of onset of fALS is significantly earlier (Orsini *et al.*, 2015; Mehta *et al.*, 2016) . Unfortunately, there is currently no cure for ALS. Although riluzole and edaravone have been approved for the treatment of ALS, they only delay the functional decline and extend survival by several months (Bensimon, Lacomblez and Meininger, 1994; Yoshino and Kimura, 2006; Morgan and Orrell, 2016).

Genetics

With the progress made in genetic technology, DNA analysis and gene-wide association studies have facilitated the identification of the genes that are implicated in ALS. As previously mentioned, 10% of ALS cases are familial (fALS) and are transmitted in a dominant manner with high penetrance. The remaining 90% of the cases are termed sporadic (sALS) in which patients have no history of genetic lineage. Thanks to multiple extensive research, over 30 genes associated with ALS have been identified (Taylor, Brown and Cleveland, 2016), with some of the most common mutations shown in Table 1. Mutations in SOD1 and C9ORF72 account for approximately 20% and 30% of fALS cases respectively, whereas FUS and TDP-43 mutations account for 5% of cases (Genetics Home Reference, 2019). In this study, we studied the changes in the $SOD1^{G93A}$ mouse model, therefore, mechanisms involved in the pathogenesis of ALS caused by SOD1 mutations will be explored in this chapter.

Gene	Implicated patho-mechanisms	References
Superoxide Dismutase 1 (SOD1)	Oxidative stress	Rosen *et al.* (1993)
RNA Binding Protein Fused in Sarcoma (FUS)	RNA metabolism	Vance *et al.* (2009)
TAR DNA-Binding Protein (TARDBP)	RNA metabolism	Kabashi *et al.* (2008)
Guanine nucleotide exchange (C9ORF72)	RNA metabolism and autophagy	Renton *et al.* (2011)
Alsin (ALS2)	Endosomal trafficking	Yang *et al.,* (2001)
Senataxin (SETX)	RNA metabolism	Chen *et al.* (2004)
Ataxin 2 (ATXN2)	RNA metabolism	Elden *et al.* (2010)
Matrin 3 (MATR3)	RNA metabolism	Johnson *et al.* (2014)
Ubiquilin-2 (UBQLN2)	Ubiquitin-proteasome system	Deng *et al.* (2011)

Table 1: Examples of genes implicated in ALS and respective patho-mechanism

SOD1

The human superoxide dismutase 1 (SOD1) gene, located on the q-arm of chromosome 21, codes for the Cu-Zn superoxide dismutase which is an antioxidant enzyme involved in the catalysation of reactive oxygen species into oxygen and hydrogen peroxide. Thus, the enzyme plays an important role in homeostasis by removing free radicals that can cause oxidative stress at cellular levels, particularly in the mitochondrial intermembrane space. Disruption in this system can have cellular consequences which would ultimately lead to apoptosis.

Amongst the genes implicated in the disease, missense mutations (such as D90A, A4V, G93A) in SOD1 gene were the first to be identified in 1993 (Rosen *et al.*, 1993). Mutations in SOD1 account for approximately 15% of fALS and 2% of sALS cases. Loss of function in SOD1 have been speculated to impair the motoneurons' ability to remove ROS which subsequently activates the downstream apoptotic pathway, resulting in neuronal death (Sau *et al.*, 2007). In contrast, gain-of-function has also been shown to underlie the patho-mechanism in ALS. Overexpression of misfolded SOD1 in mitochondrial intermembrane space results in SOD1 protein aggregation which in turn hinder the enzyme's dismutase activity, leading to progressive oxidative stress and mitochondrial dysfunction (Kaur *et al*., 2016). Overall, the majority of the findings implicate that mutant SOD1 misfolds resulting in aggregates, which in turns associate with cellular proteins causing dysfunctions in cellular homeostasis and function (Brown and Al-Chalabi, 2017; Hardiman *et al.*, 2017).

Models of ALS

Patient tissue can only be utilised post-mortem and therefore only provides information about the pathomechanisms at the end stage of disease (time of death). Therefore, it is hard to distinguish the putative underlying mechanisms that eventually lead to neurodegeneration. The discoveries of the

mutations associated with ALS and the ability to manipulate genomes have enabled scientists to develop animal models of ALS in order to study the patho- mechanisms underlying motoneuron degeneration. Over the past decades, animal models such as *Drosophila,* zebrafish, tadpoles and particularly mice have provided substantial evidence in deciphering the cellular mechanisms and disease progression in ALS. Even though successful therapeutics have not yet been developed, animal models have contributed to the understanding of the pression of the disease. However, there are limitations to consider when using these animal models as the validity of these models can be questionable.

Cellular models such as yeast, immortal human and primary cell lines have been helpful in deciphering the mechanisms underlying protein aggregation which is a common feature of ALS. Yeast has been particularly helpful in studying cytotoxicity induced by dipeptide protein aggregation. For example, the RNA-binding protein ATXN2 has been identified to interact with TDP-43 and its associated toxicity. Yeast possesses approximately 25% homologous genes to humans and several of its genes have been validated in higher models. As a result, the mutation in ATXN2 has been discovered to be a genetic risk factor in ALS (Elden *et al.*, 2010). Similarly, rodent primary neuronal cultures have enabled investigation of the neurotoxicity associated with many mutant ALS genes including glutamate toxicity in $SOD1^{G93A}$ (Van Damme *et al.*, 2005) and proteotoxicity in MATR3 and C9ORF72. Not only have such culture models facilitated the assessment of the consequences of mutant genes, but they have also allowed researchers to decipher how RNA dysfunction can lead to dysfunction in nucleic acid binding and mislocalisation and aggregation of mutant proteins (Webster *et al.*, 2016; Malik *et al.*, 2018). Although cellular models can permit to study of the consequences of gene mutations, they do not allow the study of the function of motoneurons in their physiological systemic environment.

The intricate nervous system and rapid lifecycle of *Drosophila melanogaster* have allowed scientists to model neurodegenerative disease by overexpressing or knocking down genes of interest using the

GAL4/UAS system (Ugur, Chen and Bellen, 2016). Aberrant C9ORF72 repeat expansion in *Drosophila* has shown reduced locomotion activity and lifespan, whilst increasing in eye degeneration (Xu *et al.*, 2013; Mizielinska *et al.*, 2014). Moreover, fly models overexpressing genes implicated in ALS such as, SOD1 (Watson *et al.*, 2008), TARDBP (Vanden Broeck *et al.*, 2013), FUS (Chen *et al.*, 2011) and ALS2 (Takayama *et al.*, 2014) exhibit cellular toxicity. One vertebrate model that has emerged as an important and useful is the zebrafish. Their optical transparency as embryos, efficiency in compound/toxin screening studies and ease of genetic modification and the high conservation of genes between zebrafish and humans contribute to their usefulness in modelling the effects of genetic mutations in ALS. As a result, this model has been used to demonstrate the gain and loss of function mechanism of C9ORF72 mutation (Ciura *et al.*, 2013; Lee *et al.*, 2013). However, there are limitations with this model as zebrafish lack upper motoneurons, are not mammals and most studies have used zebrafish at their embryonic stage which may not be ideal for the study of an adult-onset disease such as ALS (Babin, Goizet and Raldúa, 2014). The discovery of SOD1 mutation in fALS by Rosen et al. (1993) led to the $SOD1^{G93A}$ transgenic mouse model which stands as the most studied animal model of ALS (Gurney *et al.*, 1994). The $SOD1^{G93A}$ mouse line has contributed to understanding of the underlying disease mechanisms of ALS, such as glutamate toxicity, protein aggregation, mitochondrial dysfunction and non-cell autonomous toxicity, that lead to neurodegeneration (Ilieva, Polymenidou and Cleveland, 2009). Most importantly, this mouse model develops motor deficits leading to paralysis and death at around 3-5 month of age; thus, reproducing most of the clinical phenotypes of ALS and aiding the investigation of presymptomatic and age- dependent stages of the disease. As a result, this has led to the development of FDA-approved therapeutics riluzole and edaravone (Lutz, 2018).

As more ALS genes have been discovered, many new mouse models of ALS representing multiple mutations have emerged to characterise their respective disease pathogenesis. Chew *et al.* (2015) developed the first C9ORF72 HRE mouse model using adeno-associated virus. Shortly after, Liu *et al.*

(2016) generated a C9ORF72 HRE mouse model by inserting bacterial artificial chromosome clone containing the human HRE into the genome of the mouse. Both models are advantageous in studying C9ORF72-ALS as they recapitulate the molecular and phenotypic feature of the disease, such as aggregation of dipeptide proteins and motor deficits (Chew *et al.* 2015; Liu *et al.* 2016)

Animal models have provided critical insights in understanding the patho-mechanisms and developing therapeutics. However, there are inherent limitations associated with the validity of each animal model, which raise questions about whether results obtained from them can be translated into humans. In addition, ALS models that are based on specific gene mutations only represent a subset of the disease. For example, overexpression of mutant genes is necessary to manifest an age-dependent phenotype during the lifespan of mouse models. This raises the question of how well these models can recapitulate the clinical phenotypes in humans and whether the mutations cause similar patho-mechanisms observed in humans. As a result, these models exist with caveats that perhaps contributed to a lack of translation to the clinic (Morrice, Gregory-Evans and Shaw, 2018).

The ability to generate induced pluripotent stem cells (iPSCs) has raised the opportunity to study multiple diseases, including ALS, using human cells derived from patients. Reprogramming human fibroblasts into iPSCs by exposing them to transcription factors OCT4, SOX2, c-Myc and Klf4 via viral constructs has enabled scientists to differentiate them into cells of interest (Takahashi *et al.*, 2007) and develop new modelling approaches for both fALS and sALS. Unlike animal models, human iPSC-based systems allow researchers to study disease mutations and their consequences when expressed at disease relevant levels in a functionally relevant cell-type. Using gene editing technology such as CRISPR/Cas9, it is now possible to generate gene-corrected lines that can be used to compare with patient lines whilst avoiding biological variability. Ultimately, there are caveats to this approach as using iPSC-derived cells as a model does not recapitulate a physiological environment in which the disease

progresses. Therefore, it is important to merge findings from multiple models in order to elucidate the pathomechanisms as a target for potential therapeutics.

Patho-mechanisms in ALS (linked with SOD1)

Due to the heterogeneity of ALS, elucidating a clear common patho-mechanism has been proven to be difficult. Various cellular mechanisms have shown to be dysfunctional in different models of ALS and importantly at different timepoints of the disease progression. It can be postulated that the initial patho-mechanism is triggered by the mutation itself. However, as the disease progression continues other pathways become dysfunctional due to secondary effects and impaired homeostatic regulations. Therefore, it is hard to pinpoint which system starts first which would ultimately result in the final disease phenotype: motoneuron degeneration.

Mitochondrial dysfunction

Mitochondria play an important role in cell metabolism and survival. Their main role is to produce ATP via oxidative phosphorylation, as well as phospholipid biogenesis, calcium homeostasis and apoptosis. Since motoneurons persist and are active throughout the lifespan of an individual, they become susceptible to accumulating damages that arises from mitochondrial dysfunction.

Mitochondrial dysfunction in ALS can arise from many different pathways including production of reactive oxygen species (ROS), defective oxidative phosphorylation and impaired calcium homeostasis. Moreover, in many identified ALS genes, mitochondrial dysfunction has been showed to be associated with other pathomechanisms such as defective axonal transport and excitotoxicity. This highlights the

fact that there can be multiple risk factors that combine to trigger pathogenic cascades and it is difficult to pinpoint which mechanism is initiated first in the disease.

Since the SOD1 model has been the most extensively research model, mitochondrial dysfunction has been one of the main mechanisms that has been explored. Mitochondrial dysfunction is a term describing defective cellular functions due to disrupted mitochondrial functions which could subsequently result in mitochondrial fusion and fission, mitochondrial phagocytosis, and apoptosis. Earlier anatomical studies in lumbar spinal cords of ALS patients revealed abnormal mitochondrial structures with vacuolated appearance (Sasaki and Iwata, 2007) and inclusions of Bunina bodies in lower motoneurons (Okamoto, Mizuno and Fujita, 2008). Similarly, overexpressing the mutant human SOD1 in the mouse model showed vacuolated degenerating mitochondria and mutant SOD1 protein aggregate inside these vacuoles led to leaks in the outer membranal space which could release apoptotic molecules that trigger apoptotic pathways (Gurney *et al.*, 1994; Higgins, Jung and Xu, 2003).

Mutant SOD1 has been shown to form misfolded aggregates in mitochondria and impair the antioxidant activity that removes ROS produced by the electron transport chain. This contributes to oxidative stress and caspase-activated apoptosis (Takeuchi *et al*., 2002; Ferri *et al*., 2006). Indeed increased ROS have been observed in the spinal cord of sALS patients, further demonstrating evidence of oxidative damage in ALS (Barber and Shaw, 2010).

In summary, all the above findings support mitochondrial dysfunction as a possible pathogenic mechanism in ALS. Mitochondria have in fact been targeted for ALS therapy. Dexpramipexole has been shown to improve mitochondrial function, reduce ROS and ameliorate neuroprotection (Gribkoff & Bozik, 2008). Unfortunately, the drug has failed to show efficacy in a phase III trial (Cudkowicz *et al.*, 2013) and development of a disease modifying therapeutic remains a challenge.

Oxidative stress

Reactive oxygen species (ROS) are natural by-products of oxygen metabolism during cellular respiration. Accumulation of ROS and suppression of antioxidant defences lead to oxidative stress, causing damage to cellular structures and impeding physiological functions. Early studies in cerebrospinal fluid of ALS patients have identified increased levels of oxidative stress markers (Barber and Shaw, 2010).

Mutations in SOD1 gene have shown associations between oxidative stress and the disease. SOD1 gene encodes superoxide dismutase enzyme which is involved in neutralising ROS into oxygen or hydrogen peroxide. Although it has long been proposed that a loss in the function of SOD1 enzyme is causative of the disease, SOD1 knockout models failed to show toxicity and develop ALS (Reaume *et al.*, 1996). Alternatively, oxidative damage as a result of the structural changes in the active site of SOD1 has been proposed as a mechanism in ALS. Structural changes due to SOD1 mutations have shown to decrease its affinity to zinc causing the build-up of the oxidant peroxynitrite and peroxynitrite-mediated cellular damage (Beckman *et al.*, 2001). To further strengthen this claim, elevated markers for peroxynitrite-mediated damage were detected in spinal cords and motoneurons of sALS and fALS patients (Beal *et al.*, 1997).

Pathogenic processes involved in ALS are multifactorial and is it unclear whether oxidative stress is the primary cause of the disease. However, it is certain that oxidative stress exacerbates other mechanisms involved in neurodegeneration. For example, increased exposure to ROS significantly disrupts glutamate re-uptake through glutamate transporters on neuronal and glial cells (Trotti, Danbolt and Volterra, 1998; Rao, Yin and Weiss, 2003). ROS are also produced as a consequence of mitochondrial dysfunction, causing cumulative oxidative damage which in turn accounts for reduced mitochondrial efficiency in SOD1-ALS (Barber and Shaw, 2010).

Defective axonal transport

Due to their large axon and dendrite polarisation, intracellular trafficking of proteins, lipids, mRNA, vesicles, and organelles, is crucial for the maintenance of structure and function of motoneurons. Axonal transport mediates the trafficking of such materials and distributes them to specialised sites through axons such as nodes of Ranvier and synaptic terminals. Moreover, axonal transport sustains the long-distance communication between the soma and the synaptic terminals that would enable motoneurons to respond to their surrounding via trafficking of proteins (Hirokawa, Niwa and Tanaka, 2010; Black, 2016).

Microtubules are polymers comprised of heterodimers α- and β- tubulin that are formed in the structure of rods. Microtubules are polarised polymers with a fast-growing positive end and a slow growing negative end. The polarity of microtubules controls the direction of the retrograde (away from soma) and anterograde (proximal to soma) movement of contractile proteins that lead to the distribution of essential molecular cargo (Millecamps and Julien, 2013). Disruption of this machinery can hinder the distribution of molecular content essential for cell survival, leading to the dysfunction of motoneurons.

Neuropathological studies in post-mortem SOD1 ALS patients revealed abnormal accumulation of neurofilaments along with lysosomes and mitochondria, in the proximal axons of motoneurons (Rouleau et al 1996). Moreover, accumulation of axonal spheroids containing lysosomes, mitochondria, neurofilaments and microtubules were found in the spinal cord of ALS patients (Corbo and Hays, 1992). These observations highlighted that defective axonal transport is indeed a pathological hallmark of ALS. Studies conducted in the mutant $SOD1^{G93A}$ transgenic mice where sciatic nerve was ligated, revealed a reduction in kinesin-1 and dynein, which are both molecular motor proteins, in presymptomatic mice

(Warita, Itoyama and Abe, 1999). Following these observations, more studies have been investigating the deficiency of motor protein and various mechanisms that are implicated in ALS, such as cellular cargo mechanisms. Studies in embryonic SOD1^{G93A} cultures and in pre-symptomatic mice showed defective dynein-mediated retrograde axonal transport which correlates with disease progression (Kieran *et al.*, 2005; Ligon *et al.*, 2005). Particularly in the SOD1^{G93A} mouse model, defects in mitochondrial transport have been widely studied. Live microscopy in SOD1^{G93A} cortical neurons showed an imbalance between retrograde and anterograde mitochondrial transport, resulting in the depletion of mitochondria from axons (De vos *et al.*, 2007). Moreover, defects in retrograde mitochondria axonal transport was observed in *in vivo* pre-symptomatic SOD1^{G93A} at P45 and at later disease stages dysfunctions in anterograde axonal transport was followed (Magrané *et al.*, 2014). Similar observations were seen in SOD1^{G93A} transgenic rat models, where impaired axonal transport correlated with reduced mitochondrial density in axons of motoneurons (Este *et al.*, 2012). Furthermore, defects in mitochondrial transport have also been observed in non SOD1 ALS mouse models such as those expressing mutant TDP-43 and ALS2 which shows that this pathomechanisms is not exclusive to SOD1 ALS and are widespread to other forms of ALS (Hadano *et al.*, 2006; Magrané *et al.*, 2014).

Axonal transport is regulated by microtubules that can assemble and disassemble to form stable structures. The stability of microtubules is modulated by microtubule associated proteins (MAPs) by directly phosphorylating them (Gibbs, Greensmith and Schiavo, 2015). Several kinases that are involved in the phosphorylation of MAPs have been associated with ALS. For example, activation of p38 mitogen-activated protein kinase triggered an increase in glutamate signalling of which the concentration was enough to induced apoptosis (Kawasaki *et al.*, 1997). Interestingly, an increase in co-localisation of p38 mitogen-activated protein kinase, as well as phosphorylated neurofilaments, have been observed in degenerating motoneurons in both symptomatic SOD1^{G93A} mice and ALS patients (Bendotti *et al.*, 2004). Similarly, overactivation of Cdk5 (a cyclin-dependent kinase) has been implicated in ALS, where

overactivation of Cdk5 leads to disruption of transport of cargos by inhibiting the activity of dynein (Nguyen, Larivière and Julien, 2001; Klinman and Holzbaur, 2015).

Overall, defects in axonal transport in ALS result in insufficient transport of essential molecules and organelles via cargo. How the depletion of certain cargos contributes to the pathophysiology of ALS and the molecular mechanisms behind these modifications remain a subject of ongoing discussion.

Impaired protein homeostasis and aggregation

Protein homeostasis, also known as proteostasis, is the cellular balance between the production and degradation of proteins that is necessary for the survival of cells. The proteostasis networks includes pathways such as protein synthesis, protein folding and trafficking, as well as protein degradation. Moreover, it also consists of pathways that responds to protein stress pathways like the unfolded protein response (UPR) in the endoplasmic reticulum (Webster *et al.*, 2017). ER stress is induced by the accumulation of unfolded and misfolded proteins, which in turns activates UPR pathways. These pathways can restore proteostasis by downregulating mRNA translation, activating chaperone proteins to encourage protein folding and upregulating the degradation pathways and autophagy to remove misfolded proteins (Hetz, 2012). There have been multiple studies that suggest ER stress to be a factor contributing to impaired proteostasis in SOD1 ALS. Granular misfolded proteins were first observed in the ER of motoneurons of post-mortem tissue of ALS patients (Sasaki, 2011), providing evidence that ER stress may be involved in the degeneration of motoneurons. Similar observations were also seen in the $SOD1^{G93A}$ mice, where increase in UPR levels was present in only vulnerable motoneurons at early pre-symptomatic age prior to disease onset. Furthermore, administration of a stress-protective agent slowed the progression of the disease and enhancing ER stress accelerated the disease onset (Saxena, Cabuy and Caroni, 2009).

Mutant SOD1 aggregates have been shown to interact with proteins that are required for proteostasis. For example, mutant SOD1 interacts with Derlin-1, a protein involved in the ER-associated degradation pathway, and in turns perturbs this pathway resulting in increased ER stress, triggering the apoptotic pathway (Nishitoh *et al.*, 2008).

Proteins involved in proteasomal activity are impaired in ALS, which hinders the cellular mechanisms that exist to maintain proteostasis. Other stages of proteostasis have been found to be perturbed by mutant SOD1. Mutant SOD1 aggregate have been shown to sequester molecular chaperone proteins that are recruited for protein folding during ER stress. Notably, hsp40 and hsp70 are sequestered by mutant SOD1 and depriving the ER of its molecular chaperones required for proteostasis (Hetz and Mollereau, 2014; Ruegsegger *et al.*, 2016).

Another system that is involved in the degradation pathway is autophagy. Autophagy is responsible for the clearance of cytoplasmic materials including impaired organelles and misfolded proteins, via the formation of a double membrane that encapsulate the substrate prior to fusing with the lysosome (Bento *et al.*, 2016). Compromised autophagy has been shown to contribute to the pathogenesis of ALS and increasing the level of autophagy can improve the course of the disease. For example, the SOD1 aggregates are substrates of compromised autophagy of misfolded SOD1 protein and inducing autophagy by administrating trehalose decreased the accumulation of SOD1 aggregates and increase the survival of motoneurons (Castillo *et al.*, 2013). Genetically inducing autophagy (by knocking down the UPR transcription factor XBP-1) also increased the clearance of SOD1 aggregates and slowed down the progression of ALS in *in vivo* SOD1 mutant mice (Hetz *et al.*, 2009).

Hence, it is evident that SOD1 aggregation can be caused by a variety of impairments in the proteostasis machinery. Overall, mutant SOD1 aggregates may reduce the protein degradation capability of motoneurons, which in turns exacerbate mutant SOD1 aggregation leading to degeneration.

Non-cell autonomous toxicity

In the past, ALS was thought to be a motoneuron disease in which muscular atrophy and motoneuron degeneration occurred because of dysfunctional and damaged neurons themselves – a process termed cell autonomous toxicity (Bergmann *et al*., 1995; Lambrechts *et al.*, 2003; Chahin & Sorenson, 2009). While these pathological events are indeed observed in the disease, there is increasing focus on the role of glial cells in the pathogenesis of ALS. There is growing evidence that non-neuronal cells such as astrocytes, microglia and oligodendrocytes contribute to motoneuron damage; a process called non-cell autonomous disease (Lee *et al.*, 2016). For example, neurodegeneration is not observed in cultures consisting only of primary mouse spinal motoneurons expressing mutant SOD1. However, the presence of astrocytes harbouring mutant SOD1 leads to motoneuronal death (Nagai *et al.*, 2007). Moreover, non-neuronal cells expressing wild-type SOD1 significantly extended the survival of motoneurons harbouring mutant SOD1 by delaying neurodegeneration (Clement *et al*., 2003).

Increase in proliferation of reactive microglia and astrocytes is observed during the disease progression and is a key contributor in motoneuron damage. As a result, inflammatory cytokines are released in the CNS which further worsen neuronal injury and facilitate glutamate-mediated excitotoxicity; all these factors accelerate disease progression (Concetta-Geloso *et al.*, 2017). Many studies support that non-neuronal cells can cause neuronal damage in ALS (Ilieva *et al.*, 2009). Deciphering the mechanisms of actions of these cells might evoke potential therapeutic interventions against this debilitating disease.

Excitotoxicity

The term excitotoxicity was first coined by Olney (1969) where neuronal cell death was observed in response to exposure to excess glutamate. In the CNS, the glutamatergic system is essential for neuronal communication in both the brain and spinal cord for functions such as learning, memory and movement. Although glutamate plays an important role, dysregulation of the glutamatergic system, particularly through the excessive glutamate-induced excitation of neurons via glutamate receptors, has been implicated in the pathophysiology of various neurodegenerative diseases such as ALS and Alzheimer's disease (Foran and Trotti, 2009).

Under normal conditions, glutamate is released from the pre-synaptic neurons and binds to N-methyl-D-aspartate (NMDA) and α-amino-3-hydroxy-5-methyl-4-isoxazole propionic acid (AMPA) receptors, as well as metabotropic glutamate receptors (mGluR), on the post-synaptic neurons, causing an influx of Na^+ and Ca^{2+} ions and once threshold is reached, would result in action potentials (Verkhratsky and Kirchhoff, 2007). Under pathological condition, excitotoxicity refers to neurodegeneration caused by excessive stimulation of usually glutamatergic inputs, resulting in a toxic influx of ions into neurons.

There are two forms of excitotoxicity described: classical and slow. Classical excitotoxicity is defined as the degeneration caused by excessive extracellular glutamate concentration which cause continuing depolarisation that would trigger cell death. Slow excitotoxicity refers to the neurodegeneration caused by weakened postsynaptic neurons (due to impairment in cellular metabolism and energetics) in the presence of normal extracellular glutamate concentration (Doble, 1999). However, in both forms of excitotoxicity glutamatergic transmission performs a crucial part in neurodegeneration.

One of the first observations that linked excitotoxicity to the pathophysiology of ALS was an increase in concentration of glutamate in the cerebrospinal fluid of ALS patients (Rothstein *et al.*, 1990; Spreux-Varoquaux *et al.*, 2002). Similar observations were later seen in the SOD1 mouse model (Alexander *et*

al., 2000). In cell culture studies, application of cerebrospinal fluid from ALS patient onto cortical neurons was observed to be neurotoxic. However, blocking glutamate receptor with CNQX prevented excitotoxic damages and cell death of cortical neurons (Couratier *et al.*, 1993), which suggests that excessive glutamate can result in neurodegeneration.

The disruption of glutamate transport has been demonstrated to contribute to excitotoxicity. When glutamate is released by the presynaptic neurons, astrocytes are responsible for 90% of the reuptake of glutamate via excitatory amino acid transporter 2 (EAAT2). This prevents excitotoxicity and the recycling of glutamate into glutamine via glutamine synthase (Kim *et al.*, 2011). Loss of EAAT2 on glial cells in the spinal cord and motor cortex of ALS patients has been correlated with increases in the concentration of glutamate in the cerebral spinal fluid (CSF) (Rothstein *et al.*, 1995). Since then, studies in transgenic SOD1 mouse models have shown that a reduction in astrocytic EAAT2 leads to decreased motoneuron survival. Importantly, deletion of EAAT2 gene causes motor deficits, induces astrogliosis and leads to spinal motoneuron loss via glutamate excitotoxicity (Howland *et al.*, 2002; Pardo *et al.*, 2006).

Linking to excitotoxicity, changes in excitability have been widely reported in the $SOD1^{G93A}$ transgenic mouse model. It is thought that changes in motoneuronal excitability are one of the fist abnormalities observed before the disease onset in this model. Excitability of motoneurons is mostly dependent on two factors: intrinsic properties and synaptic inputs. Chapter 2 and Chapter 3 will examine in detail the role of changes intrinsic properties and synaptic inputs in motoneurons excitability in SOD1 ALS, respectively.

Selective vulnerability in motor units in ALS

In many neurodegenerative diseases like ALS, it has been widely shown that only a subpopulation of neurons is gradually affected preclinically and symptoms can be observed depending on the type of neurons that is affected. In mammals, 3 subtypes of motoneurons have been identified and each can be distinguished on the basis of the type of muscle they innervate. Alpha(α)-motoneurons comprise the majority of all motoneurons and innervate the extrafusal muscle fibres that are responsible for movement and postural modulation. Gamma(γ)-motoneurons on the other hand, innervate the intrafusal muscle fibres and are involved in proprioception. Hence, γ-motoneurons do not play a role in modulating muscle force. Beta(β)-motoneurons innervate both extrafusal and intrafusal muscle fibres (Chalif and Mentis, 2022; Smith and Brownstone, 2022).

Many studies have identified the physiological subtypes of motoneurons affected in the time course of the disease. By studying the innervation of muscle fibres in the hindlimb in SOD1 mouse model of ALS, it has been shown that different types of motoneurons have differing vulnerability to the disease. From the α-motoneurons group, firstly, the muscle fibres that are innervated by the fast-fatigable (FF) motoneurons denervate before clinical symptoms are shown. The fast-resistant (FR) motoneurons become affected at the symptom onset where they are disconnected from their muscle fibres. In contrast, the slow (S) motoneurons were resistant until the terminal stage of the disease, although they also detach from their muscle fibres then (Frey *et al.*, 2000; Pun *et al.*, 2006). Electrophysiological studies in contracting muscle fibres showed that the motoneurons innervating the F-type (FF and FR) fibres showed a delayed firing pattern upon a pulse onset stimulation. On the other hand, the motoneurons innervating the resistant S-type fibres showed an immediate firing pattern upon the same stimulation (Delestrée *et al.*, 2014; Leroy *et al.*, 2014; Martínez-Silva *et al.*, 2018; Sharples and Miles, 2021). Since F-type fibres are vulnerable in the disease, we focused only on the delayed firing

motoneurons that innervate them. From now on, the delayed firing motoneurons will be known as fast-type motoneurons, and the immediate firing motoneurons will be known as slow-type motoneurons.

In the following chapters, we will explore the changes in intrinsic properties (Chapter 2) and synaptic inputs (Chapter 3) in the fast-type motoneurons of $SOD1^{G93A}$ mice. In Chapter 4, we investigated the anatomical structure of excitatory and inhibitory post-synaptic density as well as their subsynaptic structures. The results of these studies provide evidence of early physiological and anatomical changes in the vulnerable fast-type motoneurons in ALS pathogenesis and support a role for synaptopathy in ALS-related MN dysfunction.

Chapter 2: Investigation of intrinsic properties in the vulnerable fast-type motoneurons in early presymptomatic stage of SOD1^{G93A} mice

To generate output in the form of action potentials, motoneurons must receive inputs that exceed a certain threshold. The way the motoneurons generate output is reliant on the synaptic input they receive from their neural networks, but also on their intrinsic properties(Chalif and Mentis, 2022; Smith and Brownstone, 2022).

The term intrinsic properties encompasses both passive and active biophysical membrane characteristics that allow the cells to shape their output to incoming stimuli by either firing or maintaining subthreshold oscillations. For example, intrinsic properties can modify the input-output relationship by increasing the frequency due to altered synaptic transduction or by altering the conductance of motoneurons with neuromodulation (Binder, Heckman and Powers, 1993).

Of the disease mechanisms studied in the $SOD1^{G93A}$ model, intrinsic hyperexcitability has been a parameter that has been extensively studied. Intrinsic hyperexcitability refers to the excessive output of motoneurons in response to an input. This excessive excitability is then suggested to lead to excitotoxicity and degeneration of motoneurons. The excitability of lower motoneurons has been investigated in ALS patients using electromyography (EMG) and nerve conduction studies (NCS). Even though these methods use indirect measures of motoneuron activity, they revealed hyperexcitability and aberrant firing of motor units (Kostera *et al.*, 2002; Piotrkiewicz, Kudina and Mierzejewska, 2008), and increase in axonal excitability due to enhanced Na^+ conductance (Bostock *et al.*, 1995; Nakata *et al.*, 2006). Though these studies have been conducted in symptomatic patients, it is difficult to predict and measure the changes in motoneurons and their motor units before the symptoms appear to find therapeutics to target the motoneurons before they degenerate.

Due to the late-diagnosis and ethical limitations in accessing human motoneurons, most studies that explored electrophysiological changes from pre-symptomatic to symptomatic stages have been conducted both *in vitro* and *in vivo*, ranging from cell cultures to animal models.

Early iPSC-derived motoneuron cultures from SOD1 ALS patients showed a hyperexcitable phenotype which could have been contributed by a reduction in the amplitude of delayed-rectifying potassium currents. The administration of retigabine, a potassium channel activator, reduced hyperexcitability and improved the survival of these iPSC-derived motoneurons (Wainger *et al.*, 2014). However, the iPSC-derived neurons switch from early hyperexcitability to late hypoexcitable at 7 weeks post-plating as they show reduced repetitive firing, reduced inward currents, increased delayed rectifying potassium current amplitude and loss of synaptic inputs (Naujock *et al.*, 2016), which is suggestive of an hyperexcitable phenotype that leads to dysfunction in the neurons and causes it to become hypoexcitable. We must consider that though this technique has proven to be advantageous in deciphering disease mechanisms and identify potential therapeutics, it does not recapitulate a physiological environment which the disease progresses in. Therefore, many studies have been conducted in mouse models of ALS that exhibit the symptoms observed in clinics.

In parallel to the findings observed in iPSC-derived motoneurons, electrophysiological recordings in embryonic cultures revealed that $SOD1^{G93A}$ neurons have higher firing frequency (Pieri, 2003), and increase in persistent inward currents (PIC) and lower spiking threshold (Kuo *et al.*, 2005). Hyperexcitability, in the form of increased f-I gain, was again observed in embryonic (E12-14) spinal motoneuron cultures (Kuo *et al.*, 2004). Similarly, Martin *et al.* (2013) also showed increased in f-I gain in E17.5 spinal neuron cultures, additionally, they have shown that these electrophysiological changes are secondary morphological changes.

Although ALS is clinically described as an adult-onset disease, these findings demonstrate that changes in intrinsic properties, in the form of hyperexcitability, occur long before the symptoms are manifested.

Hyperexcitability has also been observed in lumbar spinal cord slices of pre-symptomatic mouse models of SOD1 ALS. Whole-cell patch-clamp recordings obtained from motoneurons of embryonic $SOD1^{G93A}$ mice (E17.5) revealed lower rheobase currents and a general hyperexcitability in comparison to controls. Moreover, these $SOD1^{G93A}$ motoneurons displayed reduced dendritic arborisation which have been suggested to act as an early compensatory mechanism to compensate for the embryonic changes in intrinsic properties (Martin *et al.*, 2013a). Similarly, Fogarty *et al.* (2017) showed that dendritic arborisation as well as length of dendritic trees in lumbar spinal cords of $SOD1^{G93A}$ mice were reduced from P28 onwards. In contrary to the findings of Martin *et al.* (2013), they have shown that dendritic arborisation and length was unchanged in younger $SOD1^{G93A}$ mice (<P15).

Transverse lumbar spinal cord slices of P0-12 $SOD1^{G93A}$ mice showed increases in Na^+ and Ca^{2+} -mediated PICs, decreases in the duration of AHPs and decreases in spike width. Even though similar changes in properties have been observed in WT, they occur later during development. Therefore, it is suggested that the rate of development in the $SOD1^{G93A}$ motoneurons is accelerated and the expedited maturation can lead to hyperexcitability in these given motoneurons (Quinlan *et al.*, 2011a). Similar findings were also reported by Pambo-Pambo, Durand and Gueritaud, (2009), in which lumbar motoneurons of P6-10 $SOD1^{G93A}$ mice had a more depolarised resting membrane potential and increased firing frequency. These alterations to intrinsic properties were not exclusive to lumbar motoneurons as similar findings such as increased persistent Na^+ current and f-I gain were observed in hypoglossal motoneurons (Van Zundert *et al.*, 2008).

Studies in a more physiological in vivo setting have shown similar intrinsic hyperexcitable phenotypes. At late pre-symptomatic to symptomatic age (P50-90), prolonged repetitive firing in response to dorsal root stimulation was observed in $SOD1^{G93A}$ motoneurons. In accordance to this finding, Jensen *et al.* (2020) have shown that $SOD1^{G93A}$ motoneurons are indeed hyperexcitable as they show higher f-I gain, lower rheobase and increased PICs.

These studies concluded that alterations in motoneuron excitability is observed mainly as hyperexcitability at early changes which would later render motoneurons hypoexcitable in the disease.

On the other hand, many studies have refuted the idea that intrinsic hyperexcitability is a factor contributing to motoneuron degeneration in ALS. Intracellular recording in early pre-symptomatic $SOD1^{G93A}$ vulnerable (fast-type) motoneurons exhibited lower f-I gain and higher voltage threshold (Filipchuk *et al.*, 2021). These finding are seemingly at odds with previous studies that have shown that $SOD1^{G93A}$ motoneurons are in contrast hyperexcitable (Kuo *et al.*, 2004, 2005; Quinlan *et al.*, 2011; Martin *et al.*, 2013). One important aspect to address concerns the fact that these previous findings did not differentiate motoneuron subtypes. As previously discussed in the introduction, out of the three main subtypes of motoneurons, the motoneurons that innervate FF muscle fibres degenerate early in the disease (Pun *et al.*, 2006). Here, Filipchuk *et al.* (2021) were able to distinguish the vulnerable motoneurons based on their firing properties which allowed them to demonstrate that the excitability in this population was indeed hypoexcitable.

To investigate changes in motoneurons in a more physiological setting, Delestrée *et al.*(2014) carried out in vivo recordings from pre-symptomatic P40-50 lumbar motoneurons in anaesthetised mice and found that the excitability in $SOD1^{G93A}$ motoneurons remained unchanged despite the input conductance being higher in comparison to WT motoneurons. Moreover, they have also shown that a significant proportion of the $SOD1^{G93A}$ motoneurons lost the capacity to fire repetitively indicating hypoexcitability as a mechanism present at the late-presymptomatic stage of the disease just before denervation of neuromuscular junctions arise.

However, changes in intrinsic excitability do not always lead to changes in neuronal activity as these alterations can act as compensatory mechanisms to maintain the activity of a given motoneuron under physiological or pathological conditions. Huh et al. (2021) recorded motoneurons from in vivo $SOD1^{G93A}$

mice at pre-symptomatic and symptomatic ages. Even though they observed larger PICs and a more hyperpolarised voltage threshold for spiking at pre-symptomatic ages, $SOD1^{G93A}$ motoneurons do not show hyperexcitability in their firing output.

Furthermore, Martínez-Silva *et al.* (2018) explored whether different subtypes of motoneurons exhibit changes in intrinsic properties during the disease progression. They performed in vivo intracellular recordings in presymptomatic P46-60 mice and found that most FF and a fraction of FR type motoneurons were not able to fire repetitively, thus becoming hypoexcitable even though their neuromuscular junctions were intact. Besides, they have also shown that the slow-type motoneurons did not show any changes in excitability. On the other hand, slow-type motoneurons that are resistant in the disease, became hyperexcitable in comparison to control (Leroy *et al.*, 2014). This may suggest that hyperexcitability could potentially have a neuroprotective role and is unlikely to be the cause of degeneration.

These findings collectively argue against the most accepted theory of glutamate-mediated toxicity and more importantly contradict the current therapeutics available for ALS, which aim to reduce motoneuronal excitability. Importantly, these finding evoke the question whether hypoexcitability could be an early pathological sign of ALS.

The literature on changes in intrinsic properties in ALS is nothing but vast. Many studies have been conducted at different time points to outline when and how these changes occur before degeneration of neurons. Deciphering these changes could be useful for the development of therapeutics that could preserve the survival of motoneurons long before degeneration.

In summary, even though all these findings do not come together to provide a conclusive answer on how intrinsic properties change, they together show that the complex alterations in motoneuronal excitability are dependent on the disease stages and the motoneuron subtype. Moreover, combining

the electrophysiological data of both fast-type and slow-type motoneurons masks the true changes that occur in the vulnerable motoneurons.

Our study aims to explore the changes in intrinsic properties only in the most vulnerable fast-type motoneurons. As mentioned previously, electrophysiological recordings in motoneurons of early postnatal $SOD1^{G93A}$ mice have not been differentiated according to their motoneuron subtypes.

Given that only fast-type motoneurons are affected in the disease, we have used an electrophysiological approach to differentiate between the subtypes (described in the methods section in Chapter 2). Although previous studies have focused on the vulnerable motoneurons in ALS, investigation in very early (pre-symptomatic changes in intrinsic properties in the vulnerable fast-type motoneurons have not been conducted previously. Therefore, in this study, we aim to explore whether changes in intrinsic properties occur in the $SOD1^{G93A}$ mouse model within the first two weeks of post-natal age.

Methods

Animals

All experimental procedures were conducted in accordance with the UK Animals (Scientific Procedures) Act 1986, Animal Welfare Ethics Committee of the University of St Andrews as well as the UK Home Office regulations. Male B6SJL-TgN (SOD1-G93A)1Gur/J ($SOD1^{G93A}$) mice (provided by Dr Richard Mead, University of Sheffield) were crossed with wildtype females on a C57BL/6 background (Charles River Laboratories). Experiments were performed on spinal cord slices obtained from $SOD1^{G93A}$ positive mice and their negative WT littermates, at postnatal days P1-20.

Genotyping

All genotyping occurred after analyses (post-hoc) were performed to blind the experimenter. Experimental $SOD1^{G93A}$ x C57 mice were post-hoc tail sampled. DNA extraction was undertaken by adding the tail samples to 75µL of alkaline lysis solution and heated on a heat-block at 95°C for 30 minutes. 75µL of neutralising solution was added to the cooled extracted DNA solution. 2µL of extracted DNA solution was added to 23µL of PCR master mix per sample and placed in a thermocycler with the following protocol: *1) 94°C, 3.00 (min.secs) ; 2) 94°C, 0.15 ; 3) 65°C, 0.15 (-0.5°C per cycle) ; 4) 68°C, 0.01 ; 5) GO TO step 2, 10x ; 6) 94°C, 0.15 ; 7) 60°C, 0.15 ; 8) 72°C, 0.01 ; 9) GO TO step 6, 28X ; 10) 72°C, 1.00 ; 11) 14 °C, hold.*

Agarose gel (1.5%, Sigma Aldrich) was prepared in 1 x TBE buffer (Sigma Aldrich) with 5 x 10^{-6} % (v/v) Redsafe DNA Stain 2000x (Chembio). Once PCR was completed, 5µL of TriTrack loading dye (6X) (Thermo Scientific) was added to each PCR sample and 10µL of the final solution was transferred onto the agarose gel. The gel was run at a voltage of 156V for 20 minutes and DNA bands were visualised under UV light. Samples were run alongside a DNA ladder, positive and negative controls.

PCR primers:

$SOD1^{G93A}$ Forward: 5'-CAT CAG CCC TAA TCC ATC TGA-3'

Reverse: 5'-CGC GAC TAA CAA TCA AAG TGA-3'

Forward Control: 5'-CTA GGC CAC AGA ATT GAA AGA TCT-3'

Reverse Control: 5'-GTA GGT GGA AAT TCT AGC ATC ATC C-3'

PCR Reagents:

Alkaline Lysis Reagent: *NaOH (25mM); Na_2-EDTA 2H2O (0.2mM) dH2O; pH=~12*

Neutralisation Solution: *Tris-HCl (40mM) in dH2O, pH=~5*

PCR Master mix: *5x KAPA 2G HS Buffer MgCl2 Free (1x); $MgCl_2$ (2.5mM); dNTP KAPA (0.2Mm); 10µM F Primer (0.5µM); 10µM R Primer (0.5µM); 10µM F Control Primer (0.5µM); 10µM Control R Primer (0.5µM); 5KAPA 2G HS Taq Polymerase 5U/µl (0.5U) in PCR-Grade H_2O.*

Tissue preparation

Mice were cervically dislocated, decapitated and eviscerated. To remove the spinal cord, animals were pinned ventral side up in a dissecting chamber filled with ice-cold potassium gluconate based dissecting aCSF (equilibrated with 95% oxygen, 5% carbon dioxide). Vertebrectomy was performed to expose the spinal cords, the cords were held and lifted at the cervical end with a pair of forceps and ventral and dorsal roots were cut with a pair of fine micro-scissors to isolate the spinal cords from their spinal columns. Spinal cords were transversely cut to isolate the lumbar segment and were secured using surgical glue (VetBond 3M) to an agar block (3% agar) that was glued to the cutting stage of slicing chamber.

The tissue was immediately immersed in ice-cold dissecting aCSF (equilibrated with 95% oxygen, 5% carbon dioxide). 300µm longitudinal slices were cut at an average speed of 15µm/s on a vibratome (Leica VT1200) and were transferred to a recovery chamber filled with recovery aCSF (equilibrated with 95% oxygen, 5% carbon dioxide at 35°C), for 30 minutes after obtaining the last slice.

Following recovery, the longitudinal slices were transferred to a chamber filled with warm recording aCSF (equilibrated with 95% oxygen, 5% carbon dioxide at 35°C) and were allowed to equilibrate to room temperature (23-26°C) for approximately one hour before experiments.

Whole cell patch-clamp recordings

Spinal cord slices were immersed in a recording chamber with recording aCSF continuously perfused at a constant rate of 1mL per second. Slices were stabilised in the recording chamber with fine fibres attached to a platinum harp. Whole-cell patch-clamp recordings were performed from spinal motoneurons located within the ventral horn (in ventro-medial and ventro-lateral pool) . Lumbar motoneurons were morphologically visualised with a x40 objective with differential interference contrast microscopy and infrared illumination.

Recording microelectrodes with resistance of 2.5-3.5 MΩ were pulled from borosilicate capillary tubes using a Flaming Brown micropipette puller (Sutter instruments Model P97). Microelectrodes were filled with intracellular solution and were attached to the membrane of motoneurons . High resistance giga-seals of more than 1 GΩ were obtained before rupturing the cell membrane using suction. Whole-cell mode was applied, and the capacitance and resistance values were corrected. Signals were amplified and filtered (4kHz low-pass Bessel filter) with a MultiClamp 700B amplifier (Molecular Devices) and acquired at ≥ 10kHz using a DigiData 1440A digitizer and pClamp software (Molecular Devices). All

recording were performed in both current-clamp and voltage-clamp mode on motoneurons with resting membrane potentials of -45mV and -80mV.

In current clamp mode, intrinsic properties were studied whilst applying a bias current to maintain the membrane potential at ~-60 mV. For a subset of experiments to measure intrinsic properties such as PIC and Ih, voltage clamp mode was used, and the membrane potential was clamped at -60 to -90 mV.

Data acquisition

Capacitance and passive input resistance were measured using a series of incremental hyperpolarising current steps. Input resistance was calculated by measuring the slope of the current-voltage relationship. This was done by measuring the difference at the initial peak voltage and the steady state voltage deflection after a series of 1s hyperpolarising current steps.

Capacitance was calculated by dividing the time constant (time taken to reach 2/3 of the peak voltage change) by the input resistance.

Rheobase and repetitive firing properties were measured using a slow, 100pA/s, depolarising current ramp. Motoneuron types were assessed using a 5s-long depolarising current ramp (described in the next section).

Single spike properties of action potentials were elicited by injecting a 10ms depolarising current (at least 1.25 times the rheobase) pulse. Spike threshold was calculated at the potential at which the derivative trace was at 10 mV/ms. Post-discharge excitability was measured by applying a 10s pulse trains at 30 Hz and the amplitude and duration of the afterdepolarisation or after-hyperpolarisation was measured from voltage at the end of the high frequency pulse to the resting membrane potential.

Persistent inward currents (PICs) were measured in voltage clamp mode by injecting a slow depolarising voltage ramp (10mV/s from -90 to -10 mV). This allowed us to calculate the voltage of the PIC onset, peak voltage, peak current amplitude, and voltage of PIC offset.

Ih was also measured in voltage clamp mode by injecting a 1s hyperpolarising 10 mV steps from either -60 mV or -40mV to -110 mV. The difference in currents between the initial and steady state currents were calculated to measure Ih.

Identification of fast and slow motoneurons

Fast and slow motoneurons were identified using a protocol established by Leroy et al. (2014) whereby motoneurons are distinguished based on the latency to the first spike in repetitive firing when injecting a 5 second square depolarising current at rheobase. This protocol identified two distinct profiles: a delayed repetitive firing with accelerating spike frequency which is characteristic of a fast-type motoneuron, and an immediate repetitive firing with a constant rate of firing frequency which is characteristics of a slow-type motoneuron.

Data Analysis and statistics

Intracellular patch-clamp recordings were analysed using Clampfit software (Molecular Devices) and exported to GraphPad Prism (version 9.2.0) for statistical analysis

Drugs and solutions

Dissecting aCSF: *130mM K-gluconate, 15mM KCl, 0.05 mM EGTA, 20 mM HEPES, 25 mM D-glucose, 3 mM kynurenic acid, 2 mM Na-pyruvate, 3 mM myo-inositol, 1 mM Na-L-ascorbate; pH 7.4, adjusted with NaOH; osmolarity approximately 345 mOsm*

Recovery aCSF: *119mM NaCl, 1.9mM KCl, 1.2mM NaH2PO4, 10mM $MgSO_4$, 1mM $CaCl_2$, 26mM $NaHCO_3$, 20mM glucose and 1.5mM kynurenic acid*.

Recording aCSF: *127mM NaCl, 3mM KCl, 2mM $CaCl_2$, 1mM $MgCl_2$, 26mM $NaHCO_3$, 1.25mM NaH_2PO_4, 10mM glucose.*

Intracellular solution for patch clamp recordings: *14mM $KMeSO_4$, 10mM NaCl, 1mM $CaCl_2$, 10mM HEPES, 1mM EGTA, 3mM Mg-ATP and 45mM Mg-GTP.*

Results

We used whole-cell patch-clamp electrophysiology to explore the intrinsic properties of lumbar motoneurons in the SOD1^{G93A} mouse model of ALS. To further characterise the vulnerable fast-type motoneurons, a protocol established by Leroy *et al.*, (2014) was used whereby a 5 second depolarising square current pulse was applied to motoneurons. Fast-type motoneurons were distinguished by their delayed firing pattern and increased firing frequency once firing has started. Motoneurons with an immediate firing pattern, which is indicative of slow-type motoneurons, were excluded from the analysis.

The passive membrane properties of motoneurons were derived from WT and SOD1^{G93A} mice at 1 (W1) and 2 (W2) postnatal weeks. Here, we show that the input resistance does not significantly change between WT and SOD1^{G93A} fast-type motoneurons at postnatal ages of W1 and W2 (Table 1. W1 WT: 45.7 ± 17.8 MΩ, W1 SOD1^{G93A}: 42.2 ± 18.8 MΩ, p= 0.99; W2 WT: 36.7 ± 20.3 MΩ, W2 SOD1^{G93A}: 24.9 ± 16.1 MΩ. p= 0.07). However, a decrease in input resistance is observed in SOD1^{G93A} fast-type motoneurons from W1 to W2 (Table 1. W1: 42.2 ± 18.8 MΩ, W2: 24.9 ± 16.1 MΩ, p=0.007). Although, no significant differences were observed between the two genotypes at the different timepoints, it can be highlighted that a trend indicating a decrease in input resistance is observed in SOD1^{G93A} fast-type motoneurons in comparison to WT, particularly in W2. This could suggest that there may be a change in the membranal ion channels at this early developmental stage in SOD1^{G93A} fast-type motoneurons. Furthermore, we did not observe significant differences in other passive properties such as the resting membrane potential (Table 1. W1 WT: -63.0 ± 6.4 mV, W1 SOD1^{G93A}: -68.0 ± 4.1 mV; W2 WT: -66.5 ± 5.3 mV, W2 SOD1^{G93A}: -67.6 ± 4.8 mV), and capacitance (Table 1. W1 WT: -63.0 ± 6.4 mV, W1 SOD1^{G93A}: -68.0 ± 4.1 mV; W2 WT: -66.5 ± 5.3 mV, W2 SOD1^{G93A}: -67.6 ± 4.8 mV).

Next, we compared the properties of single spikes. Two-way ANOVA showed most parameters including spike threshold (Table 1. W1 WT: -44.6 ± 3.8 mV, W1 SOD1^{G93A}: -43.8 ± 3.6 mV; W2 WT: -48.0 ± 5.3 mV, W2 SOD1^{G93A}: -45.0 ± 9.4 mV), spike amplitude (Table 1. W1 WT: 82.3 ± 3.6 mV, W1 SOD1^{G93A}: 78.1 ± 6.0

mV; W2 WT: 78.0 ± 5.0 mV, W2 SOD1^{G93A}: 78.0 ± 7.7 mV), AHP amplitude (Table 1. W1 WT: -7.5 ± 2.1 mV, W1 SOD1^{G93A}: -8.1 ± 2.1 mV; W2 WT: -7.1 ± 2.7 mV, W2 SOD1^{G93A}: -8.2 ± 3.1 mV) and AHP duration (Table 1. W1 WT: 153.8 ± 43.5 ms, W1 SOD1^{G93A}: 143.8 ± 39.1 ms; W2 WT: 138.1 ± 45.6 ms, W2 SOD1^{G93A}: 121.0 ± 52.9 7.7 ms) to be comparable between both genotypes at W1 and W2 No developmental changes in action potential parameters were observed in SOD1^{G93A} fast-type motoneurons. However, we did observe a decrease in the spike half width only between W1 and W2 SOD1^{G93A} motoneurons. However, no differences were seen between WT and SOD1^{G93A} motoneurons (Table 1. W1 SOD1^{G93A}: 0.87 ± 0.2 ms, W2 SOD1^{G93A}: 0.68 ± 0.2 ms; p=0.01).

	Week 1 (W1)			Week 2 (W2)			p value comparison between W1 and W2 $SOD1^{G93A}$
	WT	$SOD1^{G93A}$	p value	WT	$SOD1^{G93A}$	p value	
Resting membrane potential (mV)	-63.0 ± 6.4	-68.0 ± 4.1	0.10	-66.5 ± 5.3	-67.6 ± 4.8	0.43	
capacitance (pF)	577.8 ± 271.2	585.5 ± 242.5	0.99	714.9 ± 438.8	805.0 ± 441.8	0.58	
Input resistance (MΩ)	45.7 ± 17.8	42.2 ± 18.8	0.99	36.7 ± 20.3	24.9 ± 16.1	0.065	W1 vs W2 $SOD1^{G93A}$ **p = 0.007
Spike threshold	-44.6 ± 3.8	-43.8 ± 3.6	0.94	-48.0 ± 5.3	-45.0 ± 9.4	0.39	
Spike amplitude	82.3 ± 3.6	78.1 ± 6.0	0.63	78.0 ± 5.0	78.0 ± 7.7	0.99	
Spike half width	0.95 ± 0.16	0.87 ± 0.2	0.91	0.82 ± 0.2	0.68 ± 0.2	0.18	W1 vs W2 $SOD1^{G93A}$ **p = 0.01
Spike AHP duration (ms)	153.8 ± 43.5	143.8 ± 39.1	0.96	138.1 ± 45.6	121.0 ± 52.9	0.93	
Spike AHP amplitude (mV)	-7.5 ± 2.1	-8.1 ± 2.1	0.99	-7.1 ± 2.7	-8.2 ± 3.1	0.87	
Spike AHP half width (ms)	69.3 ± 15	64.3 ± 15.7	0.94	64.7 ± 21.6	53.7 ± 24.2	0.63	

Table 1: Electrophysiological passive and single spike properties of week 1 and 2 of fast-type motoneurons in WT (W1: N = 3, n = 10; W2: N= 14, n= 16) and $SOD1^{G93A}$ (W1: N = 4, n = 21; W2: N = 14, n = 21) mice. 'N' denotes number of mice and 'n' denotes the total number of cells in each group. **p<0.01; Two-Way ANOVA, statistical analysis performed on individual cells recorded from WT and $SOD1^{G93A}$ mice.

Next, we wanted to explore the firing properties of motoneurons as these are the triggered output to a given input. The minimal current required to generate repetitive firing, which is also known as the rheobase, was measured using a 100pA/s depolarising current ramp (Fig 1A). The rheobase of WT and $SOD1^{G93A}$ fast-type motoneurons were not significantly different at both W1 and W2 (Fig 1B. W1 WT: 275.1 ± 205.7 pA, W1 $SOD1^{G93A}$: 366.2 ± 247.2 pA; W2 WT: 497.5 ± 371.3 pA, W2 $SOD1^{G93A}$: 501.9 ± 313.1 pA). This demonstrates that $SOD1^{G93A}$ motoneurons are neither hyperexcitable nor hypoexcitable at this early presymptomatic stage of the disease. Furthermore, to compare the frequency-current (f-I) relationship, the slope of the linear portion of the traces were calculated. This allowed us to determine the relationship between the input stimulus (the increasing current) and the frequency of the action potentials produced by the motoneurons. Here we show that there is no significant difference in the F-I slope between WT and $SOD1^{G93A}$ at both W1 and W2 (Fig 1C. W1 WT: 0.0199 ± 0.008 Hz/pA, W1 $SOD1^{G93A}$: 0.0233 ± 0.006 Hz/pA; W2 WT: 0.0238 ± 0.012 Hz/pA, W2 $SOD1^{G93A}$: 0.0193 ± 0.006 Hz/pA).

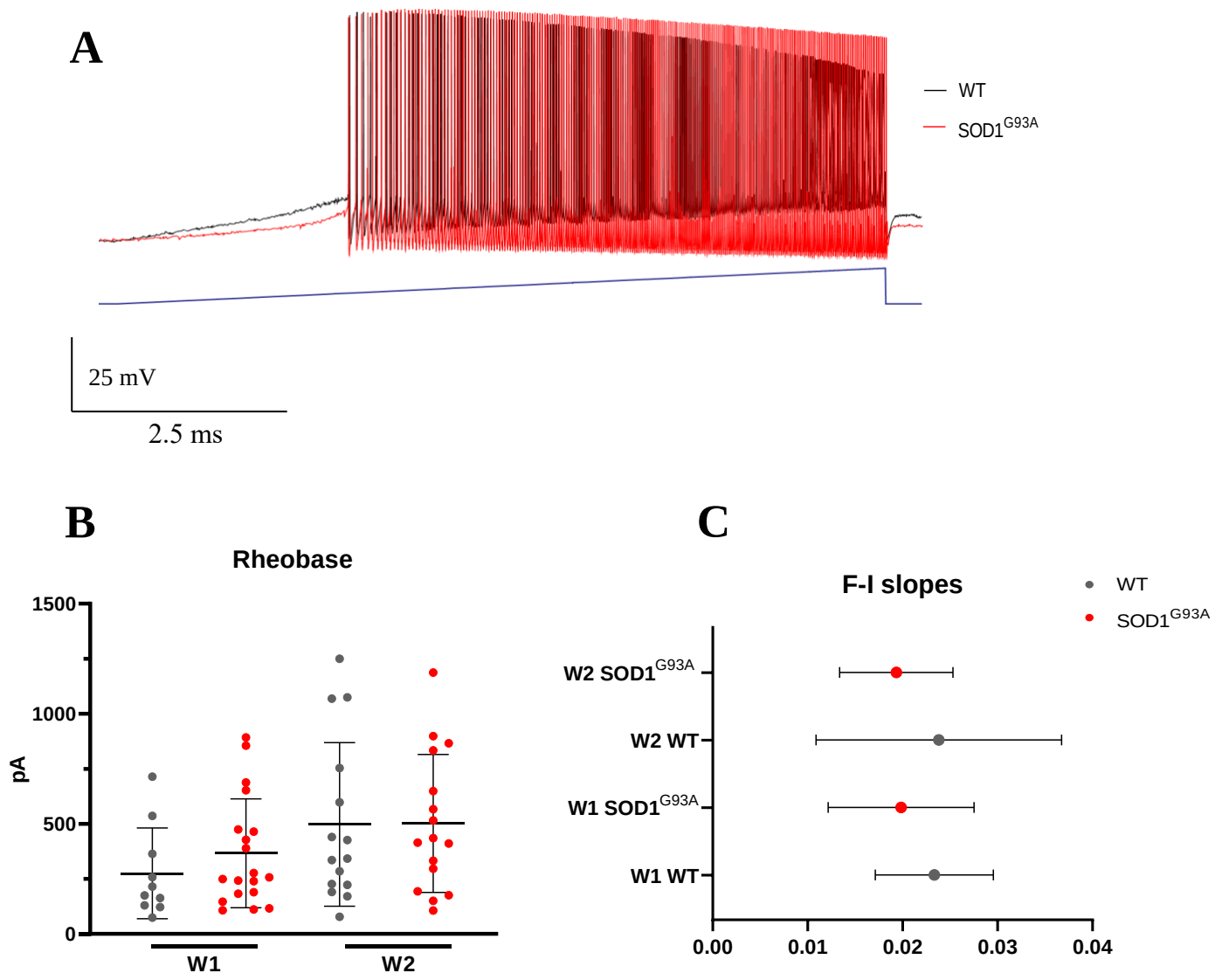

Figure 1: **Firing properties do not change in SOD1^{G39A} fast-type motoneurons in the first and second postnatal weeks.** (A) Representative raw traces of repetitive firing of WT (black) and SOD1^{G39A} (red) motoneurons. (B) Rheobase and (C) F-I slopes of fast-type motoneurons in W1 (WT: n= 10, N = 3; and SOD1^{G39A}: n= 19, N = 4) and W2 (WT: n= 15, N= 14 and SOD1^{G39A}: n=16, N = 14). No significant difference, 2-Way ANOVA.

Although we did not observe any difference in most of the passive properties, spike properties and firing properties, we expected that there may be a difference in other properties that underlie the post-discharge activity (which refers to the activity of neurons after a period of prolonged activity) of $SOD1^{G93A}$ fast-type motoneurons that could influence their excitability.

We next wanted to characterise the post-discharge activity of fast-type motoneurons and explore whether these properties are altered after a prolonged period of activity, in the vulnerable $SOD1^{G93A}$ motoneurons. All fast-type motoneurons recorded showed a post-discharge activity in the form of an afterdepolarisation (ADP). ADP can be characterised by the depolarisation of the membrane after discharge (as seen in Fig 2A). A 10 second pulse train at 30Hz was applied and the amplitude and the duration of the ADP was measured. At both W1 and W2, two-way ANOVA revealed that there are no significant differences in the amplitude of ADP (Fig 2C. W1 WT: 8.3 ± 2.7pA ; W1 $SOD1^{G93A}$: 9.1 ± 3.3 pA; W2 WT: 7.4 ± 4.8 pA; W2 $SOD1^{G93A}$: 9.5 ± 4.3 pA). Furthermore, there was no difference in the ADP duration between the WT and $SOD1^{G93A}$ fast-type motoneurons as they exhibited similar recovery time back to the RMP (Fig 2B. W1 WT: 16.7 ± 13.3 ms ; W1 $SOD1^{G93A}$: 19.0 ± 11.3 ms; W2 WT: 16.4 ± 13.9 ms; W2 $SOD1^{G93A}$: 12.2 ± 6.2 ms)

Overall, this indicated that there are no differences in the post-discharge activity following the firing of fast-type motoneurons. We next wanted to investigate if changes in the underlying current that contribute to this post-discharge activity exist.

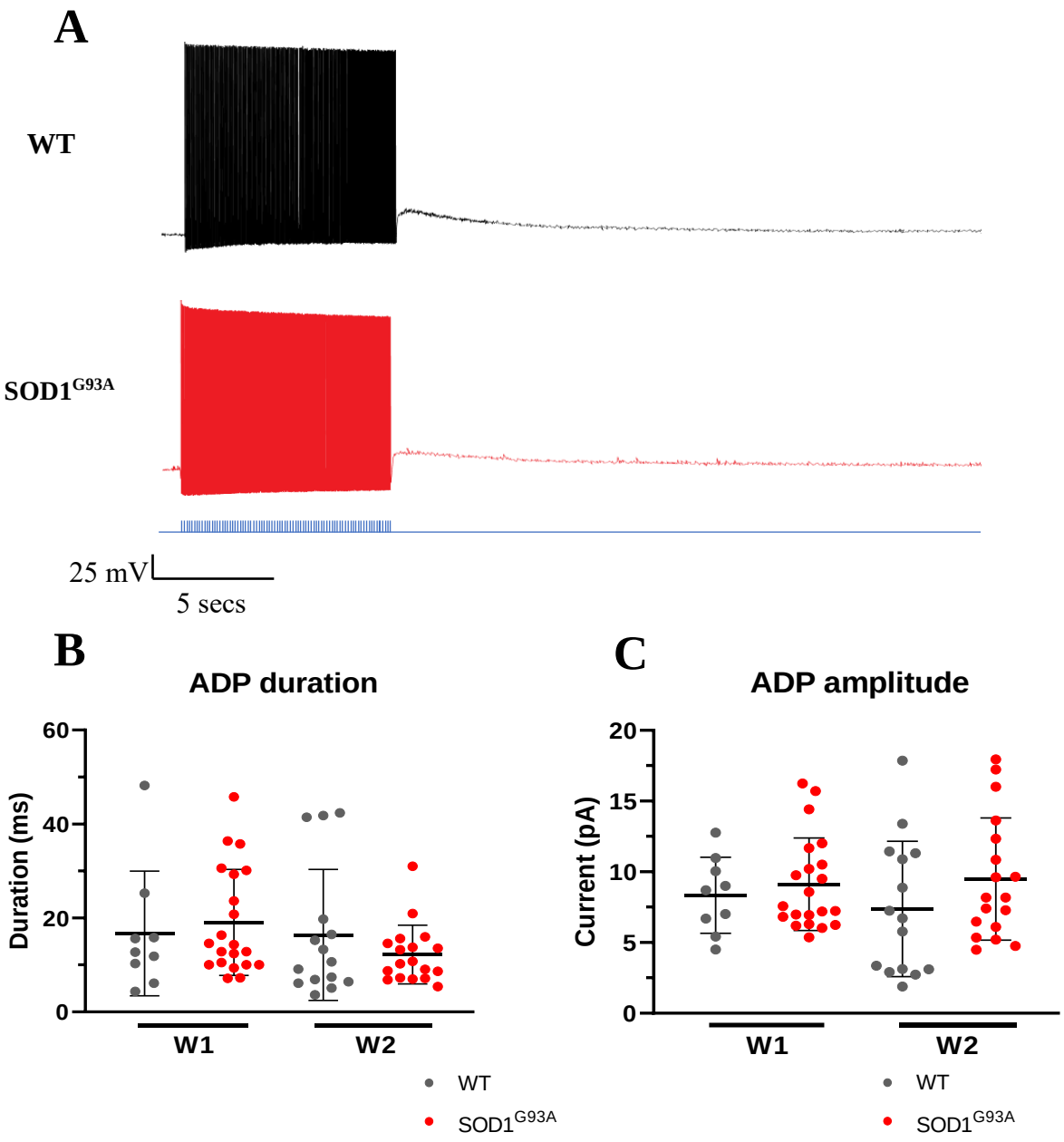

Figure 2: **Fast-type motoneurons in SOD1^{G39A} do not show significant difference in post-discharge activity properties**. (A) Raw electrophysiological trace of motoneurons displaying an afterdepolarisation (ADP) after a period of prolonged 10 seconds firing (WT in black; SOD1^{G39A} in red). (B) Duration and (C) amplitude of ADP in W1 (WT: n=9; SOD1^{G39A}: n=21) and W2 (WT: n=15 ; SOD1^{G39A}: n=18) fast-type motoneurons in WT and SOD1^{G39A}. No significant difference, Two-way ANOVA.

Other underlying currents that are involved in modulating the firing behaviour of motoneurons are persistent inward currents (PICs). PICs, generated by both Na^+ and Ca^{2+} channels, influence net neuronal excitability by increasing the firing rate, prolonging the firing after cessation of inputs and self-sustaining neuronal firing (ElBasiouny, Schuster and Heckman, 2010). Furthermore, the generation of PICs through activation of L-type Ca^{2+} channels and persistent inward Na^+ channels can also influence the generation of post-discharge ADPs (Heckman *et al.*, 2008). Even though we did not observe differences in the post-discharge ADP amplitude or duration, we wanted to investigate if there are differences in PICs in $SOD1^{G93A}$ fast-type motoneurons as previous studies have shown that PICs contribute to hyperexcitability in $SOD1^{G93A}$ motoneurons. For example, an upregulation in this inward current has been shown by previously mentioned studies (Kuo *et al.*, 2004, 2005; Van Zundert *et al.*, 2008). As these studies in PIC properties in pre-symptomatic $SOD1^{G93A}$ have not differentiated motoneurons according to subtypes, we examined whether PIC properties change only in the fast-type motoneurons.

The underlying PICs were measured in fast-type motoneurons of week 2 mice, in voltage-clamp during a slow 10mV/s depolarising voltage ramp (Fig. 3A). Here, we show that there are no differences in the onset voltage of PICs between WT and $SOD1^{G93A}$ fast-type motoneurons (Fig 3C. WT: -55.1 ± 6.8 mV; $SOD1^{G93A}$: -52.8 ± 7.1 mV). There are no differences in the PIC amplitude (Fig 3E. WT: 360.7 ± 216.8 pA; $SOD1^{G93A}$: 417.6 ± 427.8 pA) or the voltage at the peak amplitude (Fig. WT : -26.2 ± 6.1mV; $SOD1^{G93A}$:-23.8 ± 7.2 mV). Lastly the voltage at which the PIC offsets is not significantly different in W2 $SOD1^{G93A}$ fast-type motoneurons compared to W2 WT (Fig 3D. WT: -34.7± 4.6 mV; $SOD1^{G93A}$:-31.9 ± 6.0 mV). These data provide evidence that PICs do not change in fast-type motoneurons of $SOD1^{G93A}$ and suggest that this underlying current does not contribute to changes in excitability of these cells (as previously seen from the studies mentioned above).

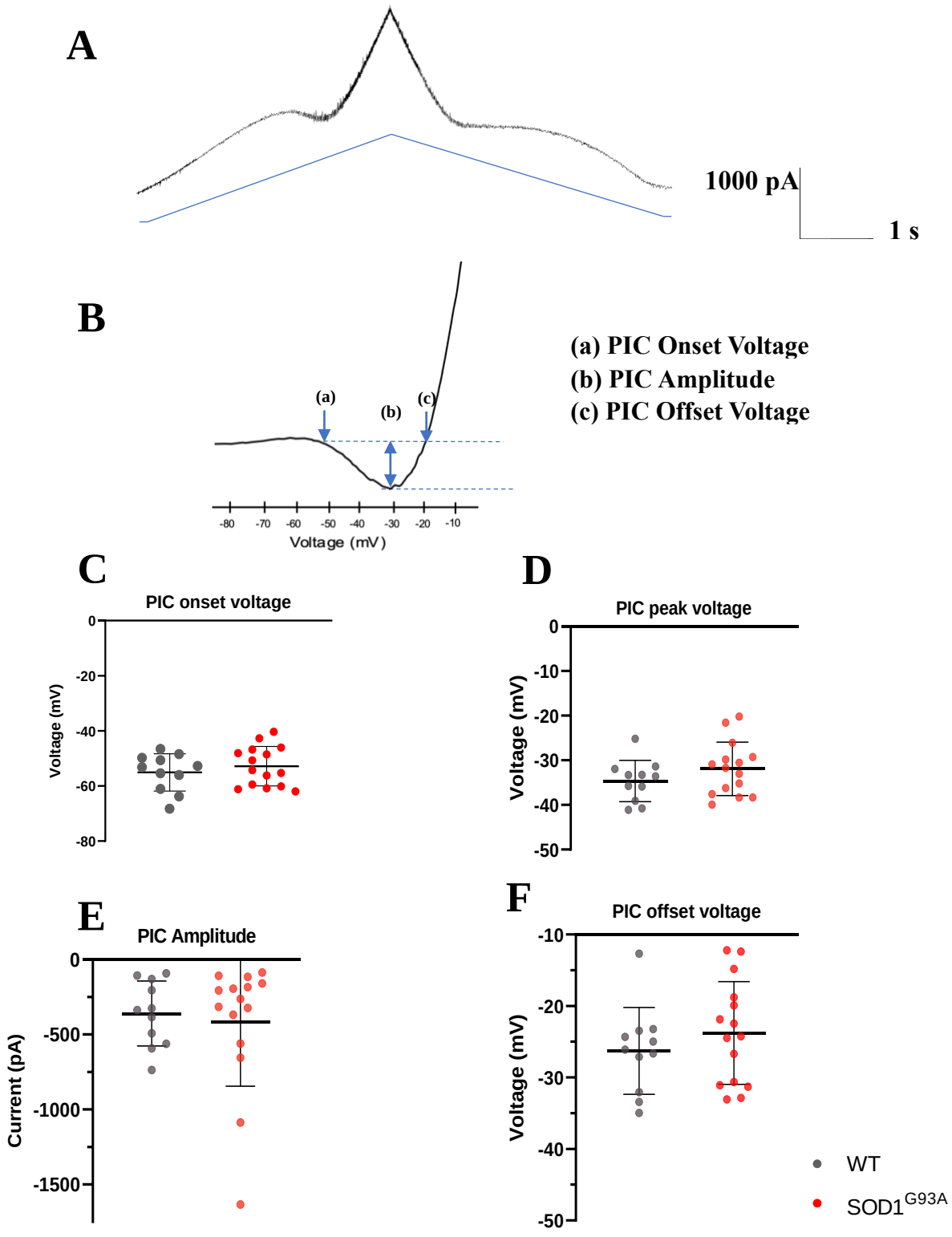

Figure 3: **Persistent inward currents (PICs) properties are not altered in W2 SOD1^{G39A} fast-type motoneurons**. (A) Raw trace used to measure underlying PICs in motoneurons using a 10mV/s depolarising voltage ramp. (B) Representative Na^+ leak subtracted, and low pass filtered trace to measure (C) voltage at PIC onset, (D) voltage at peak PIC, (E) PIC amplitude and (F) voltage at PIC offset in W2 WT (n=11) and SOD1^{G39A} (n=15) fast-type motoneurons. No significant difference, Mann-Whitney test.

We next considered other active properties that may contribute to changes in intrinsic excitability in fast-type motoneurons. Hyperpolarization-activated cyclic nucleotide-gated (HCN) channels, that are found on the soma and proximal dendrites of motoneurons, are involved in producing hyperpolarisation-activated inward currents (Ih) (Milligan, Edwards and Deuchars, 2006). As the HCN channels are active near and below the RMP, the inward current counteracts the hyperpolarising K^+ currents and allows the motoneurons to maintain their RMP. Ih has been shown to contribute to the rebound potential following inhibition (Bayliss *et al.*, 1994; Kiehn *et al.*, 2000; Engbers *et al.*, 2011). Rebound bursting can act as a switch to stop inhibition and reset excitation in motor networks (Sivaramakrishnan et al., 2017). Therefore, changes in Ih currents could potentially contribute to changes in excitability in the vulnerable motoneurons in ALS.

To measure Ih, we applied incremental hyperpolarising voltage steps (-10mV/step) and measured the difference between the initial and steady-state current (Fig 4A). Given that fast-type motoneurons have an average resting membrane potential of –63 mV and –68 mV, in WT and $SOD1^{G93A}$ mice respectively, we initially hyperpolarised the membrane to -70mV which was around or below the RMP and measured Ih. Two-way ANOVA revealed no significant difference in Ih between WT and $SOD1^{G93A}$ fast-type motoneurons at W1 (Fig 4B. WT: -6.7 ± 11.8 pA; $SOD1^{G93A}$: -7.1 ± 6.0 pA). However, a significant increase in Ih was observed in $SOD1^{G93A}$ fast-type motoneurons at W2 in comparison to WT (Fig 4B. WT: -9.0 ± 12.2 pA; $SOD1^{G93A}$: -49.2 ± 43.2 pA). Moreover, during this early development period, $SOD1^{G93A}$ fast-type motoneurons show increased Ih from W1 to W2 (Fig 4B. W1: -7.1 ± 6.0 pA; W2: -6.7 ± 11.8 pA)

Since Ih is activated at more hyperpolarised voltages below the RMP, we further hyperpolarised the motoneurons to see whether there is a difference in Ih between the disease and control. Here, we show that around –80mV (which is showed to be around the physiologically measured AHP (Table 1))

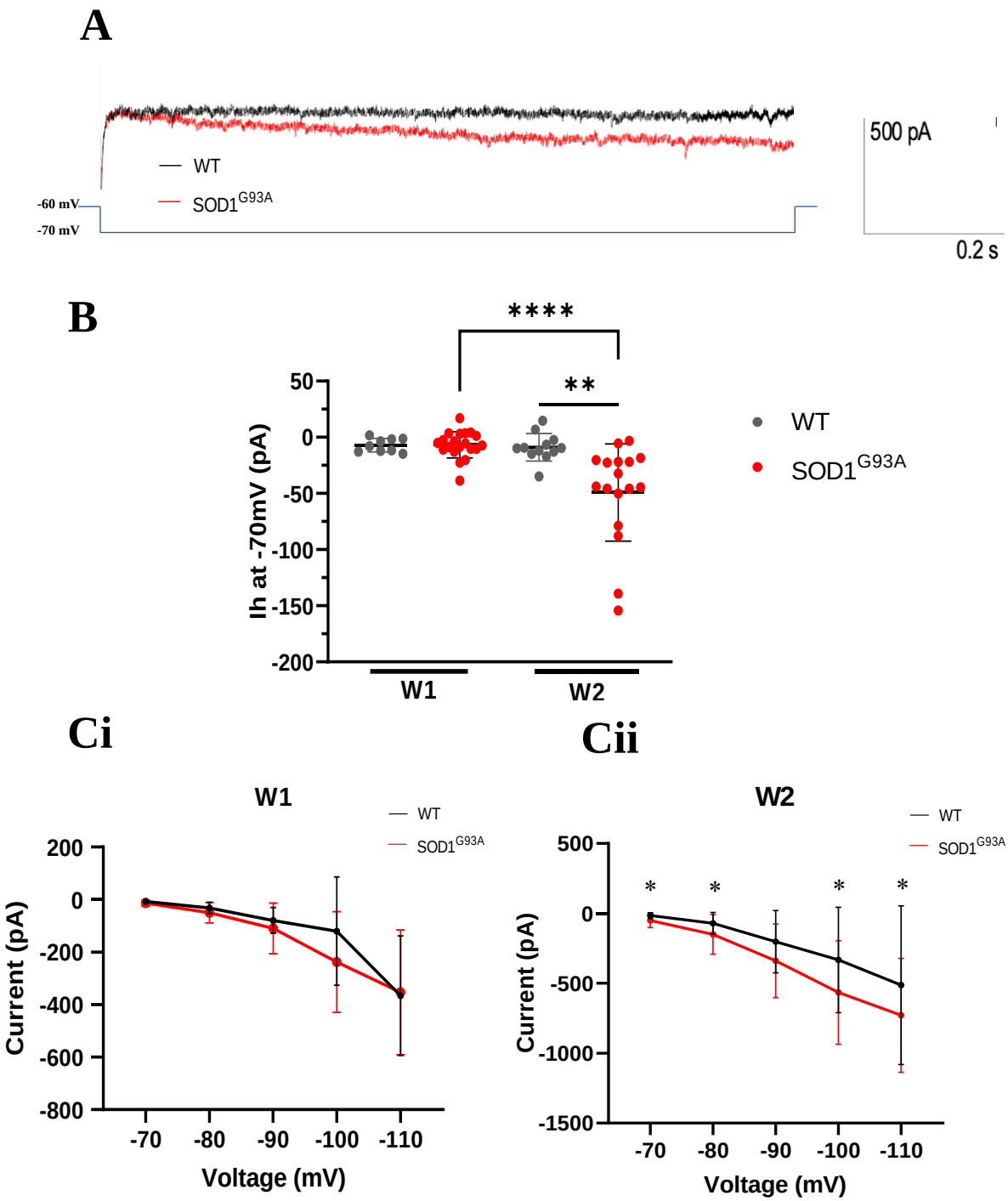

Figure 4: **Increase in Ih current is observed in week 2 fast-type SOD1^{G39A} motoneurons.** (**A**) Representative trace of Ih current measured by applying hyperpolarising current steps in voltage clamp from WT (black) and SOD1^{G93A} (red) fast-type motoneurons. (**B**) Ih measured at −70mV from week 1 (W1) (WT: n=9; SOD1^{G93A}: n=20) and week 2 (W2) (WT: n=12 ; SOD1^{G93A}: n=17) fast-type lumbar motoneurons. * p<0.05, ** p<0.01, **** p<0.001; 2-Way ANOVA. Ih current at voltages from −60 to −110 mV in week 1 (**Ci**) and week 2 (**Cii**) fast-type WT and SOD1^{G39A} motoneurons. * p<0.05; Mann-Whitney. Figures show mean ± SD

there is a significant increase in Ih current activation only in week 2 $SOD1^{G93A}$ motoneurons in comparison to WT (Fig. Cii: WT: -71.1 ± 77.0 pA; $SOD1^{G93A}$: -150.1 ± 142.3 pA). No significant differences in Ih were observed between W1 $SOD1^{G93A}$ and WT fast-type motoneurons when the cells were hyperpolarised from -70 to -110 mV (Fig 4Ci). However, when hyperpolarised from -70 to -110 mV, W2 $SOD1^{G93A}$ motoneurons exhibited a significant increase in Ih at all voltages except at -90 mV, in comparison to the WT (Fig C4ii).

To summarise, no changes in active Ih current are observed in fast-type motoneurons of $SOD1^{G93A}$ mice at W1. Although, difference in Ih current are observed in W2 $SOD1^{G93A}$ motoneurons in comparison to WT. A greater Ih current near the resting membrane potential and AHP potential is observed in the fast-type motoneurons which could lead to changes in excitability of fast-type motoneurons in SOD1 ALS, particularly when motoneuron firing follows a prolonged period of inhibition in which would activate Ih.

Discussion

In this chapter, we investigated the changes in intrinsic properties of the vulnerable fast-type lumbar motoneurons in the SOD1^{G93A} mouse model of ALS at an early pre-symptomatic age of up to postnatal two weeks. We first characterised the passive properties of fast-type motoneurons to see if these physiological properties could influence the output of motoneurons. We have shown that most passive intrinsic properties in SOD1^{G93A} fast-type motoneurons do not change at early pre-symptomatic ages of post-natal 2 weeks, in comparison to WT. However, we observed a developmental change in the input resistance of W2 fast-type motoneurons in comparison to W1 in the SOD1^{G93A} mice. A plausible explanation for this observed decrease in input resistance could be due to the size of the fast-type motoneurons as they would be larger with development. Since we do not see a significant change in input resistance between W1 and W2 WT fast-type motoneurons, we can speculate that SOD1^{G93A} fast-type motoneurons develop quicker than WT motoneurons. Whether this change can act as a developmental disorder that will later contribute to the pathogenesis of ALS cannot be known. The input resistance is determined by the size of the cell and the number of open ion channels (Kernell, 1966). The larger the size of the motoneuron, the lower the input resistance as there is more surface area for the current to pass through. Moreover, more open channels can also lower the input resistance as conductance (g) = 1 / resistance. As well as the size, increased input resistance observed in this study which could also indicate alterations in the ion conductance in transgenic motoneurons. To further investigate whether these alterations exist, we need to measure ion conductance of Na^+ and K^+ ions.

Similar findings were also observed in another SOD1 transgenic mouse model where a decrease in input resistance was also observed in SOD1^{G85R} motoneurons in neonates (Bories *et al.*, 2007)

Some studies that have undertaken patch-clamp electrophysiological in pre-symptomatic SOD1^{G93A} mice (of similar age to this study) have not shown differences in input resistance (Van Zundert *et al.*, 2008; Quinlan *et al.*, 2011b). Pun *et al.* (2006) have shown that the fast-fatigable motoneurons with lowest input resistance are vulnerable in the SOD1^{G93A} models, whereas the slow motoneurons with higher

input resistance are resistant to the disease. Given this, merging the properties of fast and slow motoneurons may have masked the changes in properties of the vulnerable motoneuron population. Hence, future studies in ALS research must take this element into account.

Neurons in the CNS can relay information in the form of action potentials. These signals can be of electrical or chemical nature, which changes the membrane potential in the form of activation and deactivation of ion channels. During a single action potential (single spike), various types of ion channels are involved and underlie the different phases of this event. Studying single spike properties would allow us to pinpoint if there were any difference in the phases of an action potential which would in turn allow us to pinpoint the ion channels that could be impaired/changed in the disease. Our results demonstrate that there are no differences in single spike properties in the fast-type $SOD1^{G93A}$ motoneurons in comparison to WT at W1 and W2. Although no difference was seen between the different genotypes, a reduction in the spike half-width was observed in $SOD1^{G93A}$ fast-type motoneurons in postnatal age of 2 weeks. This reduction in the width of the spike at half-maximal amplitude could imply that there may be an increase in potassium conductance in $SOD1^{G93A}$ motoneurons (Viana, Bayliss and Berger, 1993).

We have shown that fast-type motoneurons do not show hyperexcitable intrinsic changes in single spike properties. In contrary to our findings, studies conducted in earlier presymptomatic stages than postnatal 1 week have shown that $SOD1^{G93A}$ motoneurons are indeed hyperexcitable as they showed reduction in spike threshold (Kuo *et al.*, 2005), increased spike half-width and RMP (Pambo-Pambo, Durand and Gueritaud, 2009). This difference could have been due to differences in methodology as some studies were conducted in embryonic or neonatal spinal cultures, however, results from Pambo-Pambo, Durand and Gueritaud (2009) were also collected from transverse spinal cord slices. One caveat

from the mentioned studies is that the subtype of motoneurons were not distinguished in the study. Leroy *et al.* (2014) showed that only the slow-type $SOD1^{G93A}$ motoneurons in transverse slices have reduced spike threshold and are overall hyperexcitable in the disease model. Since only the fast-type motoneurons are affected and the slow-type motoneurons are resistant in the disease (Pun *et al.*, 2006), pooling the data from both subtypes may have given a biased overall impression that $SOD1^{G93A}$ motoneurons show hyperexcitable phenotypes at early pre-symptomatic stages of the disease.

Next, we investigated the firing properties of the fast-type motoneurons and found that $SOD1^{G93A}$ and WT have comparable parameters in terms of rheobase and F-I slopes. This suggests that there are no differences in neuronal output in $SOD1^{G93A}$ fast-type motoneurons in response to the same brief current stimulus applied to WT fast-type motoneurons. This finding is rather in intriguing as many studies in $SOD1^{G93A}$ mouse models and humans have supported the widely accepted hyperexcitability hypothesis whereby motoneurons only show signs of prolonged repetitive firing and firing frequency before degeneration (Pieri, 2003; Kuo *et al.*, 2004, 2005; Martin *et al.*, 2013b). Slow type motoneurons are hyperexcitable (Leroy *et al.*, 2014), therefore the hyperexcitability phenotype seen in numerous studies may have been resulted from pooling data acquired from both fast- and slow-type motoneurons.

Ion channel dysfunction has become a widely recognised potential mechanism in many neurodegenerative disease such as Parkinson's and Alzheimer's disease (Chang *et al.*, 2019). One class of ion channels involved in the modulation of neuronal excitability are HCN channels. HCN channels are activated by the hyperpolarisation of neuronal membrane (approximately below the resting membrane potential) and these channels are responsible for the conductance of Ih (Santoro *et al.*, 2000). Moreover, along with other currents, Ih is an important contributor to the RMP of motoneurons. For

example, knockdown of HCN1 channel decreases Ih which in turns can hyperpolarise the RMP of neurons (Tsay, Dudman and Siegelbaum, 2007).

In this study we observed an increase in Ih in SOD1^{G93A} fast-type motoneurons in comparison to WT. Although it has been shown that Ih can affect the RMP and intrinsic excitability of neurons, here we do not see any differences in the RMP and firing properties of fast-type motoneurons between the two genotypes, indicating that this change in Ih do not alter other intrinsic parameters. However, it is interesting to observe that pharmacologically blocking HCN channels using ZD7288 or ivabradine hyperpolarised the RMP in fast-type motoneurons. This could have been due to the active currents that oppose Ih (Sharples and Miles, 2021). Therefore, it can be implied that other currents that oppose Ih, such as the transient K^+ current, Na^+/K^+ pump current and M-current mediated by voltage-gated K^+ channel, may be active to mask the changes in Ih seen in W2 SOD1^{G93A} motoneurons (MacLean *et al.*, 2003; Picton, Zhang and Sillar, 2017; Buskila *et al.*, 2019).

In a study conducted by Sharples and Miles (2021) whereby the postnatal development of Ih was studied in WT fast-type motoneurons, it was observed that the size of the Ih increases with development. We could postulate that the SOD1^{G93A} motoneurons may have a more pronounced maturation in comparison to WT at W2. This early alteration in Ih could set up the motoneurons for failure at an early developmental stage, with progressive worsening with development. Whether this change is due to the disease or hypervigilant homeostasis to compensate for changes caused by the disease is unknown, however given these early changes in current changes, we could speculate that ALS may be a developmental disorder.

Our study on the electrical properties of the vulnerable fast-type motoneurons do not support the changes found in other studies that support hyperexcitability as a pathological sign of ALS. We do not observe any changes in the passive properties such as spike threshold and rheobase, which have been

shown to change towards a hyperexcitable phenotype (Kuo *et al.*, 2005; Van Zundert *et al.*, 2008; Martin *et al.*, 2013a).

Our results show that fast-type motoneurons do not display changes in intrinsic properties that have been reported by previous studies. In contrary to the standard hypothesis of intrinsic hyperexcitability, lumbar fast-type SOD1^{G93A} motoneurons do not show signs of hyperexcitability that would render them hyperexcitable and trigger degeneration at early pre-symptomatic stage. Even though we observed changes in intrinsic properties such as decrease in capacitance and increased in Ih in SOD1^{G93A} fast-type motoneurons, we do not see overt changes in the output of these motoneurons which could imply that there are homeostatic mechanisms in place that can compensate for these early changes which would preserve the functional output of the motoneurons. Perhaps, faults in this homeostatic maintenance could results in changes that would push the fast-type motoneurons from becoming either hyperexcitable or hypoexcitable at a later stage before degeneration. It is widely known that the root cause of ALS is not arisen by single factor but is instead caused by many factors spanning from a cellular to a system-level. Since we show no clear evidence of hyperexcitability nor hypoexcitability at the first postnatal two weeks of development, the possibility of whether that initial perturbation arise at this time point cannot be ruled out. Compensating for the changes in electrical properties seen in our studies and other studies (Huh, Charles J Heckman and Manuel, 2021) could pose a metabolic burden to the fast-type motoneurons. FF motoneurons have higher metabolic needs than S motoneurons and are therefore more vulnerable to metabolic dysfunction (Le Masson, Przedborski and Abbott, 2014).

Given that these motoneurons encompass the SOD1^{G93A} mutation that disrupts the mitochondrial function, increasing the metabolic demand may in fact decrease their chance of survival and rendering them more vulnerable in ALS.

In summary, we have shown that the vulnerable fast-type motoneurons do not exhibit changes in intrinsic properties aside from changes in input resistance and Ih. Despite the changes observed, fast-type motoneurons do not show changes in their output which demonstrates that they are neither hyperexcitable nor hypoexcitable. In fact, the F-I slope and rheobase emphasise that at postnatal age of 2 weeks, $SOD1^{G93A}$ fast-type motoneurons maintain normal excitability. Perhaps, there are other components of cellular mechanisms that are involved in maintaining homeostasis.

Chapter 3: Investigation of synaptic inputs in the vulnerable fast-type motoneurons in early presymptomatic stage of SOD1^{G93A} mice

Neural circuits in the spinal cord are responsible for the coordination of locomotion. This arrangement of the spinal circuit comprises of motoneurons, interneurons and glial cells such as astrocytes and microglia. This physiological network that is responsible for generation and maintenance of the pattern of movement, relies on the interaction of excitatory and inhibitory neurotransmission as well as modulatory transmission (Ramírez-Jarquín and Tapia, 2018). Motoneurons receive excitatory, inhibitory, and modulatory synaptic inputs onto their soma and dendritic structures that can shape their output that underlies the activity of muscle fibres. In other words, these inputs are determinants of whether action potentials can be generated or not.

Synapses are neuronal structures that are essential for the facilitation of coordinated transfer of information between neurons and consist of pre- and post-synaptic domains. Two main factors that contribute to the discharge activity of motoneurons are intrinsic properties and synaptic inputs. Despite the intense research that has focused on the changes in intrinsic properties of motoneurons in ALS, there are increasing evidence arguing for synaptic abnormalities such as perturbation in their structure and function, known as synaptopathy (Fogarty et al 2017).

Many studies undertaken in rodents have shown synaptic dysfunction to be a mechanism in the disease, particularly within the motor cortex. Post-mortem analysis in ALS patients showed that synapses were significantly reduced on the dendrites of the upper motoneurons, called Betz cells, that send their axons down to the spinal cord via the corticospinal tract (Genç *et al.*, 2017). In rodent models of ALS, an increase in excitatory synaptic inputs in parallel to decreases in inhibitory inputs have been observed in the cortex, and this shift in the excitation to inhibition ratio (E:I) towards excitation is considered to result in excessive excitation leading to subsequent excitotoxicity (Nieto-Gonzalez 2011, Saba et al 2016).

Although there has been numerous evidence of synaptopathy in the brain, as we are interested in the changes in excitability in lower motoneurons, we will be discussing the changes in synaptic function in spinal motoneurons.

Post-mortem observations in ALS patients revealed evidence for synaptic pathology in the disease. Decreases in synaptophysin, a membrane protein expressed in presynaptic vesicles, were observed in the anterior horn of ALS patients with only degeneration in the lower motoneurons (Sasaki & Maruyama, 1994). Interestingly, there was also a loss in the number of synapses on the axon hillocks on the proximal axons of anterior horn neurons (Sasaki & Iwata, 1995) and the loss of synaptophysin correlated to the loss of lower motoneurons (Matsumoto et al., 1994).

Consistent with the post-mortem findings, anatomical studies in the $SOD1^{G93A}$ mouse model also revealed loss in synaptophysin-positive pre-synaptic boutons on lumbar motoneurons at the pre-symptomatic stage (Zang, Lopes and Cheema, 2005). Furthermore, the dendritic spine represents the site of synaptic contact in neurons and in neonatal $SOD1^{G93A}$ mice, the dendritic spine density was increased; however, it was found to be decreased from the pre-symptomatic age to disease onset of P28-35 (Fogarty et al 2017). Whether this change occurs because of maladaptive changes or is indeed a protective homeostatic change cannot be identified.

Overall, these findings provide evidence that synaptic changes are clearly present in the disease and many studies have been conducted with the goal to explore how these changes in synaptic inputs contribute to the disease. Thus, these studies have investigated how the excitatory and the inhibitory circuits and synapses are affected in ALS.

As the output of a neuron is dependent on the balance of excitatory and inhibitory input it receives, the imbalance of this ratio biased towards excitation could elicit hyperexcitability and trigger

neurodegeneration. This can be resulted in two ways: 1) motoneurons receive excessive excitatory inputs, 2) there is insufficient inhibition on motoneurons or within the spinal network itself.

Changes in excitatory inputs

Glutamate is the major neurotransmitter in the CNS and glutamatergic transmission has been widely studied in the context of ALS and thus far it is considered, by some researchers, as the most contributing factor in the disease. In ALS patients, cortical hyperexcitability has been widely documented and is thought to be the preceding mechanism that results in motoneuron degeneration through glutamate-induced toxicity (Vucic, Nicholson and Kiernan, 2008; Geevasinga *et al*., 2016; Menon *et al.*, 2020).

Motoneurons in the ventral horn of the spinal cord receive excitatory glutamatergic inputs from the motor cortex, brainstem, sensory afferents and excitatory spinal interneurons (Brownstone and Bui, 2010). These excitatory inputs to lower motoneurons have shown abnormalities in ALS. For example, motoneurons receive glutamatergic proprioceptive inputs that are recruited during muscle stretch reflexes. Irregular action potential bursts in the proprioceptive Ia afferent in the brainstem were observed in P8-14 $SOD1^{G93A}$ mice. This disrupted firing pattern has been shown to be as a result of reduced $Nav_{1.6}$ channels and these excitability changes were only limited to muscle spindle afferent proprioceptive neurons (Seki *et al.*, 2019). Moreover, functional elimination of Ia afferent input on motoneurons increased the survival of the vulnerable α-motoneurons, however, it did not halt the progression of the disease (Lalancette-Hebert *et al.*, 2016).

Furthermore, one of the earliest alterations in synaptic inputs has been observed in the hypoglossal motoneurons. Van Zundert *et al.* (2008) showed that these motoneurons received significantly more glutamatergic inputs as well as spontaneous inhibitory PSCs, in the first week of age in $SOD1^{G93A}$ mice.

Further work in adult sacral spinal cord of SOD1^{G93A} mice revealed that excitatory synaptic inputs persisted as sacral SOD1^{G93A} motoneurons manifested higher frequency of excitatory post-synaptic potential (Jiang *et al.*, 2017). Since both studies show changes in frequency not amplitude of the events, it can be inferred that there is an increase in the probability of neurotransmitter release from the pre-synaptic neurons or an increase in the number of synapses. The similarity in the amplitude of the synaptic events between the disease and control could tentatively indicate that there are no changes in the structure and function of the post-synaptic density (PSD) (Choi and Lovinger, 1997).

Besides electrophysiological studies of motoneurons, some studies have investigated the role of excitatory neurotransmission using pharmacological interventions. Administration of glutamate receptor agonists and excitatory amino acids in WT animals revealed symptoms that are similarly observed in symptomatic SOD1^{G93A} animals, which included hind limb weakness, motoneuronal loss and gliosis (Hirata *et al.*, 1997; Nakamura *et al.*, 1997). Moreover*, in vivo* acute administration of AMPA receptor agonist in the lumbar spinal also mimicked SOD1 ALS symptoms by showing motoneuronal loss as well as muscle hyperexcitability and hind limb paralysis. The loss of motoneurons was attributed to the heightened Ca^{2+} entry though AMPA receptors (Corona and Tapia, 2004, 2007).

When taken together, it is possible that the increase in excitatory inputs seem to negatively impact motoneurons in ALS by rendering them more excitable leading to excitotoxicity. However, excitatory neurotransmission isn't the only factor altered in ALS. Altered inhibitory neurotransmission has also been observed in animal models of SOD1 ALS and is summarised in the next section.

Changes in inhibitory inputs

The excessive excitatory synaptic innervation onto motoneurons emphasises the glutamate excitotoxicity and hyperexcitability theories in ALS. However, the balance of excitatory and inhibitory drive on motoneurons may be altered by not only an increase in excitation, but also by a decrease in inhibitory inputs. Spinal motoneurons express glycine and GABA receptors and receive GABAergic and glycinergic innervations from several inhibitory interneurons which regulate their excitability (Goulding, 2009). Post-mortem studies in ALS patients have shown significant reduction in glycine binding sites in the anterior horn of the spinal cord (Hayashi et al., 1981) and the mRNA expression of GABA receptors were significantly reduced in the motor cortex at the time when motoneuron loss was prevalent (Petri *et al.*, 2003).

Recurrent inhibition that is mediated by Renshaw cells has also shown to be impaired in SOD1-ALS. Spinal motoneurons can regulate their own activity by projecting synapses onto Renshaw cells and simultaneously receiving inhibitory inputs from Renshaw cells, and as a result inhibit motoneurons through glycinergic mechanisms (Eccles, Fatt and Koketsu, 1954). A loss of presynaptic motor axons input onto Renshaw cells have been observed in symptomatic $SOD1^{G93A}$ mice which suggests that motoneurons lose this recurrent feedback inhibition of firing (Wootz, Fitzsimons-Kantamneni, *et al.*, 2013). In a study performed by Özyurt *et al.* (2020), they compared the spinal recurrent inhibition and post-activation depression on the soleus muscle of lumbar affected ALS patients and found that both spinal circuits were significantly reduced in comparison to healthy individuals as well as non-lumbar affected ALS patients. This further depicts that spinal inhibitory circuits are selectively impaired in ALS at the lumbar spinal cord level and importantly shows how heterogenous symptoms can be depending on where the degeneration is. Previous studies have reported dysfunctions in inhibitory inputs in SOD1 ALS, particularly in glycinergic inputs. Loss in glycinergic receptors was observed in the anterior horn of the spinal cord of ALS patients (Hayashi et al., 1981). Similar observations were made in the ventral and

dorsal horns of lumbar spinal cords of ALS patients, where there was a reduction in the level of glycine but no significant changes in GABA levels (Malessa et al., 1991)

In early symptomatic $SOD1^{G93A}$ mice, the density of glycine transporter-2 (GlyT2) boutons was considerably lower on lateral motoneurons, and the number of calbindin-positive Renshaw cells were reduced in comparison to control. Furthermore, this reduction of Renshaw inhibition was observed prior to the degeneration of motoneurons (Chang and Martin, 2009), which suggests that changes in the pre-motor circuits are present before motoneurons are lost.

In whole-cell patch-clamp experiments, glycinergic miniature inhibitory post-synaptic currents (miPSCs) were smaller and correlated with a decrease in mRNA expression of the GlyRα1 subunit in $SOD1^{G93A}$ embryonic cultures (Chang and Martin, 2011). They also showed that these glycinergic miPSCs and glycine-evoked currents were reduced in larger motoneurons, however the smaller motoneurons (presumably slow-type motoneurons) exhibited currents and miPSC that were comparable to controls. This deficit in glycinergic transmission in different subtypes of motoneurons further validates that selective vulnerabilities are present in ALS. In line with this finding, Cavarsan et al (2022) showed that the excitability of glycinergic interneurons is reduced in very early presymptomatic (P6-10) $SOD1^{G93A}$ mice and this possible loss in inhibitory innervation could indeed affect the excitability of motoneurons by increasing the excitation: inhibition (E:I) synaptic inputs on motoneurons, favouring excitability.

In comparison to slow-type motoneurons that innervate slow twitch muscle, the fast-type motoneurons that innervate FF and FR motor units often have more excitatory synapses than inhibitory synapses, thus having a higher E:I ratio (Conradi *et al.*, 1979; Brännström, 1993). Given that the fast-type motoneurons are affected first in ALS, an increase in excitation could potentially contribute to this selective vulnerability and it is therefore important to differentiate between each motoneuron subtype when studying changes in synaptic inputs. Following this, Allodi et al. (2021) investigated inhibitory inputs in

the vulnerable motoneuron population in the context of ALS. They found that the vulnerable fast-type motoneurons have many inhibitory glycinergic synapses and receive significantly more inhibitory inputs than slow-type motoneurons. However, in $SOD1^{G93A}$ fast-type motoneurons, a selective loss in these glycinergic synapses is observed during the disease progression before the degeneration of motoneurons. Furthermore, these neurons were positive for the V1 interneurons marker En1, and the silencing these spinal interneurons induces ALS locomotor phenotypes. Therefore, loss of V1 interneurons can also contribute to fast-type motoneuron vulnerability before motoneuron degeneration (Allodi *et al.*, 2021).

Even though these findings suggest alteration in only glycinergic inputs, histological studies in post-mortem tissue of ALS patients showed reductions of GABAergic interneurons in the anterior horn of the spinal cord (Stephens *et al.*, 2006). Similarly, Niessen and colleagues (2007) showed that $GABA_A$ receptors were significantly reduced in the spinal cords of late pre-symptomatic (P75) $SOD1^{G93A}$ mice. Immunohistochemical studies using pre-synaptic markers can provide anatomical information about possible changes in synaptic inputs. Hossaini *et al.* (2011) showed a reduction in GlyT2 and GAD65/67 which are glycinergic and GABAergic presynaptic markers respectively, in the ventral horn of $SOD1^{G93A}$ mice at the end stage of the disease. Importantly, they have shown that these changes in inhibitory interneurons manifest prior to motoneuron degeneration. This implies that the degeneration in pre-motor circuits may facilitate the degeneration of motoneurons. In line with this finding, a loss of the vesicular GABA transporters (VGAT) that are expressed in both GABAergic and glycinergic presynaptic neurons suggests that less of the inhibitory neurotransmitters GABA and glycine are recycled into synaptic vesicles in SOD1 ALS (Saito *et al.*, 2010; Sunico *et al.*, 2011). Overall, these findings suggest that deficits in inhibitory innervation of spinal motoneurons could serve as a mechanism that leads to motoneuron hyperexcitability.

Whilst most studies have shown a bias toward excitatory transmission due to a decrease in the opposing inhibitory transmission, some studies on the other hand argue that excessive inhibition may be a neuropathological feature in ALS. In a study conducted in early symptomatic SOD1^{G93A} mice, a loss in the glutamatergic pre-synaptic markers, VGLUT1 and VGLUT2 in VAChT-positive motoneurons was found whilst no change in the inhibitory pre-synaptic marker VIAAT was observed (Schütz, 2005). This finding indicates that excitatory glutamatergic interneurons may be lost before the inhibitory interneurons and would therefore suggest that changes in the E:I towards increased inhibition. Similar findings were also observed when visualising synapses using electron microscopy in SOD1^{G93A} embryonic cultures, where more inhibitory synapses were present in comparison to excitatory synapses (Avossa *et al.*, 2006). Both studies point towards that over-inhibition, rather than over-excitation, may be a patho-mechanism that enhances the progression of the disease.

In summary, there is clear indication that synaptic inputs are altered in SOD1-ALS, however, elucidating a clear patho-mechanism from the available literature can be challenging. Even though the SOD1^{G93A} mouse has proven to be a popular model to study ALS, differences in the time points studied and method used can make it difficult to draw comparisons amongst studies and to better understand putative changes to synaptic inputs in ALS.

From the previous chapter, we have shown that irrespective of some changes in intrinsic properties, the output of fast-type motoneurons were not different in SOD1^{G93A} mice in comparison to WT at a postnatal age of two weeks. We studied these intrinsic properties by applying an artificial current stimulation as the input and from this we did not observe any overt changes in intrinsic properties (aside from input resistance and Ih) and in firing properties in SOD1^{G93A} fast-type motoneurons. Application of controlled current stimulation does not replicate the physiological inputs that the motoneurons receive. Therefore, the actual physiological inputs that fast-type motoneurons receive may differ, resulting in variable degree of motoneuronal activity/output that we may have missed by controlling the inputs

ourselves. Consequently, we wanted to investigate if changes in synaptic inputs exist in the vulnerable fast-type SOD1^{G93A} lumbar motoneurons at an early pre-symptomatic age.

Methods

Animals, tissue preparation and whole-cell patch-clamp recording protocols are as described in Chapter 2.

Data acquisition and analysis

Whole-cell patch-clamp recordings were obtained from fast-type motoneurons in voltage-clamp mode. Post-synaptic currents (PSC) were obtained in voltage-clamp mode at a holding potential of -60 mV and -40 mV. 6 minutes of recording was obtained from each motoneuron for PSC analysis. Recordings were analysed using DataView (version 11.7). Traces were debuzzed, corrected for DC shift and smoothed using a moving average. The threshold for the detection of events was set at 3 times the root mean square. The frequency of events was measured from the processed trace and the amplitude of individual events were obtained from the raw trace. Data are reported as mean ± SD. Two-way ANOVA was used to compare the mean when more than two groups were compared. Unpaired t-test was used to compare the difference in mean between two groups if data passed the normality test. If normality test was not passed, Mann-Whitney test was used to compare the mean between two groups. Kolmogorov-Smirnov test was used to test the difference in the distribution of inter-event intervals and amplitude of PSC.

Solutions and drugs

Dissecting aCSF: *130mM K-gluconate, 15mM KCl, 0.05 mM EGTA, 20 mM HEPES, 25 mM D-glucose, 3 mM kynurenic acid, 2 mM Na-pyruvate, 3 mM myo-inositol, 1 mM Na-L-ascorbate; pH 7.4, adjusted with NaOH; osmolarity approximately 345 mOsm*

Recovery aCSF: *119mM NaCl, 1.9mM KCl, 1.2mM NaH_2PO_4, 10mM $MgSO_4$, 1mM $CaCl_2$, 26mM $NaHCO_3$, 20mM glucose and 1.5mM kynurenic acid*.

Recording aCSF: *127mM NaCl, 3mM KCl, 2mM $CaCl_2$, 1mM $MgCl_2$, 26mM $NaHCO_3$, 1.25mM NaH_2PO_4, 10mM glucose.*

Intracellular solution for patch clamp recordings: *14mM $KMeSO_4$, 10mM NaCl, 1mM $CaCl_2$, 10mM HEPES, 1mM EGTA, 3mM Mg-ATP and 45mM Mg-GTP.*

Tetrodotoxin (TTX), 2R)-amino-5-phosphonovaleric acid (APV) and 6-cyano-7-nitroquinoxaline-2,3-dione (CNQX) were obtained from Tocris. Bicuculline and strychnine were obtained from Sigma-Aldrich. Concentration of drugs used in experiments were as follows: TTX, 0.5μM; bicuculline, 20μM; strychnine 2μM; APV, 50μM and CNQX, 10μM.

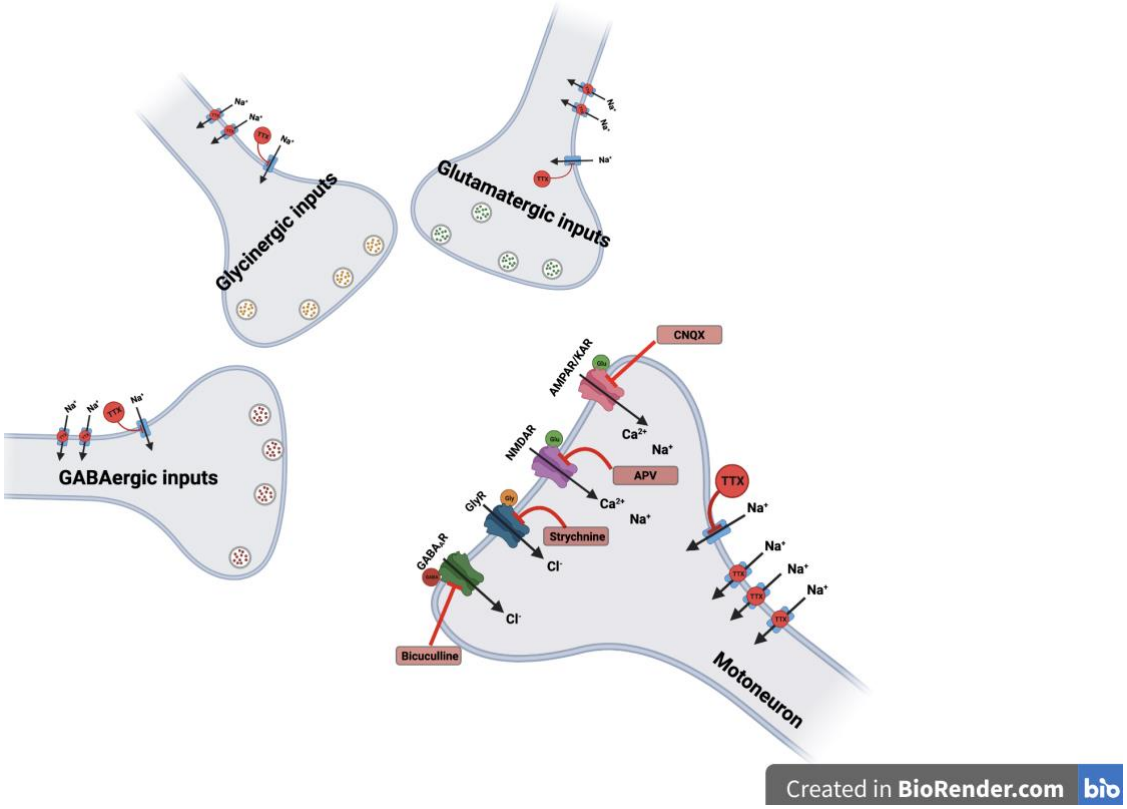

Schematic diagram showing the different receptor channels found on the post-synaptic membrane of motoneurons and their antagonists. To inhibit action potentials being generated, the Na^+ channel blocker tetrodotoxin (TTX) was used to measure miniature post-synaptic current (mPSCs). To block glutamatergic transmission, NMDA receptor antagonist APV and AMPA and kainate (KAR) receptor antagonist CNQX were used. GABAergic transmission was inhibited by the application of $GABA_A$ receptor antagonist bicuculline. Glycinergic transmission was inhibited by the application of glycine receptor (GlyR) antagonist strychnine.

Results

Given the evidence that observed no overt changes in the output (firing) of motoneurons, we next investigated the role of synaptic inputs on motoneuron excitability in fast-type motoneurons in $SOD1^{G93A}$ mice. To investigate whether there are changes to premotor inputs onto motoneurons in early postnatal $SOD1^{G93A}$ mice, voltage-clamp recordings of fast-type motoneurons held at -60 mV were performed (Fig 1A.), and the frequency and amplitude of the spontaneous PSCs were measured. We found that the frequency of mixed spontaneous PSCs was increased in week 2 (W2) $SOD1^{G93A}$ motoneurons in comparison to W2 WT (Fig 1Bi. WT: 3.5 ± 3.2 Hz, $SOD1^{G93A:}$ 8.1 ± 8.2 Hz). However, this difference was not observed between WT and $SOD1^{G93A}$ motoneurons at week 1 (W1) (Fig 1Bi. WT: 4.1 ± 2.5 Hz, $SOD1^{G93A:}$ 3.9 ± 3.4 Hz). Moreover, the cumulative frequency distribution shows comparable inter-event time between events at W1 in $SOD1^{G93A}$ and WT, but the inter-event time between mixed PSC is reduced in W2 $SOD1^{G93A}$ in comparison to WT (Fig 1Biii, $p<0.0001$ Kolmogorov-Smirnov test). In contrast, the amplitude of the mixed spontaneous PSCs remained comparable between WT and $SOD1^{G93A}$ at both W1 (Fig Ci. WT: 57.8 ± 6.3 pA, $SOD1^{G93A:}$ 54.9 ± 10.3 pA) and W2 (Fig Ci. WT: 55.4 ± 5.6 pA, $SOD1^{G93A}$: 56.8 ± 12.4 PA). In addition, no significant differences were observed in the distribution of the PSC amplitude in $SOD1^{G93A}$ and WT motoneurons at both W1 and W2 (Fig Cii and Ciii). Although we observed a trend in an increase in the frequency of mixed spontaneous PSC between W1 and W2 fast-type $SOD1^{G93A}$ motoneurons, the difference was not statistically significant (Fig Bi. W1: W2: $p=0.14$).

Although these findings demonstrate changes in the frequency of synaptic transmission in fast-type motoneurons, we cannot distinguish whether these inputs are excitatory or inhibitory due to the reversal potential of Cl^- as both types of spontaneous inputs are depolarising at a holding potential of -60 mV. To distinguish spontaneous inhibitory PSCs, the holding potential was held at -40 mV at which the inhibitory PSCs are hyperpolarising and can be distinguished from the excitatory PSCs (Fig 2A). Here, we found no significant difference in the average frequency and amplitude of inhibitory spontaneous PSCs in $SOD1^{G93A}$ fast-type motoneurons in comparison to WT, at both W1 (Fig 2Bi. WT:

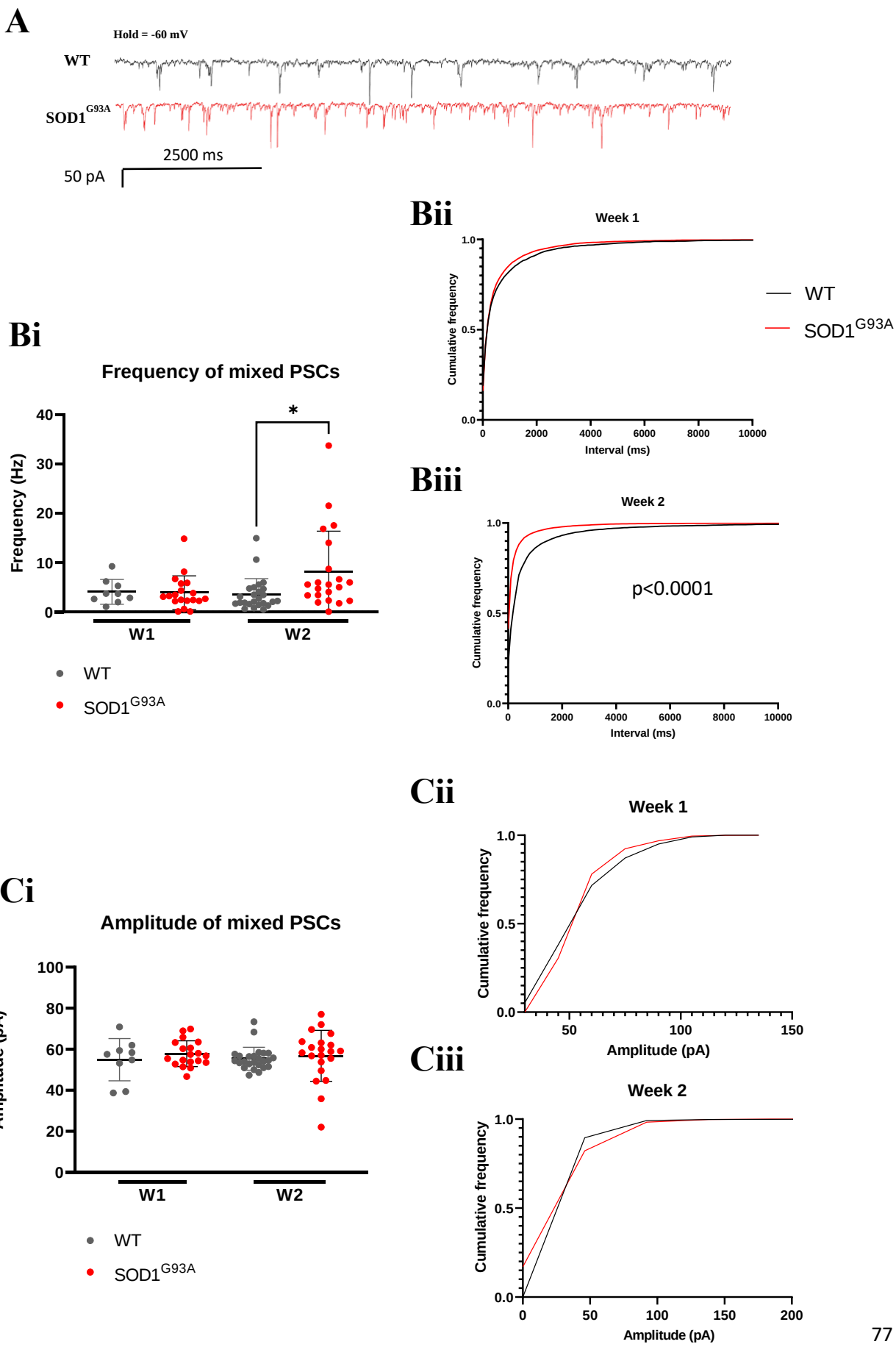
A
Hold = -60 mV
WT
SOD1G93A
2500 ms
50 pA
Bi
Frequency of mixed PSCs
Frequency (Hz)
W1
W2
WT
SOD1G93A
Bii
Week 1
Cumulative frequency
Interval (ms)
WT
SOD1G93A
Biii
Week 2
p<0.0001
Cumulative frequency
Interval (ms)
Ci
Amplitude of mixed PSCs
Amplitude (pA)
W1
W2
WT
SOD1G93A
Cii
Week 1
Cumulative frequency
Amplitude (pA)
Ciii
Week 2
Cumulative frequency
Amplitude (pA)

Figure 1. **Frequency of mixed post-synaptic currents is increased in week 2 SOD1^{G93A} fast-type, lumbar motoneurons.** (A) voltage-clamp recording recorded from W2 fast-type motoneurons from WT (black) SOD1^{G93A} (red) mice held at -60 mV. (Bi) Average frequency of mixed PSCs in WT and S SOD1^{G93A} at postnatal age of week 1 and week 2. Cumulative frequency plots of interval between events in W1 (Bii) and W2 (Biii), WT and SOD1^{G93A} motoneurons. (Ci) Average amplitude of mixed PSCs in WT and SOD1^{G93A} at postnatal age of week 1 and week 2. (Cii) Cumulative frequency plots of amplitude in W1 (Cii) and W2 (Ciii), WT and SOD1^{G93A} motoneurons. All datapoints show the mean for each recording. Column graphs show mean ± SD; W1 – WT: n=9 cells, SOD1^{G93A}: n=19. W2 – WT: n=25, SOD1^{G93A} : n=21. * $p<0.05$, Two-way ANOVA. Cumulative frequency graphs were plotted using individual events. Kolmogorov-Smirnov test was used to compare the cumulative distribution.

6.0 ± 4.7 Hz, SOD1^{G93A}: 7.9 ± 2.5 Hz) and W2 (Fig 2Bi. WT: 7.6 ± 3.1 Hz, SOD1^{G93A}: 10.3 ± 3.9 Hz). However, the cumulative frequency distribution reveals that a greater proportion of inhibitory PSC in in SOD1^{G93A} motoneurons have shorter inter-event time between each event at both W1 (Fig Bii., $p<0.001$, Kolmogorov-Smirnov test) and W2 (Fig Biii., $p<0.0001$, Kolmogorov-Smirnov test), suggesting that there are more frequent events in SOD1^{G93A} fast-type motoneurons. Even though the two-way ANOVA showed no significant difference in the average frequency, a trend towards an increase in the average frequency can be observed between the two genotypes. Similar to mixed PSCs, we observed no differences in the mean amplitude of inhibitory PSC between the two genotypes at W1 (Fig2 Ci. WT: 64.9 ± 14.5 pA, SOD1^{G93A}: 81.7 ± 20.3 pA) and W2 (Fig2 Ci. WT: 60.9 ± 13.9 pA, SOD1^{G93A}: 78.0 ± 45.2 pA), nor their distribution at both weeks (W1: Fig 2Cii. W2: Fig 2CiiI $p>0.99$, Kolmogorov-Smirnov test).

Increases in synaptic activity could be attributed to an increase in the input from pre-synaptic neurons, due to changes in their firing rate, or modulation of synaptic transmission via pre- or post- synaptic mechanisms. To distinguish between the two possibilities, we applied tetrodotoxin (TTX) to measure action potential independent miniature post-synaptic currents (mPSC) that are resulted from the release of vesicular neurotransmitters quanta release from the pre-synaptic neurons. Here, we measure the amplitude and frequency of mixed (excitatory and inhibitory) mPSCs received onto fast-type SOD1^{G93A} and WT motoneurons (Fig 3)

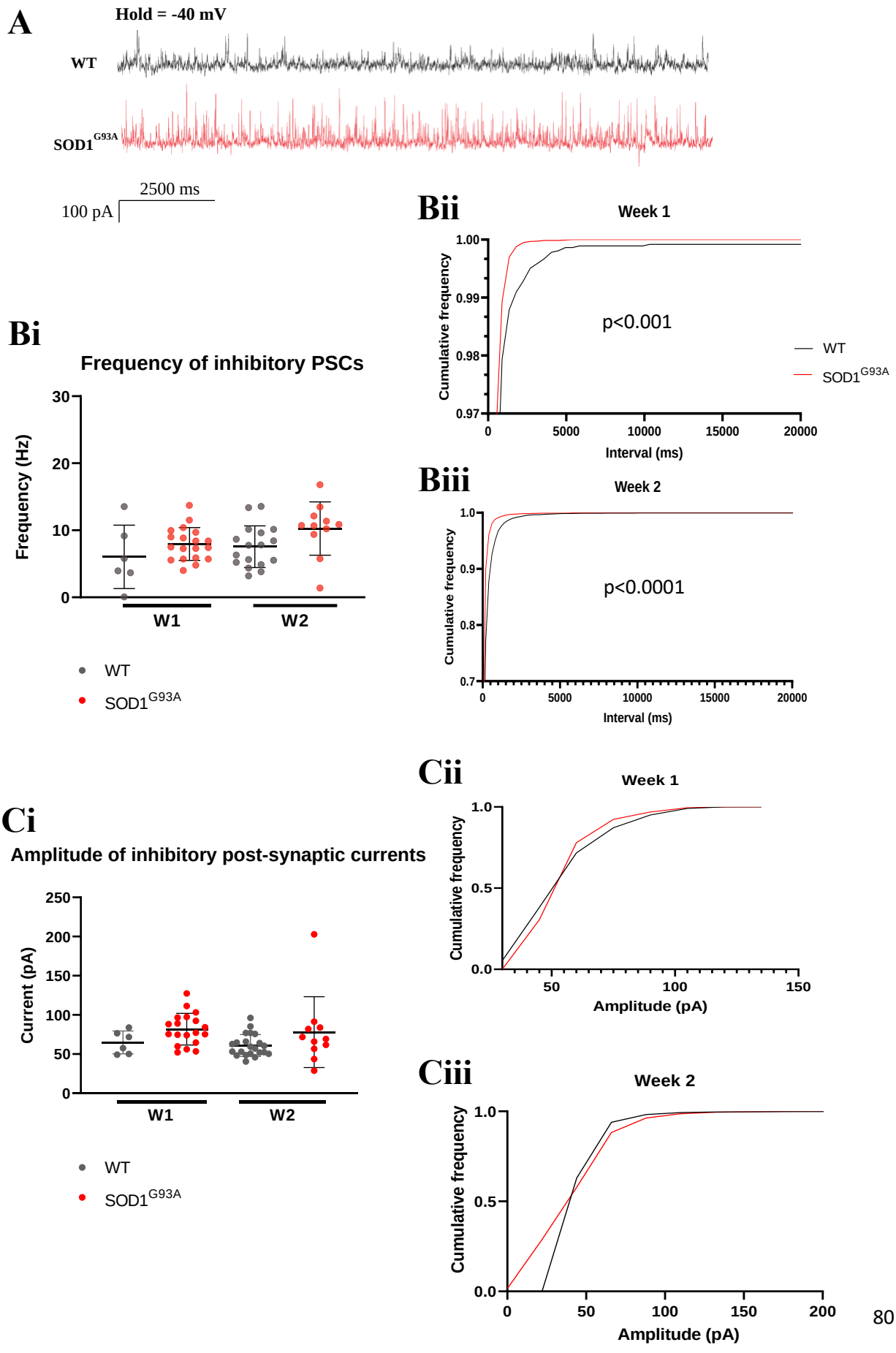
A
Hold = -40 mV
WT
SOD1G93A
2500 ms
100 pA
Bi
Frequency of inhibitory PSCs
Frequency (Hz)
W1
W2
WT
SOD1G93A
Bii
Week 1
Cumulative frequency
p<0.001
Interval (ms)
WT
SOD1G93A
Biii
Week 2
Cumulative frequency
p<0.0001
Interval (ms)
Ci
Amplitude of inhibitory post-synaptic currents
Current (pA)
W1
W2
WT
SOD1G93A
Cii
Week 1
Cumulative frequency
Amplitude (pA)
Ciii
Week 2
Cumulative frequency
Amplitude (pA)

Figure 2**. Frequency and amplitude of inhibitory PSCs show a trend in increase in both week 1 and week 2 SOD1^{G93A} fast-type lumbar motoneurons**. (A) Voltage clamp recording from fast type lumbar motoneurons in WT (black) and SOD1^{G93A} (red) held at -40 mV, at a potential at which inhibitory PSCs are hyperpolarising and therefore can be distinguished from excitatory PSCs. (Bi) Average frequency of inhibitory PSCs in WT and SOD1^{G93A} motoneurons at postnatal age of week 1 and week 2. Cumulative frequency of interval between events in week 1 (Bii) and week 2 (Biii) WT and SOD1^{G93A} motoneurons. (Ci) Average amplitude of inhibitory PSCs in WT and SOD1^{G93A} motoneurons at postnatal age of week 1 and week 2. Cumulative frequency plot of amplitude in week 1 (Cii) and week 2 (Ciii) WT and SOD1^{G93A} motoneurons. All datapoints show the mean for each recording. Column graphs show mean ± SD. W1 – WT: n=6 cells SOD1^{G93A} : n=19. W2 – WT: n=11, SOD1^{G93A} : n=14; Two-way ANOVA. Cumulative frequency graphs were plotted using individual events. Kolmogorov-Smirnov test was used to compare the cumulative distribution.

Application of 0.5μM TTX halted repetitive firing in neurons in the slice preparations and enabled measurement of action potential-independent mPSCs at a holding potential of -60 mV (Fig 3A). Since changes in spontaneous PSCs were observed between WT and $SOD1^{G93A}$ fast-type motoneurons at W2, we chose to explore changes in mPSC in that age group. The frequency of mixed mPSC events was found to be increased in $SOD1^{G93A}$ fast-type motoneurons (Fig 3Bi. WT: 3.6 ± 2.1 Hz, $SOD1^{G93A}$: 12.7 ± 9.1 Hz) and the cumulative frequency shows that a greater proportion of mixed mPSC events have a shorter inter-event time(Fig 3Bii. $p<0.0001$, Kolmogorov-Smirnov test). Although, it may seem that the average amplitude of the mixed mPSC in $SOD1^{G93A}$ is not different in comparison to WT motoneurons (Fig. 3Ci), the cumulative frequency graph shows that a greater proportion of the events have higher amplitude in the disease in comparison to WT fast-type motoneurons (Fig 3Cii. $p<0.0001$, Kolmogorov-Smirnov test).

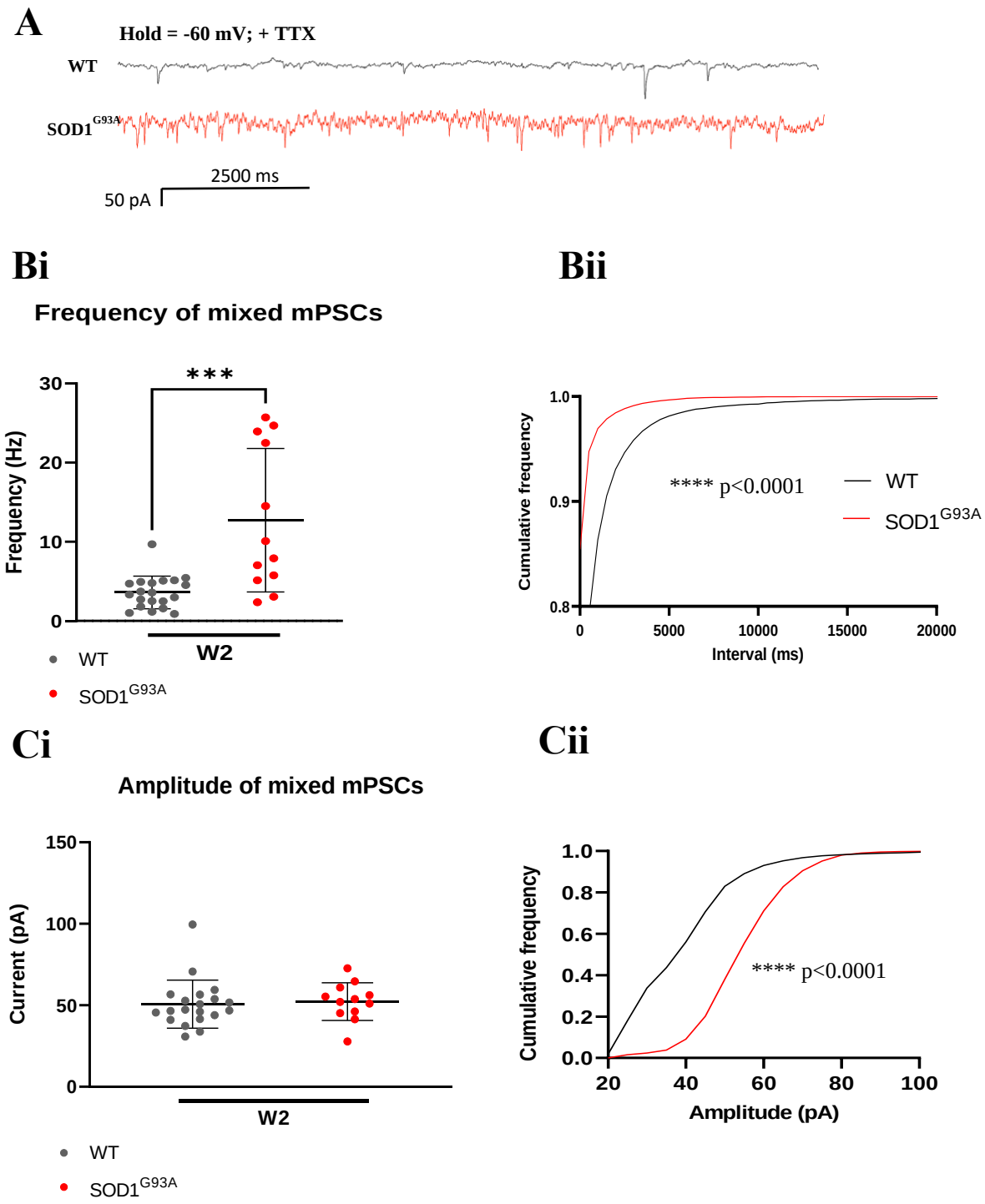

Figure 3. **Frequency of mixed miniature post-synaptic currents (mPSCs) is increased in week 2 SOD1^{G93A} fast-type lumbar motoneurons in the presence of 0.5µM TTX.** (A) Voltage clamp recording from fast type lumbar motoneurons in WT (black) and SOD1^{G93A} (red) held at -60 mV.(Bi) Average frequency of mixed mPSCs in WT and SOD1^{G93A} at postnatal age of week 2. (Bii) Cumulative frequency of intervals between events in week 2 WT and SOD1^{G93A} motoneurons. (Ci) Average amplitude of mixed mPSCs in WT and SOD1^{G93A} at postnatal age of week 2. (Cii) Cumulative frequency plot of amplitude in week 2 WT and SOD1^{G93A} motoneurons. All datapoints show the mean for each recording. Column graphs show mean ± SD; W2 – WT: n=20 cells, SOD1^{G93A}: n=12; *** p<0.001, Mann-Whitney test. Cumulative frequency graphs were plotted using individual events. Kolmogorov-Smirnov test was used to compare the cumulative distribution.

An increase in the frequency of mixed mPSCs could reflect increased input, due to greater neurotransmitter vesicles being released from presynaptic neurons that could influence the excitability of motoneurons and therefore their output. However, the nature of the synaptic transmission, whether it is excitatory or inhibitory, cannot be determined. To differentiate the miniature excitatory PSCs (mePSCs), 20μM bicuculline and 2μM strychnine along with 0.5μM TTX were added to aCSF to block $GABA_A$ and glycine receptors respectively. Under these conditions, we observed that the frequency of mePSCs was significantly reduced in $SOD1^{G93A}$ motoneurons in comparison to WT (Fig 4Bi. WT: 12.1 ± 7.4 Hz, $SOD1^{G93A}$: 7.6 ± 5.6 Hz) and a large proportion of the events had longer inter-event time in $SOD1^{G93A}$ fast-type motoneurons (Fig 4Bii. $p<0.0001$, Kolmogorov-Smirnov test). On the other hand, we did not observe a significant difference between the mean amplitude of mePSCs (Fig 4Ci. WT: 63.3 ± 17.4 pA, $SOD1^{G93A}$: 68.8 ± 13.7 pA) and in the distribution of amplitude of the events (Fig 4Cii) between $SOD1^{G93A}$ and WT fast-type motoneurons.

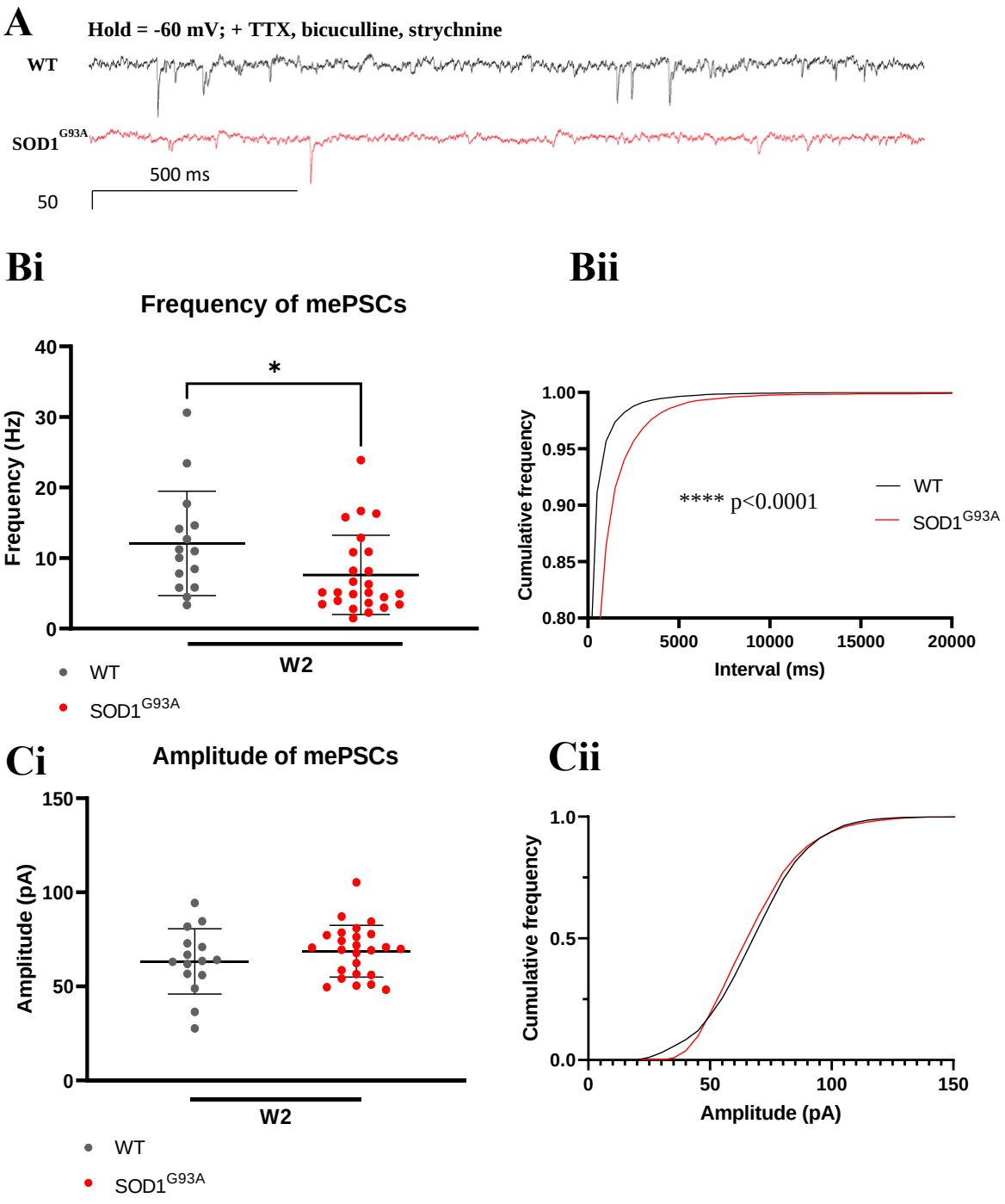
A
Hold = -60 mV; + TTX, bicuculline, strychnine
WT
SOD1G93A
500 ms
50
Bi
Frequency of mePSCs
Frequency (Hz)
40
30
20
10
0
*
W2
WT
SOD1G93A
Bii
Cumulative frequency
1.00
0.95
0.90
0.85
0.80
**** p<0.0001
WT
SOD1G93A
0
5000
10000
15000
20000
Interval (ms)
Ci
Amplitude of mePSCs
Amplitude (pA)
150
100
50
0
W2
WT
SOD1G93A
Cii
Cumulative frequency
1.0
0.5
0.0
0
50
100
150
Amplitude (pA)

Figure 4. **Frequency of miniature excitatory post-synaptic currents (mePSCss) is decreased in week 2 SOD1^{G93A} fast-type lumbar motoneurons in the presence of 0.5µM TTX, 2µM strychnine and 20µM bicuculline.** (A) Voltage clamp recording from fast type lumbar motoneurons in WT (black) and SOD1^{G93A} (red) held at -60 mV. (Bi) Average frequency of mePSCss in WT and SOD1^{G93A} at postnatal age of week 2. (Bii) Cumulative frequency of intervals between events in week 2 WT and SOD1^{G93A} motoneurons. (Ci) Average amplitude of mePSCss in WT and SOD1^{G93A} at postnatal age of week 2. (Cii) Cumulative frequency plot of mePSCs amplitude in week 2 WT and SOD1^{G93A} motoneurons. All datapoints show the mean for each recording. Column graphs show mean ± SD; W2 – WT: n=15 cells, SOD1^{G93A}: n=25; * $p<0.05$, Mann-Whitney test. Cumulative frequency graphs were plotted using individual events. Kolmogorov-Smirnov test was used to compare the cumulative distribution.

To differentiate the miniature inhibitory PSCs (miPSCs), the NMDA-receptor antagonist APV (50μM) and AMPA/kainate- receptor antagonist CNQX (10μM) were added to the aCSF. The analysis of the miPSCs demonstrated that the mean frequency of the miPSCs was increased in $SOD1^{G93A}$ fast-type motoneurons in comparison to WT (Fig 5Bi . WT: 2.3 ± 1.4 Hz, $SOD1^{G93A}$: 3.3 ± 1.4 Hz). This is further reiterated by the shorter duration of the inter-event intervals seen in the $SOD1^{G93A}$ motoneurons (Fig 5Bii. $p<0.0001$. Kolmogorov-Smirnov test). Similar to the frequency, the mean amplitude of miPSCs was also found to be larger in the $SOD1^{G93A}$ motoneurons in comparison to WT (Fig 5Ci. WT: 85.9 ± 9.8 pA, $SOD1^{G93A}$: 97.13 ± 9.9 pA). This was also shown in the cumulative frequency distribution as a greater proportion of miPSC had larger amplitudes in comparison to WT (Fig 5Cii. $p<0.0001$. Kolmogorov-Smirnov test).

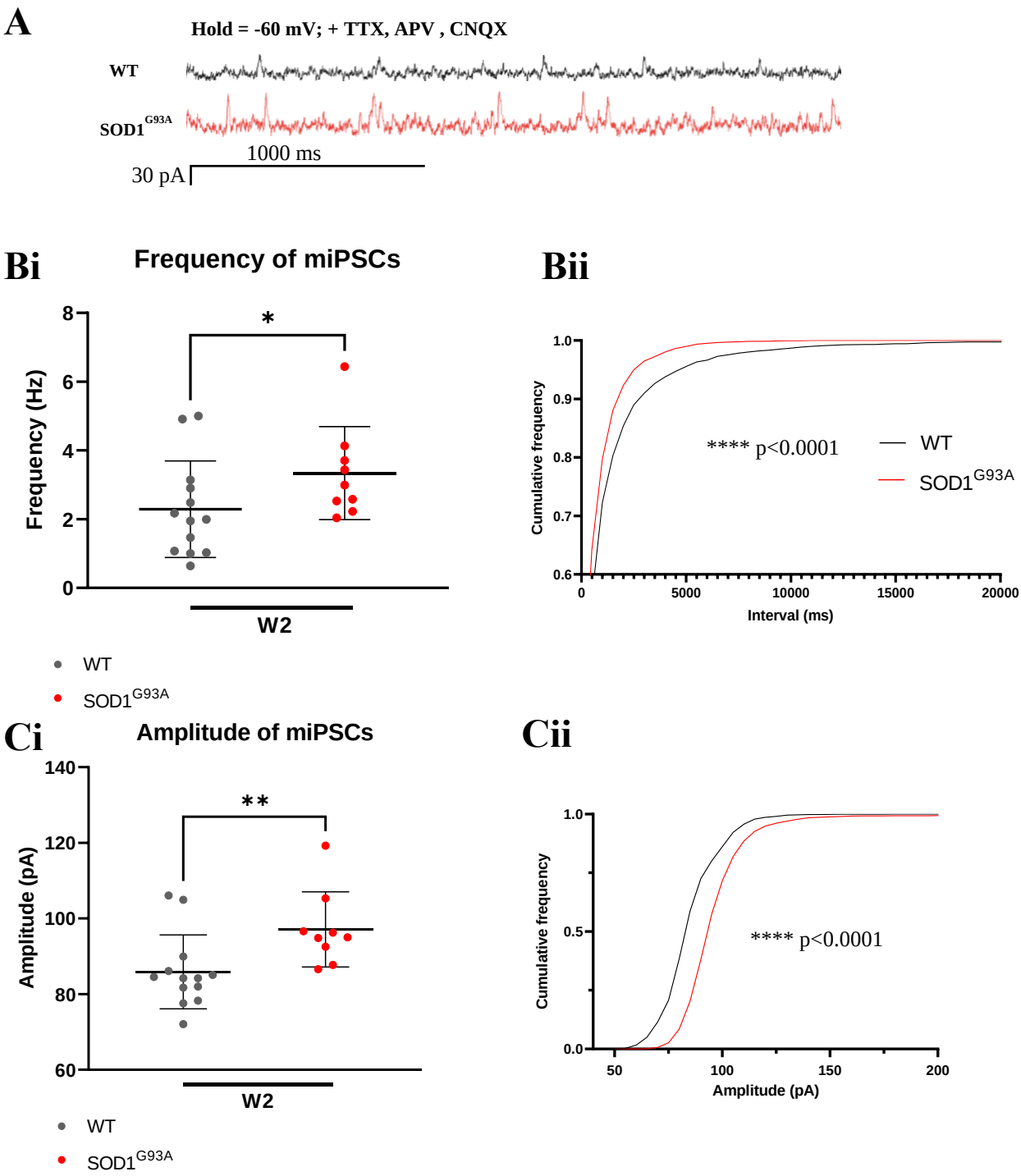
A
Hold = -60 mV; + TTX, APV , CNQX
WT
SOD1G93A
1000 ms
30 pA
Bi
Frequency of miPSCs
Frequency (Hz)
*
W2
WT
SOD1G93A
Bii
Cumulative frequency
**** p<0.0001
WT
SOD1G93A
Interval (ms)
Ci
Amplitude of miPSCs
Amplitude (pA)
**
W2
WT
SOD1G93A
Cii
Cumulative frequency
**** p<0.0001
Amplitude (pA)

Figure 5. **Frequency and amplitude of miniature inhibitory post-synaptic currents (miPSCs) is increased in week 2 SOD1^{G93A} fast-type lumbar motoneurons in the presence of 0.5µM TTX, 10µM CNQX and 0.5µM APV.** (A) Voltage clamp recording from fast type lumbar motoneurons in WT (black) and SOD1^{G93A} (red) held at -60 mV. (Bi) Average frequency of miPSCs in WT and SOD1^{G93A} at postnatal age of week 2. (Bii) Cumulative frequency of intervals between events in week 2 WT and SOD1^{G93A} motoneurons. (Ci) Average amplitude of miPSC in WT and SOD1^{G93A} at postnatal age of week 2. (Cii) Cumulative frequency plot of miPSC amplitude in week 2 WT and SOD1^{G93A} motoneurons. All datapoints show the mean for each trace. Column graphs show mean ± SD; W2 – WT: n=13 cells, SOD1^{G93A}: n=9; * $p<0.05$, Mann-Whitney test. Cumulative frequency graphs were plotted using individual events. Kolmogorov-Smirnov test was used to compare the cumulative distribution.

Discussion

In this chapter, we aimed to characterise if changes in synaptic inputs were present at early presymptomatic stages of postnatal 2 weeks in fast-type motoneurons of SOD1^{G93A} mouse model. The selective vulnerability in the motoneuron types in the disease has been widely documented, however, most studies exploring changes in synaptic inputs have not considered this. From our study in Chapter 2, we showed that unlike previous finding (Van Zundert *et al.*, 2008; Quinlan *et al.*, 2011a) the firing properties of fast-type SOD1^{G93A} motoneurons remained unchanged at this early presymptomatic stage.

It is important to note that the absence of changes in intrinsic properties in SOD1^{G93A} fast-type motoneurons could be due to intrinsic or circuit compensatory homeostatic mechanisms (Lambo and Turrigiano, 2013; Huh, Charles J Heckman and Manuel, 2021). Given that neuronal excitability depends on two main factors: intrinsic properties and synaptic inputs, we wanted to investigate if changes in synaptic inputs in fast-type motoneurons existed in the second post-natal week in SOD1^{G93A} mice.

In this study, unlike most studies that used whole-cell patch-clamp recording, we decided to use longitudinal slices instead of transverse slices. Motoneurons receive synaptic inputs on their somas and dendrites, however, a greater proportion of the inputs are received on the dendrites (Kishore and Fetcho, 2013). When transverse slices are cut, most of the dendritic structures are cut away. Therefore, by cutting the spinal cord longitudinally, we tried to preserve as much of the dendrites on the lumbar motoneurons as we could, to get a more accurate representation of the inputs received by the motoneurons.

First, we measured the frequency and amplitude of spontaneous mixed PSCs in fast-type motoneurons of WT and SOD1^{G93A} mice at W1 and W2. We found that the frequency of these events was increased only in W2 SOD1^{G93A} fast-type motoneurons in comparison to WT. Moreover, the amplitude and frequency at W1 remained comparable between both genotypes. We suggest that this increase in frequency at W2 indicates a probable alteration in the inputs received from the pre-synaptic neurons by

the fast-type motoneurons. The increase in frequency of PSC could be attributed to an increase in neurotransmitter vesicular release, indicating alterations on the pre-synaptic neurons; or it could also indicate that the presynaptic neurons are more active ;or an increase in the number of synapses on fast-type motoneurons which would have been resulted changes on PSD of fast-type motoneurons (Choi and Lovinger, 1997; Turrigiano and Nelson, 2004). Increase in the neurotransmitter transporter has been observed in SOD1^{G93A} motoneurons of postnatal age of 60, however, by P110 the expression of VGLUT2 is significantly reduced in the ventral horn (Schütz, 2005; Sunico *et al.*, 2011). The increase in VGLUT2 puncta could indicate that more excitatory synapses are present on motoneurons before P60 and could therefore be a plausible explanation for the observed increase in the spontaneous mixed PSC (Fig). In line with clinical study and observations in the motor cortex in SOD1^{G93A} mice, increased glutamatergic neurotransmission may contribute to the pathogenic mechanism in SOD1 ALS. In contrast, the similarity in the amplitude of mixed spontaneous PSC events between the disease and control could tentatively indicate that there are no changes in the structure and function of the post-synaptic density (PSD) (Choi and Lovinger, 1997). Moreover, the dendritic structure of motoneurons is important for the integration of all types of synaptic inputs and alteration in these structures have been reported in a previous study where the dendritic spine density in neonatal mice is significantly increased in spinal motoneurons (Fogarty *et al.*, 2017). This morphological change could also contribute to the observed increase in frequency and amplitude of spontaneous mixed PSC as more surface area for synapse contacts may have been present. Although, this may be a plausible explanation to link the change in morphology with the physiology, this study did not differentiate between fast- and slow- type motoneurons. Therefore, for future studies, investigating the dendritic structure of fast-type motoneurons by retrogradely labelling fast-twitch muscle fibres such as the tibialis anterior should be investigated in SOD1^{G93A} neonatal mice.

Our electrophysiological measurements of spontaneous PSC contain a combination of excitatory and inhibitory synaptic inputs. To differentiate between the two, we applied a holding potential of -40 mV to reveal the spontaneous IPSCs. We have showed that even though we do not observe any difference in the average frequency and amplitude of IPSCs between WT and $SOD1^{G93A}$ fast-type motoneurons, we did observe that a significant proportion of the event had shorter inter-event interval times. This indirectly suggests that the fast-type $SOD1^{G93A}$ motoneurons exhibit more frequent spontaneous IPSC events. Even though we see a trend toward an increase in the average frequency between the WT and $SOD1^{G93A}$ fast-type motoneurons, the difference was not significantly different. Although we measured the IPSC by changing the voltage clamp, we did not fully pharmacologically block the ePSC transmission. To measure the spontaneous IPSC events more accurately, future experiments should utilise antagonists such as APV and CNQX to block excitatory transmission.

In line with our results, findings in hypoglossal motoneurons in P4-10 $SOD1^{G93A}$ motoneurons showed that spontaneous IPSC events had an increase in frequency with a trend towards higher amplitudes (van Zundert et al 2008). Although there are discrepancies between findings, some studies have shown agreement on GABA-mediated currents remain unaltered in $SOD1^{G93A}$ motoneurons (Petri *et al.*, 2005; Chang and Martin, 2011). We did not distinguish between glycinergic and GABAergic transmission, but we can speculate that there may be a change in receptor density on motoneurons. However, none of these studies have differentiated between inputs to fast and slow-type motoneurons. As a future study, investigating the differences in the glycine and GABA receptors in MMP9-positive fast-type motoneurons can be undertaken to decipher if changes in post-synaptic density can be a pathogenic change in SOD1-ALS.

So far, the spontaneous PSC that were measured consisted of a mixture of synaptic currents caused by firing of pre-synaptic neurons and miniature synaptic currents. We applied TTX to measure the action potential-independent synaptic currents caused by the spontaneous vesicle release from pre-synaptic neurons. Application of TTX allowed us to measure the single release events, removing the possibility that the changes in inputs we observed were due to changes in the firing rate of the premotor interneurons. By doing this, we demonstrated that there was indeed an increase in the average frequency of mixed mPSC, again reinforcing the fact that there may be more neurotransmitter vesicular release from pre-synaptic neurons. Although we didn't observe any changes in the average amplitude of mPSC, we cannot ignore from the distribution of the mPSC that most of these events recorded from fast-type $SOD1^{G93A}$ motoneurons were skewed towards higher amplitudes. This difference may have been masked by the biological variability between each trace obtained from individual motoneurons as we calculated the average for each trace to make comparisons between the groups. However, the distribution of the events showed that there was a clear difference in the strength of the amplitudes in $SOD1^{G93A}$ fast-type motoneurons. In theory, total synaptic strength can be regulated through changes in receptor density, presynaptic neurotransmitter release and reuptake by the presynaptic neurons and the number of functional synapses (Turrigiano and Nelson, 2004). This could imply that there are both alterations on the pre-synaptic side and in the density of receptors on the post-synaptic side.

Application of bicuculline and strychnine in addition to TTX enabled us to measure the frequency and amplitude of mePSCs and it was found that the frequency of these events was reduced in fast-type $SOD1^{G93A}$ motoneurons in comparison to WT. Unlike the widely accepted theory of excitotoxicity, whereby motoneurons receive excessive excitatory inputs that lead to degeneration, we showed that fast-type motoneurons do not receive heightened excitatory inputs at the post-natal age of 2 weeks.

Unfortunately, in our study, we did not explore the source of these excitatory inputs but there are circuit-mediated changes in ALS.

For example, motoneurons receive excitatory inputs from proprioceptive afferents (Rossignol, Dubuc and Gossard, 2006) and it may be possible that these synaptic contacts may be impaired in ALS. When investigating Ia synaptic response in FF motoneurons, the presence of hyperexcitation was absent in pre-symptomatic *in vivo* SOD1^{G93A} mice. Also contradicting the glutamatergic excitotoxicity models, the excitatory post-synaptic potentials (EPSP) evoked by sensory inputs were observed to be reduced in motoneurons of SOD1^{G93A} (Bączyk *et al.*, 2020). Moreover, (Vaughan *et al.*, 2015) showed that proprioceptive synapses on α-motoneurons are reduced during the symptomatic phase in SOD1^{G93A} mice. Taken together, we may speculate that there could be changes in the proprioceptive afferents early on during the early-presymptomatic state in neonatal fast-type motoneurons (the observed decrease mePSCs frequency), to pre-symptomatic (P45-55) FF motoneurons until the symptomatic stage of the disease, highlighting that decrease in excitatory inputs may be a hallmark of ALS.

Finally, APV, CNQX and TTX were applied to measure miPSC. Interestingly, we showed that the average frequency and amplitude of miPSC were significantly higher in fast-type SOD1^{G93A} motoneurons. This increase in the amplitude of miPSC could either originate from spontaneous release of multiple vesicles from inhibitory interneurons or could result from a higher density of receptors on the post-synaptic motoneurons. In contrast to our finding, Chang and Martin (2011) showed a reduction in miPSCs in cultured Hb9+ embryonic SOD1^{G93A} neurons. Using pharmacological interventions, they observed that only glycine-mediate miPSCs were reduced and reported a reduction in the expression of glycine receptor α1 subunit on SOD1^{G93A} spinal neurons. In addition, no difference in GABA-mediated miPSCs were found in SOD1^{G93A} neurons in comparison to WT. We must acknowledge this study did not selectively record from the most vulnerable population of motoneurons in the disease as they targeted

Hb9+ neurons, a marker of motoneurons that does not distinguish between the different subtypes. Therefore, it cannot be claimed that the observed reduction in glycinergic transmission is seen in some motoneurons but may not be observed in the vulnerable fast-type motoneurons. Moreover, there are caveats to this approach as using cell culture techniques does not recapitulate the physiological environment which motoneurons develop and ALS progresses in. Although, we did not differentiate between glycine and GABA-mediated miPSCs, it can be speculated that changes in glycinergic inputs are present in fast-type motoneurons. Fast-type motoneurons receive stronger glycinergic inputs in comparison to slow-type motoneurons and these inputs have been shown to derive from V1 populations (Allodi *et al.*, 2021). In $SOD1^{G93A}$ mice, these inputs have been shown to reduce from the pre-symptomatic age of P63 (Allodi *et al.*, 2021). Interestingly, the cause of this retraction of inhibitory synapses from fast-type motoneurons is still unknown. However, it would be interesting to explore whether this retraction is indeed due to increased inhibitory inputs in the $SOD1^{G93A}$ fast-type motoneurons, due to these interneurons being hyperexcitable.

This increase in inhibitory transmission can perhaps serve as a compensatory mechanism to maintain circuit homeostasis and possibly to prevent the fast-type motoneurons from receiving excessive excitation as phenotypic signs of ALS are mostly prevalent once a substantial proportion of motoneurons have degenerated (Pun *et al.*, 2006). One of these mechanisms has been suggested to apply to Renshaw cells as an increase in calbindin-positive synapses were observed in pre-symptomatic $SOD1^{G93A}$ motoneurons (Wootz, FitzSimons-Kantamneni, *et al.*, 2013). Even though, the study did not differentiate the quantification of synapses between fast and slow-motoneurons, this anatomical increase may go hand in hand with our functional increase in miPSC frequency and amplitude. However, the number of Renshaw cells is decreased during the symptomatic stage of the disease when muscle wastage is prevalent (Chang and Martin, 2009), which could indicate that motoneurons receive less of these

inhibitory inputs as the disease progresses. Whether increase in inhibitory transmission is in indeed a compensatory mechanism or a pathogenic mechanism, is yet to be uncovered.

Although glycinergic interneurons, particularly Renshaw cells, have shown to have reduced excitability in P6-10 SOD1^{G93A} mice(Cavarsan *et al.*, 2022), our results have shown that fast-type motoneurons receive higher frequency and amplitude of miPSC at the same timepoint. Neurons in the CNS have been shown to be able to compensate for changes in synaptic inputs to maintain their outputs. For example, inhibiting excitatory transmission onto motoneurons can cause an increase in mePSCs amplitude due to upregulation of glutamatergic receptors, to compensate for the decrease in the excitatory inputs (O'Brien *et al.*, 1998). Similarly, a reduction in inhibitory inputs could lead to an increase in miPSC amplitude to compensate for the decrease in inhibitory transmission. Given that we see an increase in miPSC amplitude in fast-type SOD1^{G93A} motoneurons, we can speculate that a degree of synaptic scaling or changes in receptor density may be present in fast-type motoneurons in two-week old SOD1^{G93A} mice.

Furthermore, pre-synaptic homeostatic plasticity has been shown to be induced in the degenerating populations of synapses to oppose the effects of motoneuron degeneration (Orr *et al.*, 2020). Given that inhibitory synapses are progressively lost towards the later stage of the disease, it can be suggested that these homeostatic changes could start during the pre-symptomatic stage but due to the pathomechanisms of the disease, compensation may be lost as the disease progresses.

Therefore, given that we observe an increase in the miPSC amplitude, we can speculate that changes in receptor density on motoneurons may occur to compensate for the decrease in inhibitory input.

Given that the development of neuronal properties and neuronal circuits are crucially dependent on plasticity, via activity-dependent changes in expression of receptors and morphology of neurons, during the early postnatal age (Turrigiano and Nelson, 2004), we suggest that these elements are altered in fast-type SOD1^{G93A} motoneurons. The decrease in excitatory inputs and increase in inhibitory inputs to

fast-type lumbar SOD1^{G93A} motoneurons suggests that there may be a perturbation in the homeostatic balance between the opposing synaptic activity. Whether this mechanism occurs to decrease the overall excitability of the fast-type motoneurons in the disease cannot be confirmed. Moreover, whether too much inhibition is indeed a pathogenic mechanism in the disease, remains an option. Essentially, it is unknown whether these changes are pathological or act as compensatory mechanisms to perturbations in the disease. Overall, we show that changes in synaptic inputs occur before overt changes in neuronal excitability of fast-type motoneuron are observed in SOD1^{G93A} at post-natal age of two weeks.

Chapter 4: Investigating changes in excitatory and inhibitory post-synaptic density and their subsynaptic nanostructures in early pre-symptomatic SOD1^{G93A} mice

Introduction

Synaptic transmission is maintained by intricate subsynaptic structures within synapses that can be altered to cause functional changes that have been observed in synaptic plasticity and neurological disorders (Tang et al 2016). Two factors that dictate the strength of synapses are the distribution of presynaptic vesicles and the organisation of post-synaptic densities (PSD) and their subsynaptic complexes, such as receptors and scaffolding proteins on the PSD. Throughout the nervous system, neuronal synapses display great structural and functional diversity. The morphology along with the nano-structural organisation can determine the strength and the function of synapses (Turrigiano and Nelson, 2004; Harris and Weinberg, 2012). In ALS, synaptopathy has been considered a factor contributing to the pathology in the disease as evidence of synapse loss in the spinal cord of $SOD1^{G93A}$ transgenic mice and prefrontal cortex of ALS patients were observed (Henstridge *et al.*, 2018; Kassa *et al.*, 2018; Allodi *et al.*, 2021).

The composition of synapses has been characterised and they have been shown to have many proteins. One of the main components of excitatory synapses is post-synaptic density 95 (PSD95). On a molecular level, PSD95 interacts with a variety of signalling molecules and receptors to form complexes within the post-synaptic density (PSD) (Broadhead *et al.*, 2020). Determining the structural organisation of PSD95 has its challenges as the small structures of synapses lie beyond the resolution of a conventional optical microscope (MacGillavry *et al.*, 2013). Here, we used gated-stimulated emission depletion (g-STED) microscopy, to investigate the distribution of postsynaptic nanostructure within the spinal cord of $SOD1^{G93A}$ mice. Super-resolution microscopy has shown that these PSD95 complexes are highly conserved in nanoclusters of approximately 150 nm. Particularly at excitatory PSD, these PSD95 nanoclusters co-localise with NMDA and AMPA receptors and align with presynaptic vesicle sites

forming trans-synaptic nanocolumns (Nair *et al.*, 2013; Tang *et al.*, 2020). Therefore, visualising PSD95 can help us determine the distribution of excitatory PSD and their nanostructures in SOD1-ALS.

Similar to excitatory PSD, it has been shown that postsynaptic inhibitory synapses are comprised of nanoscale subsynaptic domains of the scaffolding protein gephyrin amongst others. Importantly, gephyrin has been shown to cluster a subset of GABA receptors, $GABA_AR$, highlighting the importance of the interaction and the arrangement between the scaffolding protein and the receptor for physiological function (Kevin C Crosby *et al.*, 2019). Furthermore, gephyrin is crucial for glycine receptor (GlyR) clustering into inhibitory synapses in the CNS (Lévi *et al.*, 2004).

The results from Chapter 3 showed changes in the amplitude as well as the frequency of both excitatory and inhibitory PSCs recorded from fast-type motoneurons in $SOD1^{G93A}$ ALS model mice. The changes observed in amplitude highlights that there may be alterations on the post-synaptic membrane of fast-type motoneurons. Since subsynaptic nanostructures in PSD can influence the strength of synaptic transmission, we wanted to explore whether these structures are altered in early development in $SOD1^{G93A}$ mice. To test this, we analysed the PSD95-positive excitatory PSD and the gephyrin-positive inhibitory PSD, and their nanoclusters in lamina IX of the spinal cord in 2 week-old $SOD1^{G93A}$ and WT mice. Furthermore, a dysfunctional shift in the E:I ratio towards excitation has been postulated to facilitate motoneuron degeneration via excitotoxic death (Saba et al., 2016). Therefore, we wanted to investigate if there are changes in the E:I ratio by quantifying the number of excitatory PSD to inhibitory PSD, in lamina IX in lumbar spinal cord slices in 2-week-old $SOD1^{G93A}$ and WT mice.

Methods

Animals

All experimental procedures conducted are in accordance with the UK Animals (Scientific Procedures) Act 1986 and approved by the Animal Welfare Ethics Committee of the University of St Andrews as well as the UK Home Office regulations. Males B6SJL-TgN (SOD1-G93A)1Gur/J ($SOD1^{G93A}$) (provided by Dr Richard Mead, University of Sheffield) were crossed with PSD95-$eGFP^{+/+}$ females (provided by Prof Seth Grant, University of Edinburgh) to produce transgenic $SOD1^{G93A}$ mice and control offspring expressing PSD95-$eGFP^{+/-}$. Experiments were performed on spinal cord slices obtained from $SOD1^{G93A}$ positive mice and their negative WT littermates, at postnatal age of 2 weeks.

Tissue preparation

Mice were transcardially perfused with 1 x phosphate buffer saline (PBS) followed by 4% paraformaldehyde and spinal cords were removed and placed in paraformaldehyde at 4°C overnight. Once fixed, the spinal cords were transferred to 30% sucrose in PBS solution at 4°C until the cords have sunken to the bottom. The spinal cords were then placed in embedding moulds with OCT and frozen at -80°C. Cryomold blocks with the lumbar spinal embedded in them were sliced at 20um using a cryostat (Leica CM1869) and slices placed onto Superfrost Gold Plus glass microscope slides (VWR).

Immunohistochemistry

Microscope slides with mounted lumbar spinal cord slices were incubated at 37°C and then washed with 1 x PBS. The slides were blocked and permeabilised with 3% Bovine serum albumin (BSA), 0.2% Triton X100 in PBS for 2 hours at room temperature (RT). After the blocking and permeabilisation period, the

slides were washed in 1 x PBS and primary antibody solution (1.5% BSA and 0.1% Triton X100 in PBS) was applied and allowed to incubate for 48 hours at 4°C. The primary antibody used was mouse anti-gephyrin (1:500, Synaptic Systems). The slides were then washed in 1 x PBS before being incubated with the secondary antibody solution (1.5% BSA) for 2 hours at RT. The secondary primary used against mouse anti-gephyrin was donkey anti-mouse A647 (Abcam). The slides were subsequently washed with 1 x PBS, dried and mounted using Vectashield mounting medium and coverslip.

Imaging

Images were acquired through confocal and gated-stimulated emission depletion (g-STED) microscopy using the Leica SP8 SMD g-STED microscope available at the Edinburgh Super-Resolution Imaging Consortium hosted by Heriot Watt University. Excitation was provided by a CW super-continuum white light laser source at 488 nm to excite eGFP and at 647 nm to excite Alexa647, with depletion provided by a 594 nm and 775 nm laser. Images were acquired with a 100 × 1.4NA STED objective lens with an optical zoom set to provide optimal xy-resolution. Images were taken from ventral laminae IX of lumbar spinal cord sections, where lateral motoneuron pools are located. The experimenter was blinded from genotype of the mice to avoid bias whilst acquiring the images.

Image analysis

Quantification of synapses was performed using FIJI. Images were processed using background subtraction and gaussian blur. To detect the expression of PSD95 and gephyrin post-synaptic densities (PSD), moment-based and some manual thresholding was applied. Maximum and minimum size were applied to exclude detection of false positive dim and large supra-synaptic structures. Thresholding

produced binarised images which were used to quantify synapses. Full width at half maximum analysis (FWHM) using Gaussian fitting was measured manually by identifying individual nanoclusters (NC) from the images and the diameters along the minimum and maximum axes were measured for each individual NC and the average from the two was calculated. The experimenter was blinded to the genotype of the mice during the analysis to avoid bias.

Statistical analysis

Data analysis and graphical representation were performed on GraphPad Prism (version 9). Data were tested for normality and when applicable an unpaired t-test or Mann-Whitney test was conducted to make comparisons between $SOD1^{G93A,}$ and WT. Statistical significance is denoted as: *= <0.05; ** = <0.01; *** = <0.001; **** = <0.0001.

Negative controls

All immunohistochemical experiments were conducted alongside a negative control which had no primary antibody in the solution. This was carried out to confirm that the secondary antibody, donkey-anti-mouse ALEXA 647, did not have non-specific binding and bound only to the desired epitope. Figure 1 shows negative control images with corresponding positive controls. We can confirm that there was no obvious non-specific binding of the secondary antibody and were assured that only our target epitope was targeted.

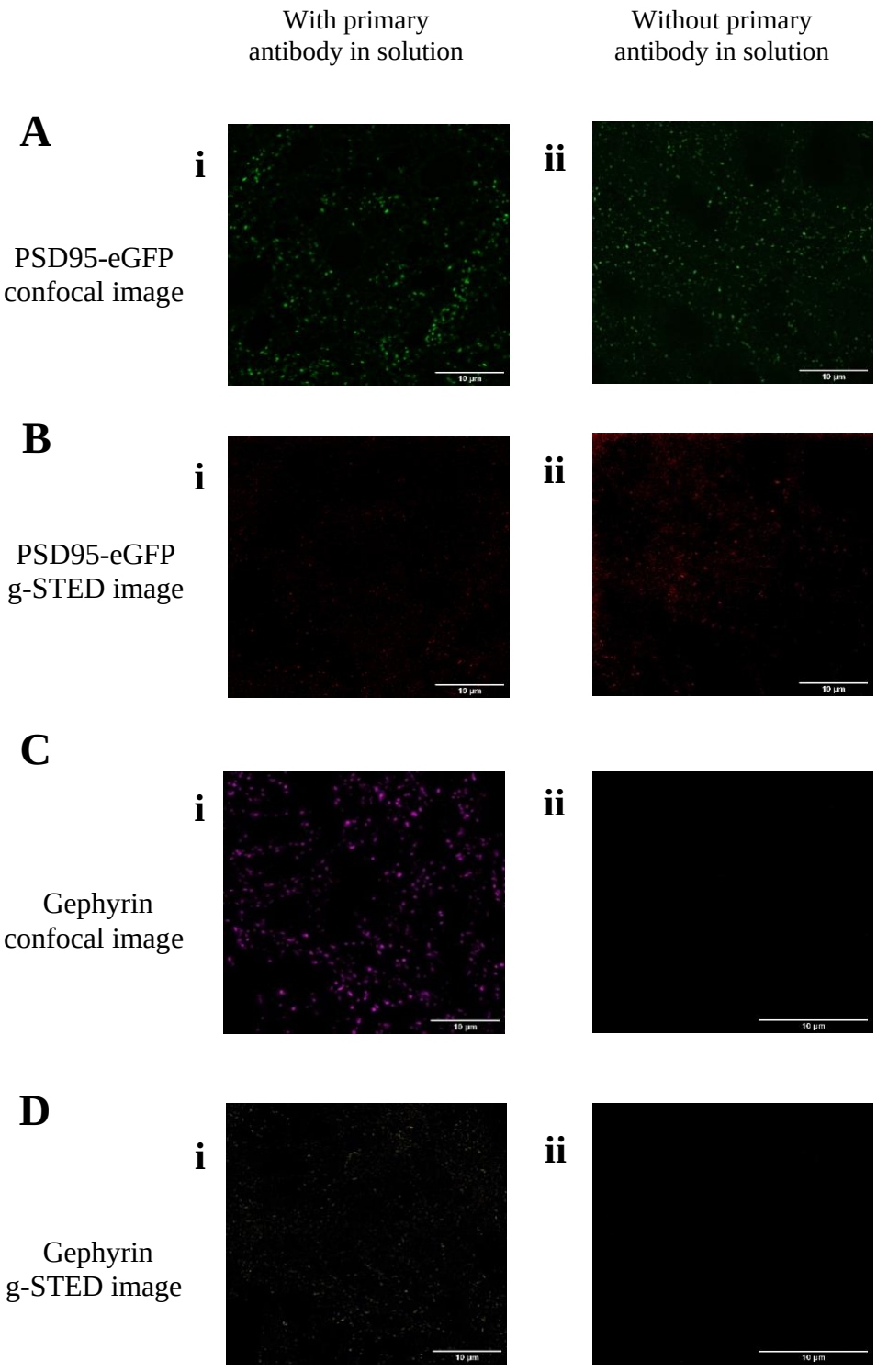

Figure 1: Images showing endogenouse PSD95-eGFP and primary antibody, mouse-anti gephyring used. PSD95-eGFP PSD with (Ai) and without (Aii) primary antibodies. (B) shows the endogenous PSD95 NC with (Bi)and without (Bii) mouse-anti gephyrin antibody. (CI) Gephyrin PSD labelled with mouse-anti gephyrin antibody (Ci) and its no primary antibody control (Cii). (Di) Gephyrin PSD labelled with mouse-anti gephyrin antibody (Ci) and its no primary antibody control (Dii).

Results

In Chapter 3, we have shown that the frequency and amplitude of PSCs are altered in SOD1^{G93A} fast type motoneurons. These findings indicate that there could be alterations in vesicular release in the pre-synaptic neurons or alterations on the post-synaptic membrane of motoneurons, or both. Given that we saw a change in amplitude of PSCs, we speculated that there may be a change in the structure on the PSD of motoneurons. We have chosen to focus on the excitatory and inhibitory PSDs in lamina IX in the ventral horn of the lumbar spinal cord as it composed of lateral motor pools that innervate the lower limbs in the mouse model.

To quantify synaptic changes in SOD1^{G93A} mice, we crossbred PSD95-eGFP$^{+/+}$ mice with SOD1^{G93A} mice. The use of the PSD95-eGFP $^{+/-}$ guaranteed that all mice used in this experiment expressed GFP tagged PSD scaffolding molecule, PSD95, at excitatory synapses throughout the CNS (Broadhead *et al.*, 2020). From here onwards SOD1^{G93A} and WT refer to mice that were bred using homozygous PSD95-eGFP+/+ mice, therefore making the offspring heterozygous for PSD95-eGFP.

High magnification images using confocal microscopy enabled the visualisation of individual PSD95-positive, excitatory synapses (Fig 1A). Our results demonstrate that, at postnatal age of 2 weeks, the average number of PSD95-positive PSD was not different in lamina IX of SOD1^{G93A} mice in comparison to WT (Fig 2B. WT = 10.7 ± 5.9, SOD1^{G93A} = 9.7 ± 4.1). We also found that there was no considerable difference in the mean and the distribution (Fig. 2Cii) of PSD95-positive PSD size between SOD1^{G93A} and WT (Fig 2Ci. WT = 0.220 ±0.063, SOD1^{G93A} = 0.210 ± 0.068)

The strength of the PSC is correlated with its size and the number of NCs per PSD (MacGillavry *et al.*, 2013). Therefore, we next used g-STED microscopy to visualise and quantify the synaptic nanostructures within the PSD (Fig 3A). When calculating the area of individual PSD95 NC after thresholding, we show that the average size of NCs is increased in SOD1^{G93A} mice in comparison to WT (Fig 3Bi. WT = 0.018 ± 0.004 μm^2, SOD1^{G93A} = 0.023 ± 0.007 μm2). Moreover, SOD1^{G93A} NCs show greater distributions of larger

NC size in comparison to WT (Fig 3Bii). Although an increase in NC size is observed, the average number of NC per PSD95-positive PSD did not differ between the genotypes (Fig 3Ci. WT = 1.6 ± 0.5, $SOD1^{G93A}$ = 1.7 ± 0.4).

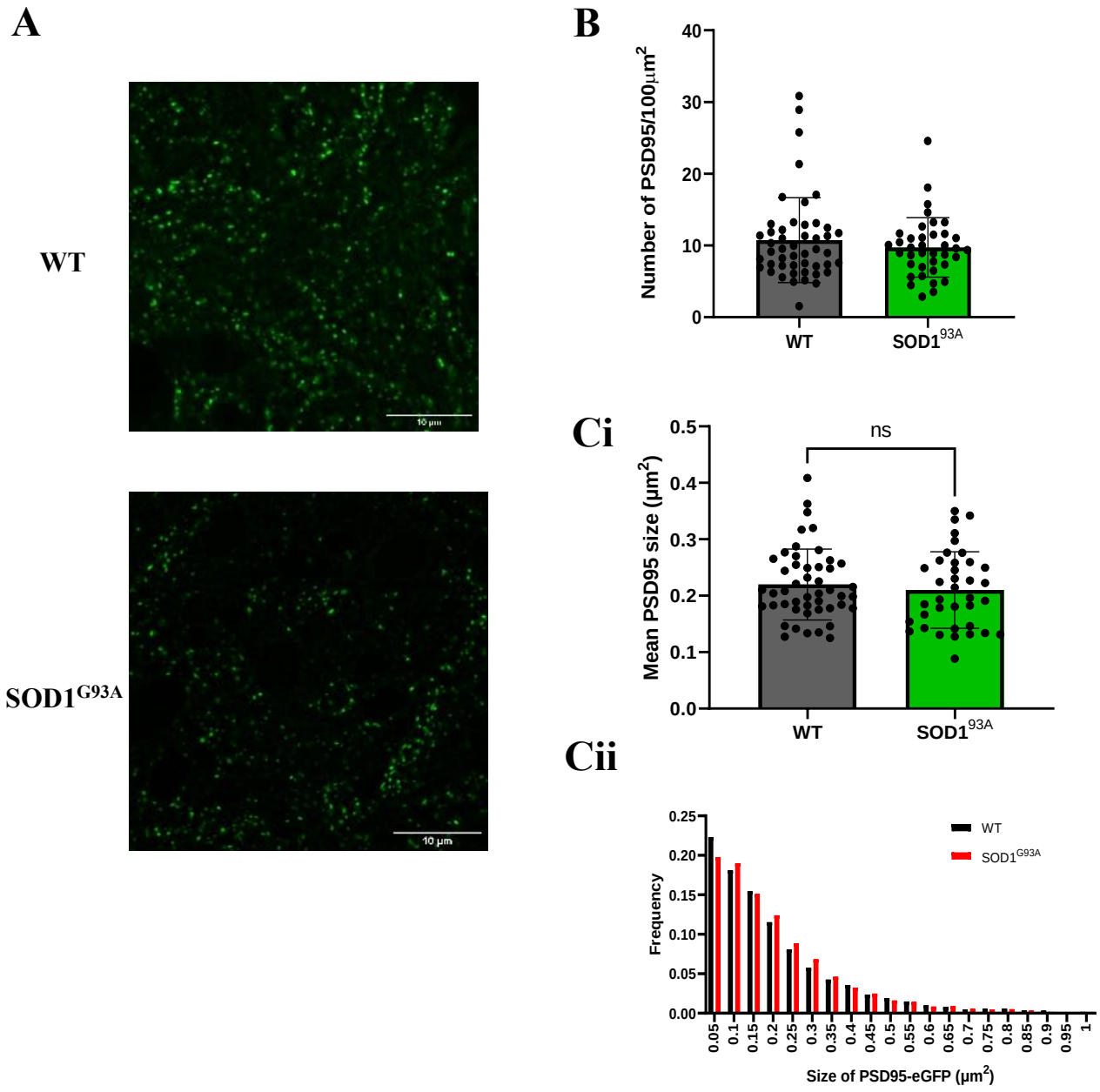

Figure 2. **Number and size of PSD95-eGFP positive excitatory PSD show no change in lamina IX of SOD1^{G93A} mice.** (A) High magnification confocal images of PSD95-positive excitatory PSD from lumbar spinal cord section of WT and SOD1^{G93A} mice. (B) Average density of PSD95-eGFP PSD per 100 µm^2 in WT and SOD1^{G93A} lumbar spinal cord. (C) Average size of PSD95-eGFP PSD (Ci) and histogram plotting the distribution of size of PSD95-eGFP PSD (Cii) in lamina IX of WT and SOD1^{G93A} lumbar spinal cord sections. At least 3 confocal images were taken from each animal and each datapoint on graph shows the average number or size of PSD of one image. Bar graphs show mean ± SD; WT: n = 8639 PSD, N = 9; SOD1^{G93A}: n = 6401 PSD, N = 9. Unpaired t-test shows no significant difference in number and size of PSD95-eGFP positive excitatory PSD.

One caveat with the method of analysing the size of NCs is that the thresholding can erroneously identify two or more overlapping NCs as one. As a result of this, the size of NCs can be overestimated and would not provide accurate interpretation of the NCs. For example, as seen in Fig 4Aiv, it can be clearly distinguished that there are two NCs marked by *, however, when quantifying the area after thresholding, those two NCs were counted as one.

To quantify the size of PSD95-eGFP NC more accurately, we manually measured the NCs by taking the full width at half maximum (FWHM) of the central bright fluorescent region of the NC. In other words, we measured along the maximum and minimum diameter of individual NCs. Unlike measuring the overall area of NC after applying threshold, FWHM analysis allowed distinction between individual NC and avoided analysis of overlapping nanostructures. Unpaired-t-test revealed a significant decrease in the mean diameter of PSD95-eGFP NCs in $SOD1^{G93A}$ mice in comparison to WT (Fig 4B. WT = 0.19 ± 0.06 μm $SOD1^{G93A}$ = 0.14 ± 0.04 μm). This is further depicted in the distribution of NCs diameter, as a greater proportion of $SOD1^{G93A}$ NC had smaller diameter of 0.15 μm in size whereas a proportion of NCs in WT still exhibited larger diameters in size (Fig 4C).

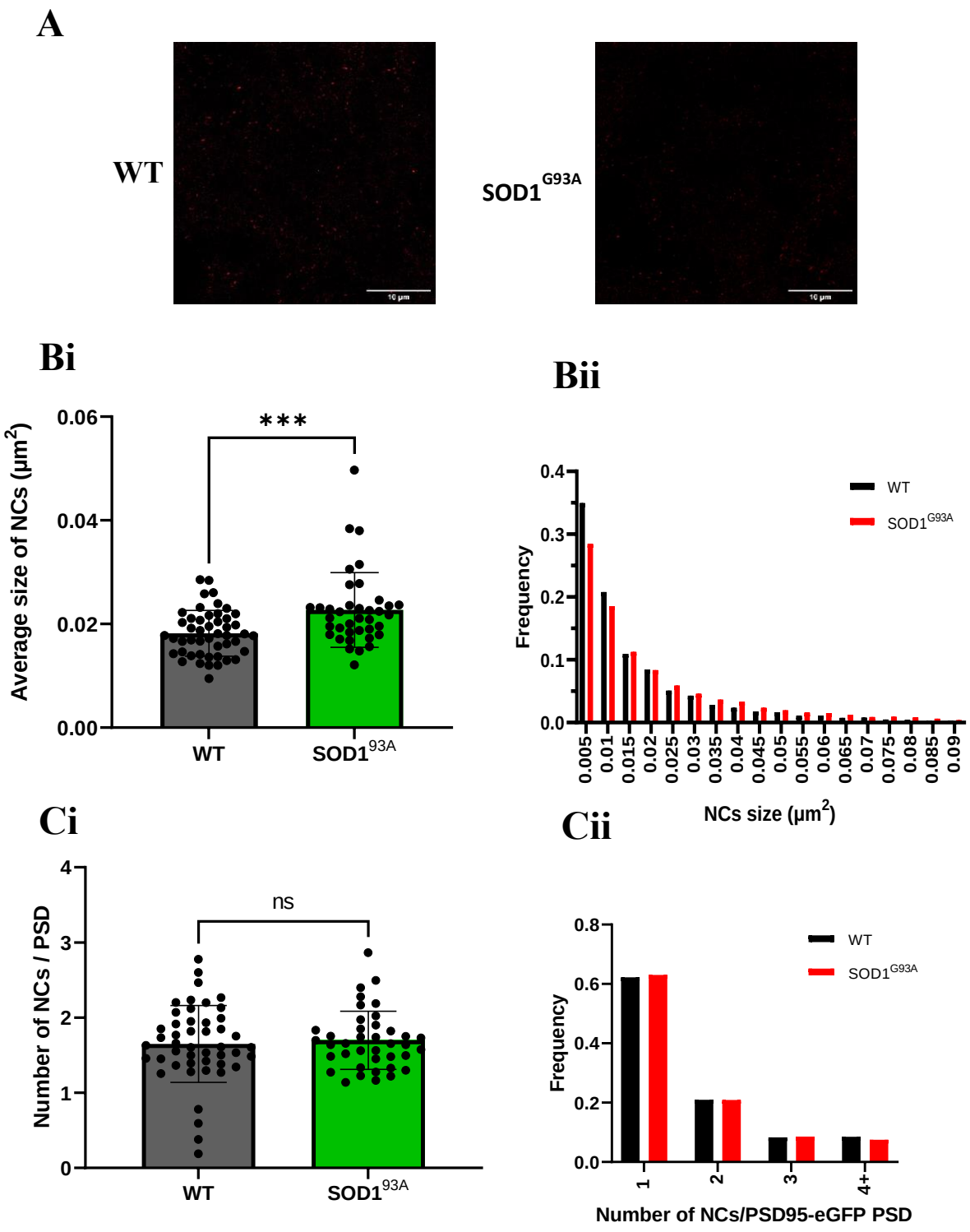

Figure 3. Size of NC is altered in lamina IX in lumbar spinal cord of 2 weeks old SOD1^{G93A} mice with no change in the number of NC per PSD (A) super-resolution images of PSD95-positive NC taken using gated-STED microscopy from lumbar spinal cord section of WT and SOD1^{G93A} mice. (B) Average size of PSD95-eGFP NC (Bi) and frequency histogram of PSD95-eGFP NC size in WT (n =9) and SOD1^{G93A} (n =9) lumbar spinal cord sections (Bii). (C) Number of PSD95-eGFP NC per PSD (Ci) and frequency histogram showing the distribution of PSD and the number of NC within the PSD (WT: n = 13543 NC, SOD1^{G93A}: n = 11666 NC) (Cii). At least 3 confocal images were taken from each animal and each datapoint on graph shows the average NC size and number of one image. Bar graphs show mean ± SD; WT: N = 9; SOD1^{G93A}: N = 9. Unpaired t-test shows that NC are significantly larger in SOD1^{G93A} mice; *** p<0.001.

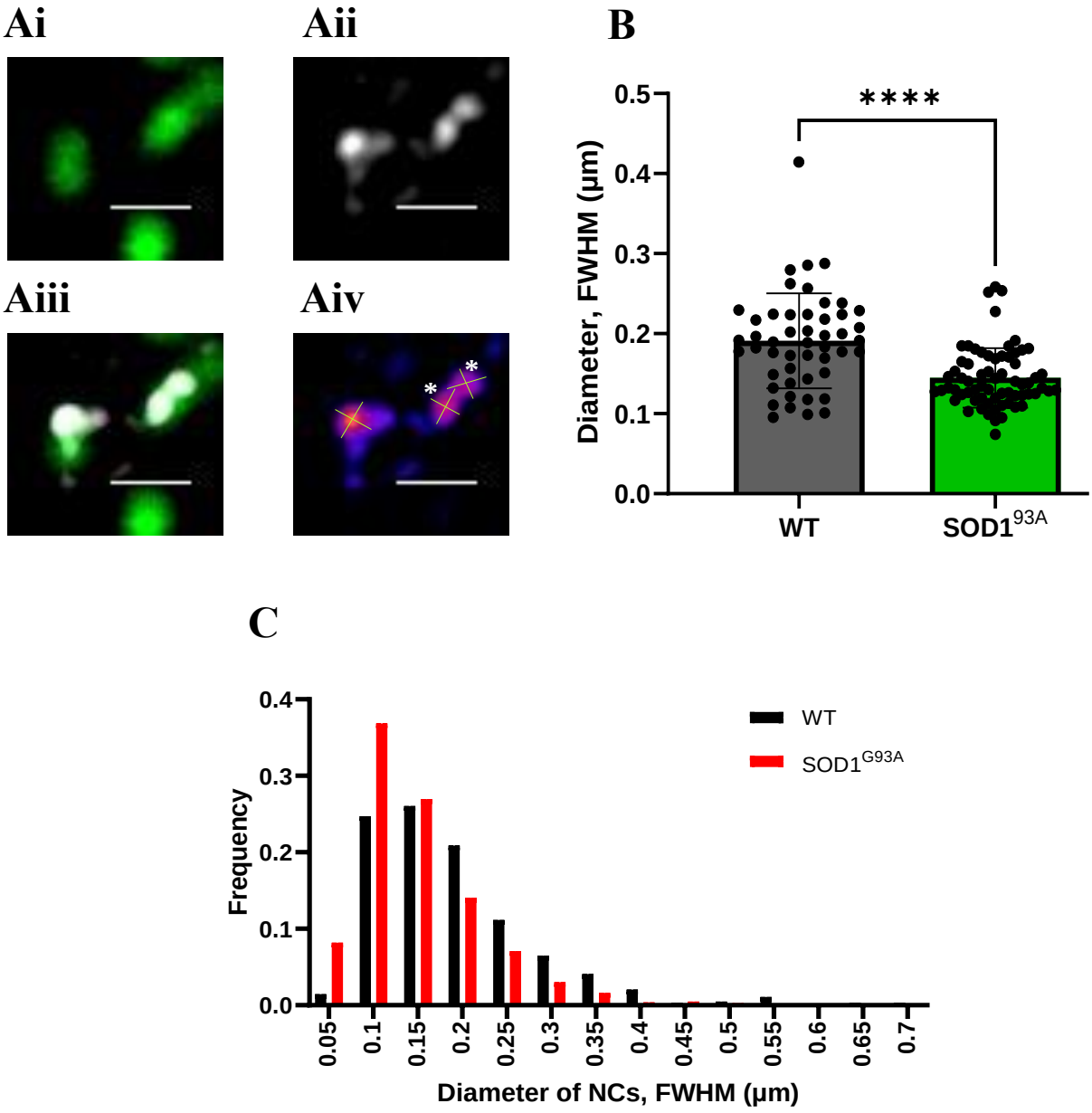

Figure 4. FWHM analysis revealed that PSD95-eGFP NC are smaller in lamina IX in lumbar spinal cords of two weeks old SOD1^{G93A} mice. (A) Example of PSD95-eGFP PSD and NC visualised in lamina IX using confocal microscopy to visualise PSDs (Ai), g-STED microscopy to visualise NC (Aii). (Aiii) Superimposed image captured from confocal and g-STED showing NC within PSD. (Aiv) Example of PSD95-eGFP NC with minimum and maximum axes length denoted for FWHM analysis. Scale bar denotes 0.5 µM.(B) Average diameter of PSD95-eGFP NC in lamina IX of 2 weeks old WT and SOD1^{G93A} mice, analysed using FWHM analysis. (C) Frequency histogram plotting the distribution of PSD95-eGFP NC of WT (n = 833 NC) and SOD1^{G93A} (n = 1061 NC) from FWHM analysis. Bar graph shows mean ± SD; WT: N = 9; SOD1^{G93A}: N = 9. Unpaired t-test shows that NC are significantly smaller in SOD1^{G93A} mice; **** p<0.0001.

We next wanted to quantify the inhibitory PSDs in lamina IX of WT and SOD1^{G93A} mice. To do this, we used mouse-anti gephyrin antibody to label the postsynaptic scaffold protein gephyrin found in inhibitory GABAergic and glycinergic PSDs (Krueger-Burg, Papadopoulos and Brose, 2017). At week 2, although the average number of gephyrin-positive PSDs per 100 µm^2 were reduced in lamina IX of SOD1^{G93A} mice in comparison to WT (Fig 5B. WT 18.7 ± 7.4, SOD1^{G93A} = 14.8 ± 7.1; $p<0.05$), the average size of PSDs were found to be comparable between the two genotypes (Fig 5Ci. WT 0.214 ± 0.078 µm^2, SOD1^{G93A} = 0.207 ± 0.059 µm^2). The comparable size of PSDs between the two groups is further shown by the histogram plot showing the distribution of PSDs in SOD1^{G93A} and WT animals (Fig 5Cii).

Given that the size of gephyrin-positive PSDs is decreased in SOD1^{G93A} mice, we next wanted to investigate if changes in NCs are present in the disease. Super-resolution g-STED microscopy and thresholding analysis revealed that the mean size of gephyrin-positive NCs is smaller in the ventral lamina IX of SOD1^{G93A} mice in comparison to WT (Fig 6Bi. WT= 0.039 ± 0.009 µm^2, SOD1^{G93A} = 0.032 ± 0.009 µm^2; $p<0.0001$). Additionally, a larger proportion of SOD1^{G93A} NC were observed to be smaller whereas WT NCs exhibited larger NC size (Fig 6Bii). Despite this change, we did not see any difference in the average number of NC per gephyrin-positive PSD (WT = 1.6 ± 0.3, SOD1^{G93A} = 1.6 ± 0.4).

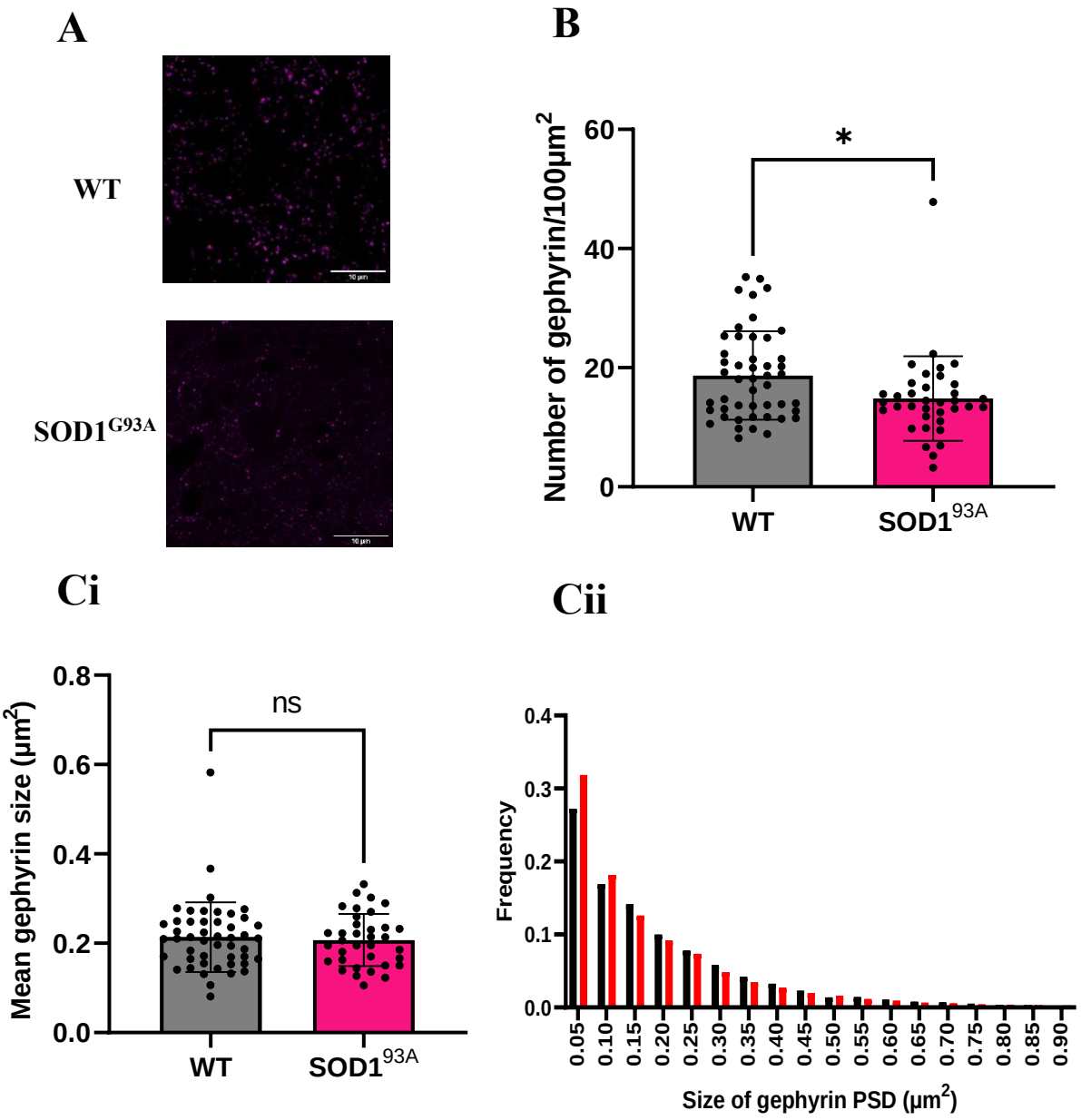

Figure 5. Number of gephyrin-positive inhibitory PSD is reduced in lamina IX in the lumbar spinal cord of 2 weeks old SOD1^{G93A} mice. (A) High magnification confocal images of gephyrin-positive inhibitory PSD from lumbar spinal cord section of WT and SOD1^{G93A} mice. (B) Average density of gephyrin-positive PSD per 100 µm^2 in WT and SOD1^{G93A} lumbar spinal cord. (C) Average size of PSD95-eGFP PSD (Ci) and frequency histogram plotting the distribution of size of gephyrin-positive PSD (Cii) in lamina IX of WT (n = 14608 PSD) and SOD1^{G93A} (n = 9386 PSD) lumbar spinal cord. At least 3 confocal images were taken from each animal and each datapoint on graph shows the average number or size of PSD per image. Bar graphs show mean ± SD; WT: N = 9, SOD1^{G93A}: N = 9. Unpaired t-test shows a reduction in the number of gephyrin-positive inhibitory PSD in SOD1^{G93A} mice; * $p<0.05$

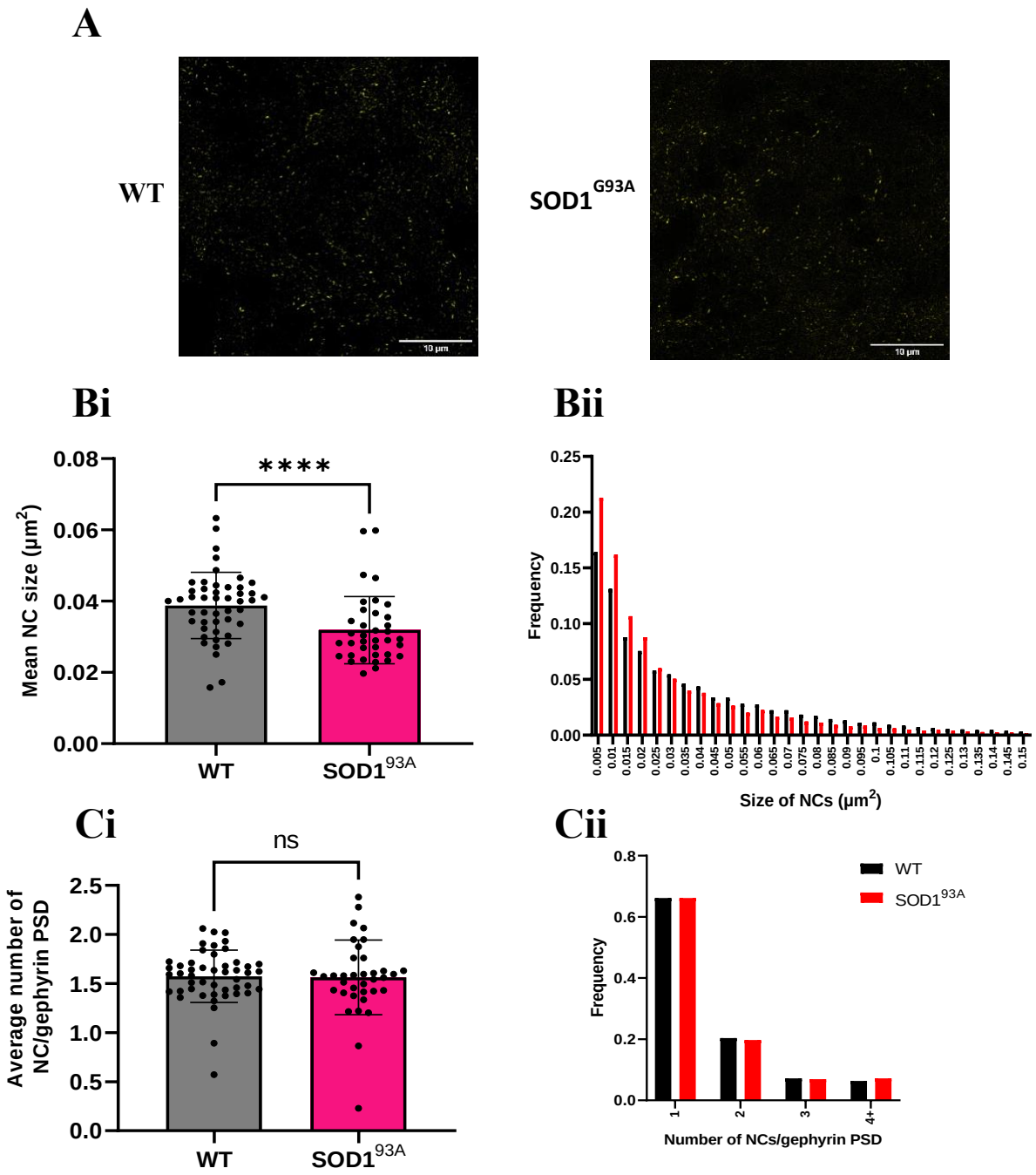

Figure 6. Size of gephyrin NC is decreased in lamina IX of the lumbar spinal cord of 2 weeks old SOD1^{G93A} mice with no change in the number of NC per PSD (A) super-resolution images of gephyrin-positive NC taken using gated-STED microscopy from lumbar spinal cord section of WT and SOD1^{G93A} mice. (B) Average size of gephyrin-positive NC (Bi) and frequency histogram of gephyrin-positive NC size in WT (n = 23576 NC) and SOD1^{G93A} (n = 14834 NC) lumbar spinal cord sections. (C) Number of gephyrin-positive NC per PSD (Ci) and frequency histogram showing the distribution of PSD and the number of NC within the PSD (WT: n = 14608 PSD, SOD1^{G93A}: n = 9386 PSD) (Cii). At least 3 confocal images were taken from each animal and each datapoint on graph shows the average NC size and number per image. Bar graphs show mean ± SD; WT: N = 9; SOD1^{G93A}: N = 9. Unpaired t-test shows that NC are significantly smaller in SOD1^{G93A} mice; **** p<0.0001.

Similar to the methodology followed to quantify the size of NCs in excitatory PSDs, we next measured the short and long axis diameter of inhibitory NCs using FWHM analysis (Fig. 7Aiv). Consistent with the results obtained by calculating the area of NC after applying the threshold, results show that the NC in ventral lamina IX of $SOD1^{G93A}$ mice are significantly smaller in comparison to WT (Fig 7B. WT = 0.221 ± 0.061 µm, $SOD1^{G93A}$ = 0.172 ± 0.46 µm; $p<0.0001$). When examining the distribution of NC short and long axis lengths using FWHM, it appears that most NC in the $SOD1^{G93A}$ mice are smaller than that of WT mice (Fig 7C).

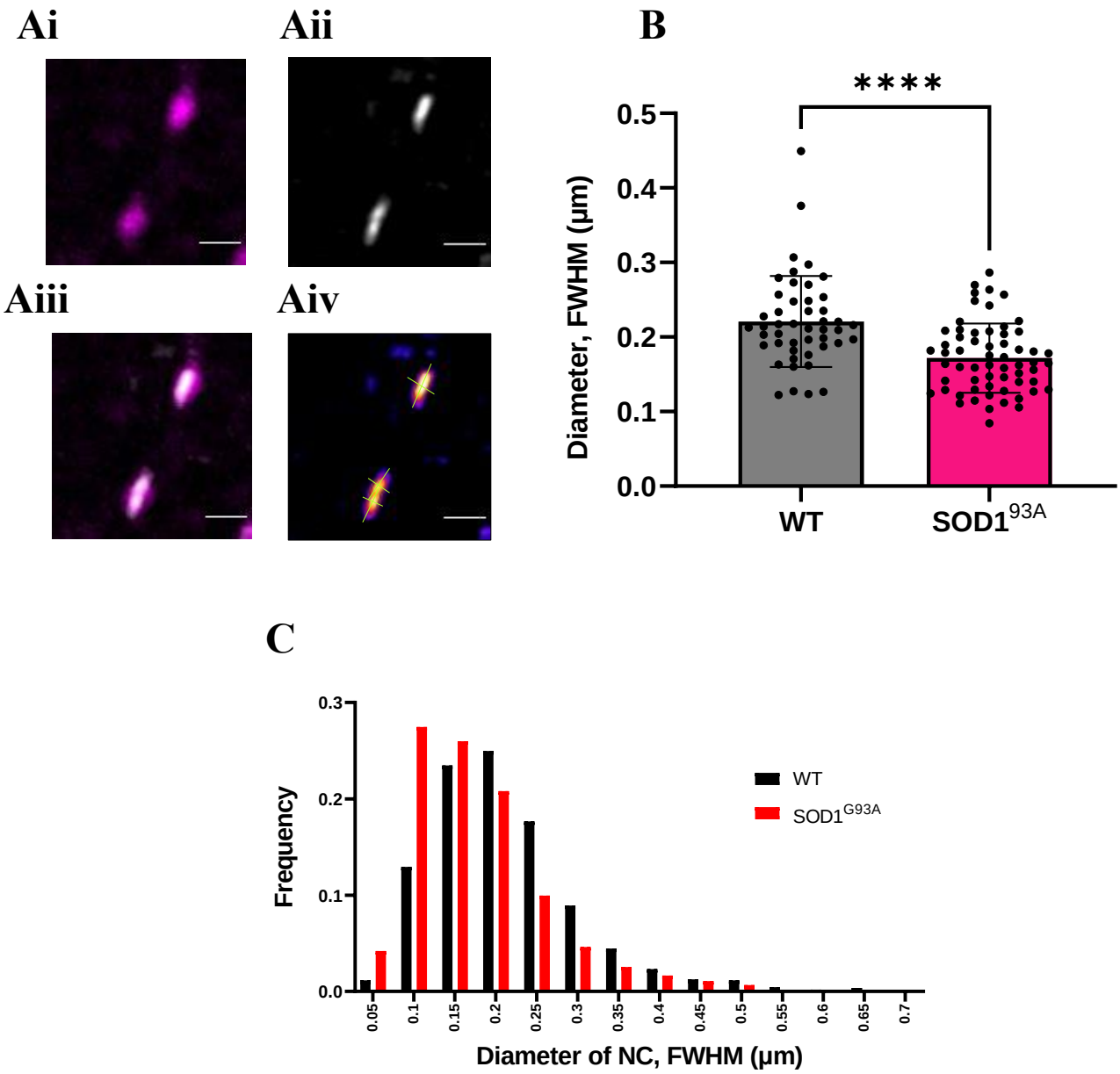

Figure 7. FWHM analysis revealed that gephyrin-positive NC are smaller in lamina IX in lumbar spinal cords of two weeks old SOD1^{G93A} mice. (A) Example of gephyrin-positive PSD and NC visualised in lamina IX using confocal microscopy to visualise PSDs (Ai), g-STED microscopy to visualise NC (Aii). (Aiii) Superimposed image captured from confocal and g-STED showing NC within PSD. (Aiv) Example of gephyrin-positive NC with minimum and maximum axes length denoted for FWHM analysis. (B) Average diameter of gephyrin-positive NC in lamina IX of 2 weeks old WT and SOD1^{G93A} mice, analysed using FWHM analysis. (C) Frequency histogram plotting the distribution of gephyrin-positive NC of WT (n = 1121 NC) and SOD1^{G93A} (n = 1216 NC) from FWHM analysis. Bar graph shows mean ± SD; WT: N = 9; SOD1^{G93A}: N = 9. Unpaired t-test shows that gephyrin-positive NC are significantly smaller in SOD1^{G93A} mice; **** p<0.0001.

The balance between excitatory and inhibitory neurotransmission can be altered by the changes in the proportion of functional excitatory and inhibitory synapses, also known as the E:I ratio. Synaptic dysfunction can cause perturbation in the E:I imbalance, which has already been observed in various neurological diseases such as ALS (Kiernan et al 2019). To determine if the E:I ratio is altered in $SOD1^{G93A}$ mice, we divided the counts of PSD95-positive excitatory PSD by the counts of gephyrin-positive inhibitory PSD collected from the same image. We show that there is no significant difference in the E:I ratio in lamina IX of $SOD1^{G93A}$ in comparison to WT control (Fig 8.WT = 0.65 ± 0.40, $SOD1^{G93A}$ = 0.77 ± 0.59). Besides the comparable E:I ratio between the two genotypes, there appears to be a bias in the ratio towards inhibitory PSD in both WT and $SOD1^{G93A}$ mice.

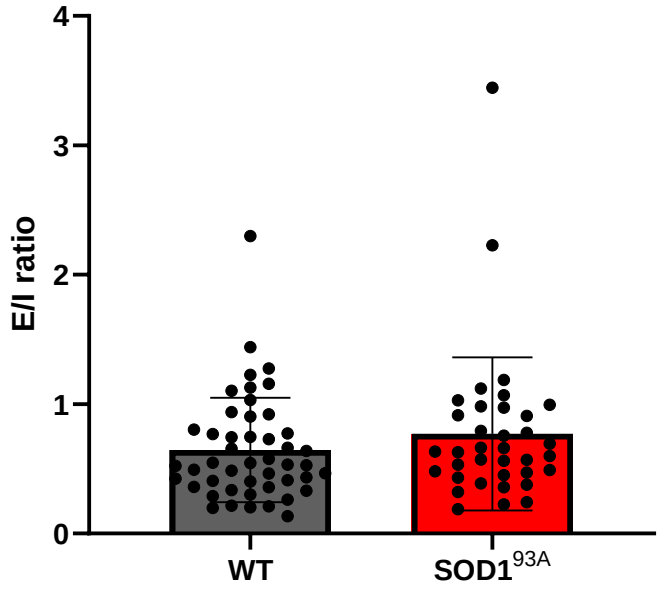

Figure 8. No difference in the E/I ratio in lamina IX of two weeks old SOD1^{G93A} mice. (A) E:I ratio in 2-week-old WT and SOD1^{G93A} mice. Bar graph shows mean ± SD; WT: N = 9; SOD1^{G93A}: N = 9. Unpaired t-test shows no significant difference between in the E:I ratio in lamina IX of the lumbar spinal cord Of WT and SOD1^{G93A} mice.

Since SOD1^{G93A} males display an earlier disease onset than females (Acevedo-Arozena *et al.*, 2011), we separated the mice according to the gender to explore whether there was a gender-based difference in the anatomy of synapses.

In male WT and SOD1^{G93A} mice, we did not observe significant changes in the average size of PSD95-positive PSD (Fig 9Ai. WT = 0.248 ± 0.059μm^2, SOD1^{G93A} = 0.234 ± 0.064μm^2), and the number of PSD95-positive PSD per 100μm^2 (Fig. 9Aii. WT = 10.4 ± 6.7, SOD1^{G93A} = 10.4 ± 4.8). When examining the PSD95 NC, the number of NC per PSD (Fig 9Aiii. WT = 1.8 ± 0.5, SOD1^{G93A} = 1.9 ± 0.3) and the average diameter of NC (Fig 9Aiv. WT = 0.179 ± 0.13μm, SOD1^{G93A} = 0.167 ± 0.11μm) were comparable in lamina IX of SOD1^{G93A} and WT mice. We next wanted to investigate whether there were changes in inhibitory synapses and their NC by quantifying gephyrin-positive PSD. Similar to the excitatory PSD95-positive PSD, we did not see significant changes in the average size of gephyrin-positive PSD between WT and SOD1^{G93A} (Fig 9Bi. WT = 0.203 ± 0.058μm^2, SOD1^{G93A} = 0.231 ± 0.042μm^2). Interestingly, the number of gephyrin-positive PSD per 100μm^2 was significantly smaller in SOD1^{G93A} mice in comparison to WT (Fig 9Bii. WT = 21.2 ± 7.7, SOD1^{G93A} = 15.6 ± 8.8). Given that the number of PSD95-postive synapses were unchanged and the gephyrin-positive synapses were reduced in the SOD1^{G93A} mice, the E:I ratio was significantly higher in lamina IX of lumbar spinal cords of SOD1^{G93A} mice in comparison to WT, showing a bias toward excitation (Fig 9C. WT = 0.53 ± 0.35, SOD1^{G93A} = 0.86 ± 0.76; $p<0.05$, Mann-Whitney test). Moreover, no significant difference was observed in the number of gephyrin NC per gephyrin-positive PSD (Fig 9Biii. WT = 1.6 ± 0.3 SOD1^{G93A} = 1.7 ± 0.3), however, FWHM analysis showed a significant reduction in the average diameter of NC in SOD1^{G93A} mice in comparison to WT (Fig 9Biv. WT = 0.222 ± 0.13μm, SOD1^{G93A} = 0.193 ± 0.12μm; $p<0.0001$, Mann-Whitney test)

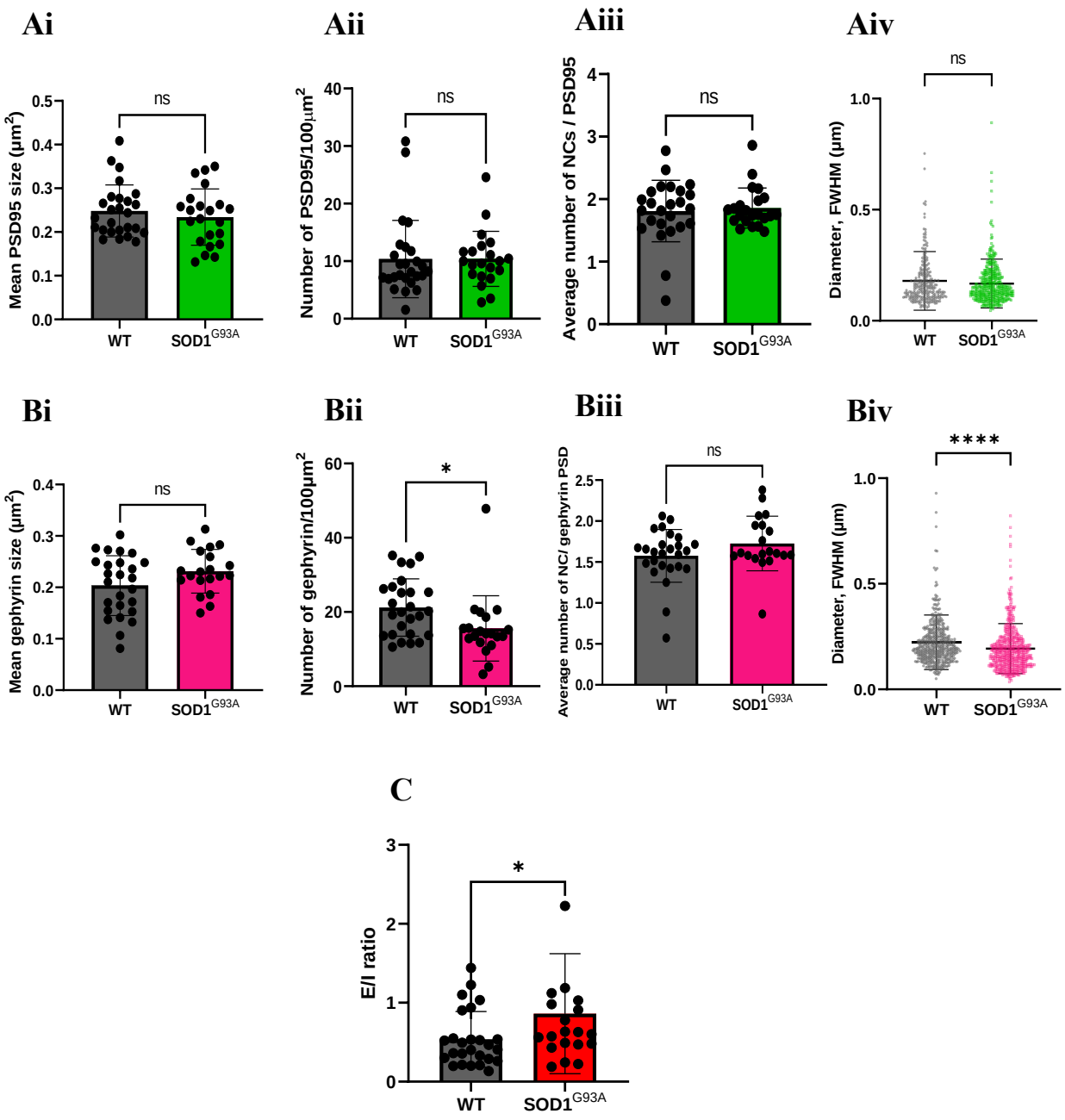

Figure 9. Quantification of PSD95 and gephyrin PSD and NC in lamina IX of lumbar spinal cord of 2 weeks old SOD1^{G93A} and WT male mice. Average size (Ai) and density (Aii) of PSD95-eGFP positive excitatory PSD. (Aiii) Number of NC per PSD (Aiii) and average diameter of PSD95-eGFP NC (Aiv). Average size (Bi) and density (Bii) of gephyrin-positive inhibitory PSD. (Biii) Number of NC per PSD (Biii) and average diameter of gephyrin NC (Biv). (C) E:I ratio in lamina IX of lumbar spinal cords sections of 2-week-old male SOD1^{G93A} and WT mice. At least 3 confocal images were taken from each animal and each datapoint on graph shows the average number or size of PSD of one image. Bar graphs show mean ± SD; WT: N=3; SOD1^{G93A}: N = 3. Unpaired t-test or Mann-Whitney test were performed; *p<0.05, ****p<0.0001.

Next, we examined if changes in excitatory and inhibitory PSD and NC in females were altered in SOD1-ALS. No significant differences were observed in the average size (Fig 10Ai. WT = 0.186 ± 0.048μm^2, $SOD1^{G93A}$ = 0.177 ± 0.059μm^2) and density per 100 μm^2 (Fig 10Aii. WT = 11.2 ± 5.0, $SOD1^{G93A}$ = 8.6 ± 3.1) of PSD95-positive PSD. Although the average number of PSD95 NC per PSD is not significantly different between $SOD1^{G93A}$ and WT mice (Fig 10Aiii. WT = 1.5 ± 0.4, $SOD1^{G93A}$ = 1.4 ± 0.3), FWHM analysis showed a significant decrease in the average diameter of PSD95 NC in female $SOD1^{G93A}$ mice (Fig 10Aiv. WT = 0.206 ± 0.101μm, $SOD1^{G93A}$ = 0.144 ± 0.082μm). For gephyrin-positive inhibitory synapses, the average size of gephyrin-positive PSD was found to be reduced in female $SOD1^{G93A}$ lamina IX in comparison to WT (Fig 10Bi. WT = 0.0.221 ± 0.096μm^2, $SOD1^{G93A}$ = 0.178 ± 0.062μm^2), however the density remained comparable between the two genotypes (Fig 10Bii. WT = 15.7 ± 5.9, $SOD1^{G93A}$ = 13.9 ± 4.2). For gephyrin NC, there was found to be no significant difference in the number of NC per gephyrin-positive PSD (Fig 10Biii. WT = 1.6 ± 0.2, $SOD1^{G93A}$ = 1.5 ± 0.2). Similar to PSD95 NC, the average diameter of gephyrin NC were significantly smaller in lamina IX of $SOD1^{G93A}$ female mice in comparison to WT (Fig 10Biv. WT = 0.220 ± 0.10μm, $SOD1^{G93A}$ = 0.167 ± 0.09μm). Overall, we found no structural difference in the E:I ratio in lamina IX of lumbar spinal cord sections of female mice across both genotypes (Fig. WT = 0.79 ± 0.4, $SOD1^{G93A}$ = 0.66 ± 0.2)

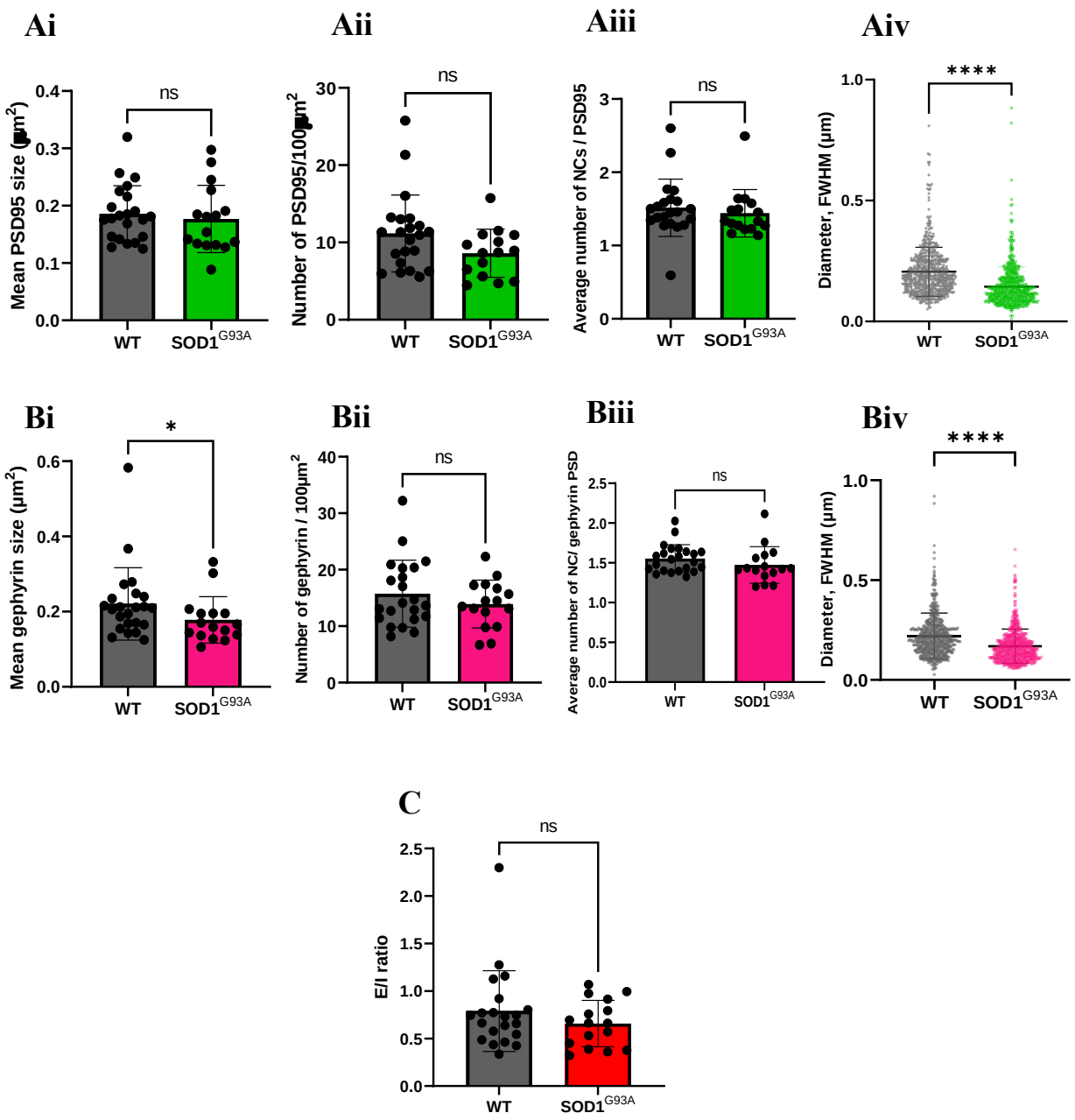

Figure 10. Quantification of PSD95 and gephyrin PSD and NC in lamina IX of lumbar spinal cord of 2 weeks old SOD1^{G93A} and WT female mice. Average size (Ai) and density (Aii) of PSD95-eGFP positive excitatory PSD. (Aiii) Number of NC per PSD (Aiii) and average diameter of PSD95-eGFP NC (Aiv). Average size (Bi) and density (Bii) of gephyrin-positive inhibitory PSD. (Biii) Number of NC per PSD (Biii) and average diameter of gephyrin NC (Biv). (C) E:I ratio in lamina IX of lumbar spinal cords sections of 2-week-old female SOD1^{G93A} and WT mice. At least 3 confocal images were taken from each animal and each datapoint on graph shows the average number or size of PSD of one image. Bar graphs show mean ± SD; WT: N=5; SOD1^{G93A}: N = 5 Unpaired t-test or Mann-Whitney test were performed; *p<0.05, ****p<0.0001.

Discussion

In this study, we provided a quantitative approach to investigate the excitatory and inhibitory synapses in lumbar spinal cords of SOD1^{G93A} mice. We used the genetically engineered mouse line, PSD95-eGFP, to visualise the scaffolding protein PSD95 that exists within excitatory PSD and provides a reliable marker for excitatory synapses (Broadhead *et al.*, 2020). To visualise the inhibitory synapses, we used an immunolabelling approach using an antibody raised against gephyrin. We imaged the anatomical lamina IX of the spinal cords, as this region is comprised of large α-, β-, γ- motoneurons and most of the synapses that are visualised in this area are on dendrites and somas of these motoneurons.

First, we demonstrated that that PSD95-positive excitatory PSD size and density are not different in the motoneuron rich area of lamina IX between SOD1^{G93A} and WT mice. When we measured the subsynaptic structure of PSD95 NC using manual thresholding, we found that the size of PSD95 NC were bigger in lamina IX of SOD1^{G93A} mice. Manual thresholding can be subjected to some degree of bias: even though a binary watershed process was applied, too little thresholding would not distinguish between NC that are too close to each other; and excessive thresholding would exclude the small NC and skew the results. To overcome this issue, we used FWHM analysis which measures the maximum transmission peak of the sub-resolution objects by manually generating line profiles of single NC and fitting these profiles with a Gaussian distribution to improve the sensitivity. The points at either side of the peak where it is half the maximum transmission is identified and the distance along the wavelength axis between the two points is measured as the width/diameter of the object (Demmerle *et al.*, 2015).

FWHM analysis showed that the diameter of PSD95-eGFP NC within PSD in SOD1^{G93A} mice were significantly shorter in comparison to WT mice, even though the PSD95-eGFP PSD size do not change. In other neurodegenerative diseases such as Alzheimer's, synapse loss and decreased level of PSD95 expression along with decrease in other scaffolding proteins were observed in the hippocampus of

patients. Moreover, expression of NMDA receptor subunits were also altered in the disease implying that these receptors are indeed less functional (Sultana, Banks and Butterfield, 2010). Shao *et al.* (2011) have also showed a time-dependent decrease of PSD95 expression, along with the progression of the disease, which was induced by the aggregation of amyloid-β and tau proteins. In our study, we investigated the expression of PSD95-eGFP PSD in the $SOD1^{G93A}$ mice model at a very early pre-symptomatic age, therefore, we can speculate that these changes are not prominent at this early stage of the disease and like the observation in Alzheimer's disease, it could potentially be altered as the disease progressed with time. Although not significant, when pooling male and female mice Broadhead *et al.* (2022) observed that $SOD1^{G93A}$ mice at 16 weeks exhibited a decreasing trend in PSD95-eGFP expression in lamina IX of lumbar spinal cord. However, a significant decrease in PSD95-eGFP PSD was observed in early symptomatic $SOD1^{G93A}$ males, highlighting the gender bias in ALS. Furthermore, the average number of PSD95 NC per PSD95-eGFP was shown to be decreased at this 16 week time point (Broadhead *et al.*, 2022). To predict if the decrease in size of PSD95-eGFP NC can contribute to the overall reduction in size and number of PSD95-eGFP PSD, a time-dependent study over the course of the disease should be undertaken.

Aggregation of SOD1 protein has been widely documented in mouse models of $SOD1^{G93A}$ and it has been shown that these aggregates can misfold at the membrane and has shown impairment at synapses of motoneurons (Lum and Yerbury, 2022). For example, association of mutant $SOD1^{G93A}$ aggregate with the Na/K-ATPase led to impairment in the activity of the Na/K-ATPase and shortened the lifespan of $SOD1^{G93A}$ mice (Ruegsegger *et al.*, 2016). Similar to the finding in Alzheimer's disease, it would be of interest to investigate whether SOD1 aggregate can misfold at PSD95 and contribute to the reduction in the diameter of PSD95-eGFP NC observed in this study.

Decrease in PSD95 expression has been shown to alter the surface of the PSD by decreasing the density of AMPA receptors as well as mePSC amplitude (Nair *et al.*, 2013). In our study on the contrary, the decrease in PSD95 NC did not coincide with a decrease in mePSC amplitude in $SOD1^{G93A}$ mice. On the other hand, we observed a change in the frequency of mePSC, where there was a significant decrease in the frequency of these events in $SOD1^{G93A}$ motoneurons in comparison to WT. We did not quantify the expression of AMPA receptors in our study, however, we can postulate that there may be an alteration in the AMPA receptor density on the PSD of $SOD1^{G93A}$ motoneurons. Although this can be assumed, PSD95 is not the only core scaffolding protein found in nanodomains and it has been shown that PSD95 and AMPA receptors in some cases do not co-localise completely. Moreover, knocking down PSD95 has been shown not to alter synaptic transmission (Nair *et al.*, 2013), therefore this could indicate that PSD95 is not the only scaffolding protein that could be involved in synaptic dysfunction in ALS.

Taken together, it is possible to conclude that alterations in the nanostructures of excitatory PSD95-positive PSD in lamina IX of $SOD1^{G93A}$ mice are prominent at an early stage of the SOD1-ALS and that these changes could worsen as the disease advances.

We next investigate the inhibitory PSD and their NC using a gephyrin antibody. We observed a significant reduction in the density of gephyrin-positive PSD as well as the diameter of gephyrin NC in $SOD1^{G93A}$ mice. On the other hand, we did not observe differences in the size of gephyrin-positive PSD and in the number of NC per PSD. Extensive studies in the hippocampus have shown that both the size and the arrangement of inhibitory PSD increase in response to increased excitatory inputs (Nusser, Cull-Candy and Farrant, 1997; Lushnikova *et al.*, 2011). Moreover, it has been shown that there is a correlation between the number of nanodomains or NC and synaptic strength (Kevin C. Crosby *et al.*, 2019). In our study we have shown that the number of both excitatory (PSD95-eGFP) and inhibitory

(gephyrin) NC remain unchanged in SOD1^{G93A} lamina IX in comparison to WT, from this which can speculate that the strength of synaptic transmission may not be implicated at this early timepoint in the disease. On the contrary, even though we did not observe changes in the number of NC, we did observe changes in the amplitude which can indicates that there could be changes in the density of receptors post-synaptic density of motoneurons (Turrigiano and Nelson, 2004). Quantitative nanoscopy of gephyrin molecules revealed that the stoichiometry between one gephyrin molecule and receptor binding sites for inhibitory neurotransmitters is 1:1 (Specht *et al.*, 2013). Our study showed that SOD1^{G93A} mice had lower density of gephyrin-positive PSD implying that there may be a decrease of glycinergic or GABAergic receptors. However, from chapter 3, an increase in miPSC amplitude was observed in fast-type motoneurons, possibly indicating that there are more receptors present on the PSD. However, even in the absence of altered receptor density, change in PSD or NC size and reorganisation of subsynaptic structures can alter synaptic transmission (MacGillavry *et al.*, 2013). Therefore, it can be inferred that there may be a compensatory mechanism involved to counteract for the decrease in inhibitory gephyrin-positive synapses observed by increasing the miPSC amplitude in SOD1^{G93A} mice.

Inhibitory SOD1^{G93A} interneurons that project onto motoneurons in lamina IX have shown to have a reduction in depolarised PIC current which could increase the excitability of motoneurons by dampening their inhibitory inputs (Cavarsan *et al.*, 2022). Although this study suggests that there is reduced inhibitory glycinergic inputs onto motoneurons, in our study we have shown that fast-type motoneurons receive, although non-significant, increased frequency of spontaneous iPSC as well as higher frequency and amplitude of miPSC. Due to changes in synaptic activity, the size of PSD can change accordingly. For example, blocking action potential-dependent synaptic currents with TTX increased the size of PSD95-positive PSD and increased the number of NC within individual PSD to compensate for reduced release of neurotransmitters (MacGillavry *et al.*, 2013). In our study, we show that only the size of gephyrin NC

is smaller in SOD1^{G93A} mice in comparison to WT which could indicate that neurons within lamina IX receive more inhibitory inputs and therefore decrease in NC size as a way of homeostatic scaling. It would be interesting to investigate if this homeostatic alteration in NC size or synaptic plasticity becomes dysfunctional thus becoming a neurodevelopmental disorder which precedes changes in gephyrin-positive PSD size in ALS. Although we did not image PSD and NC after application of TTX, it would be of interest to see whether SOD1^{G93A} PSD are capable of changing PSD size to compensate for changes via homeostatic scaling of synaptic substructure.

Broadhead *et al.*, (2022) showed that synapses formed between excitatory VGLUT2-positive presynaptic membrane, PSD95-positive postsynaptic membrane, and astrocytes, called tripartite synapses are the most vulnerable in post-natal 16-week-old SOD1^{G93A} mice and spinal cords of non-SOD1 ALS patients. It is possible that changes in inputs as well as astrocytes can contribute to changes in sub-synaptic structures in excitatory. However, less in known about astrocytes and their contribution to changes in inhibitory synapses in ALS.

Concurrent with the incidence in clinical cases of ALS (Cacabelos *et al.*, 2016) , studies have shown pronounced gender bias in SOD1^{G93A} mice, with males exhibiting an earlier onset of disease and faster disease progression (Acevedo-Arozena *et al.*, 2011). When looking at the males, we found no significant difference in PSD95-eGFP positive excitatory PSD and NC between SOD1^{G93A} and WT mice. However, we found that the density of gephyrin-positive inhibitory PSD is significantly reduced only in SOD1^{G93A} males in comparison to female SOD1^{G93A} and WT mice. As a result of this we observed a significant increase in the E:I ratio in SOD1^{G93A} males at this early stage of the disease which suggests that there are more excitatory synapses in motoneuron-rich area of lamina IX. In contrast, the E:I ratio between female SOD1^{G93A} and WT remained comparable.

When examining the excitatory PSD95 NC, only SOD1^{G93A} females showed a significant decrease in size. However, both males and females SOD1^{G93A} show decrease in inhibitory gephyrin NC size. Although the mechanism behind the alteration of NC size in ALS is unknown, given that male SOD1^{G93A} mice exhibit earlier onset of ALS, we could postulate that dysfunction in synaptic scaling and E:I ratio could be factors underlying pathological changes in early pre-symptomatic SOD1^{G93A} males.

Although it is known that the fast-type motoneurons are the most vulnerable in ALS, this study did not investigate the changes in the excitatory and inhibitory synapses on fast-type motoneurons. Due to technical issue, markers for fast-type motoneurons were not used in this study. To further explore changes on fast-type motoneurons, primary antibodies raised against MMP9 to distinguish the fast-type motoneurons, along with retrograde labelling to label dendrites, can be used to quantify the excitatory and inhibitory synapses to investigate if similar changes are observed on the vulnerable population of motoneurons in ALS.

In summary, our study demonstrates that both excitatory and inhibitory PSD are altered in early pre-symptomatic SOD1^{G93A} mice at post-natal age of 2 weeks. We present that there are not only changes in excitatory and inhibitory PSD, but also in their subsynaptic structures. These anatomical data could support the previous functional observations that also showed difference in the PSCs. This current study provides evidence that changes in synapses are evident in early pre-symptomatic stages of ALS and could be a patho-mechanism that contributes to the progression of the disease.

Concluding remarks

ALS is a devastating neurodegenerative disease that affects millions of individuals throughout the world. Like with most neurodegenerative diseases, it remains incurable despite intensive efforts to discover therapies. Although the majority of the cases of ALS are sporadic, clinical manifestation of both familial and sporadic ALS are comparable. Therefore, using disease models of fALS, elucidating the mechanisms underlying the pathogenesis of fALS would indeed provide insights into the mechanisms of sALS. Since the development of the $SOD1^{G93A}$ transgenic mouse model (Gurney *et al.*, 1994), many advancements have been made to improve our understanding into the several mechanisms that are implicated in ALS, such as mitochondrial dysfunction, oxidative stress, impaired proteostasis and excitotoxicity. Although changes in electrophysiological properties have been observed throughout the progression of the disease (from embryonic to disease-onset) (Pieri, 2003; Kuo *et al.*, 2004; Van Zundert *et al.*, 2008; Martin *et al.*, 2013a; Jensen *et al.*, 2020), most studies, particularly those conducted in pre-symptomatic mice, did not explore the changes in the vulnerable population of motoneurons that are affected in ALS. In the $SOD1^{G93A}$ mouse model, it is known that the FF and FR motoneurons are affected prior and at symptom-onset respectively, whereas S motoneurons remain resistant in the disease. The changes in electrophysiological properties in $SOD1^{G93A}$ adult vulnerable FF and FR motoneurons (late pre-symptomatic and symptomatic stages) have recently been extensively studied (Delestrée *et al.*, 2014; Leroy *et al.*, 2014; Martínez-Silva *et al.*, 2018; Jensen *et al.*, 2020), yet, the outcomes of these studies are contadicting amongst them. In this study, we were interested in exploring the changes in electrophysiological properties in very early pre-symptomatic fast-type motoneurons in the $SOD1^{G93A}$ transgenic mouse model. We used an established electrophysiological protocol that distinguished the vulnerable fast-type motoneurons that displayed a ‘delayed-firing’ response to a current pulse from the resistant slow-type motoneurons that exhibited a ‘immediate-firing’ response to a current pulse.

For the first part of the study, described in Chapter 2, we demonstrated that the vulnerable fast-type SOD1^{G93A} motoneurons do not exhibit overt difference in most intrinsic properties including RMP, spike properties, PIC which demonstrate that at this stage of the disease, the fast-type motoneurons retain normoexcitability in comparison to WT. However, fast-type SOD1^{G93A} motoneurons had lower input resistance and showed larger Ih.

In Chapter 3, the synaptic inputs to fast-type motoneurons were investigated in SOD1^{G93A} mice at the pre-symptomatic stage of the disease. In order to preserve more dendritic structures of the motoneurons, unlike the conventional transverse sections, we prepared longitudinal slices of the lumbar spinal cord. We show that SOD1^{G93A} fast-type motoneurons received increased frequency of mixed PSCs at postnatal age of 2 weeks. Whole-cell patch-clamp recordings performed in the presence of TTX showed that the frequency of miniature PSCs was indeed higher in SOD1^{G93A} fast-type motoneurons in comparison to WT. These findings proposed that both action potential-dependent and action-potential-independent inputs are altered in early SOD1^{G93A} model. To characterise the nature of the miniature PSCs, we pharmacologically blocked excitatory and inhibitory receptors and measured the input received onto fast-type in SOD1^{G93A} motoneurons. Application of bicuculline, strychnine along with TTX showed that the frequency of miniature excitatory PSCs was lower in SOD1^{G93A} motoneurons but no change in amplitude was observed. It is possible that the change in the frequency along with the absence in change in amplitude could suggests that the premotor networks are more active at this early change in the disease (Turrigiano and Nelson, 2004). Application of CNQX, APV along with TTX revealed that the frequency and amplitude of miniature inhibitory PSCs were higher in fast-type SOD1^{G93A} motoneurons. Fast-type motoneurons have been shown to receive more inhibitory inputs in comparison to slow-type motoneurons, however at the symptomatic age SOD1^{G93A} fast-type motoneurons lose inhibitory synapses (Allodi *et al.*, 2021). We can speculate that increased inhibition may be a pathogenic change in SOD1^{G93A} that could set-up the network for progressive dysfunction later in the disease.

Moreover, given that previous studies have shown increase in excitatory inputs in SOD1 motoneurons (Van Zundert *et al.*, 2008; Jiang *et al.*, 2017), it would be interesting to address whether this increase in inhibitory input is indeed a mechanisms for hypervigilant homeostasis.

Findings from Chapter 3 demonstrated that changes on PSDs could have been present in $SOD1^{G93A}$ fast-type motoneurons. We utilised the PSD95-eGFP transgenic model and crossed it with $SOD1^{G93A}$ transgenic disease line to allow us to visualise excitatory PSDs, and the anti-gephyrin antibody to visualise inhibitory PSDs. In Chapter 4, we found anatomical evidence of changes at a nanoscale resolution in the subsynaptic organisation of PSD. Both excitatory and inhibitory PSD in lamina IX of $SOD1^{G93A}$ show some degree of alteration. No changes were observed in the structures of excitatory, PSD95-eGFP positive PSD, however, at this early pre-symptomatic age, the subsynaptic individual NC within excitatory PSDs are smaller in the disease. Both the gephyrin-positive inhibitory PSD and NC were smaller in lamina IX of $SOD1^{G93A}$. Moreover, the density of the inhibitory PSD was also smaller in the $SOD1^{G93A}$ mice. These observations provide evidence that changes in synapses is evident in early pre-symptomatic stages of ALS and could be a patho-mechanism that contributes to the progression of the disease. For future work, it would be of interest to investigate the changes on fast-type motoneurons.

Although ALS is characteristically considered as an adult-onset disorder, from this study we know that changes in motoneurons, varying from alterations in intrinsic properties, synaptic inputs, and PSD structures, are present long before the manifestation of motor deficits. Whether these developmental changes are indeed adaptation of the CNS to preserve the vulnerable motoneurons or maladaptive changes that exacerbate the disease progression remains unknown. From this study, we can conclude that dysfunction in synapses plays role during the early pre-symptomatic stage of $SOD1^{G93A}$ ALS. Further

studies into these changes to gain deeper understanding of the role synaptopathy in ALS could provide as a target for therapeutics to prevent or even reverse the progression of ALS, long before the degeneration of the vulnerable motoneurons.

References

Acevedo-Arozena, A. *et al.* (2011) 'A comprehensive assessment of the SOD1 G93A low-copy transgenic mouse, which models human amyotrophic lateral sclerosis', *DMM Disease Models and Mechanisms*, 4(5), pp. 686–700. doi: 10.1242/dmm.007237.

Alexander, G. M. *et al.* (2000) 'Elevated cortical extracellular fluid glutamate in transgenic mice expressing human mutant (G93A) Cu/Zn superoxide dismutase.', *Journal of neurochemistry*. England, 74(4), pp. 1666–1673. doi: 10.1046/j.1471-4159.2000.0741666.x.

Allodi, I. *et al.* (2021) 'Locomotor deficits in a mouse model of ALS are paralleled by loss of V1-interneuron connections onto fast motor neurons', *Nature Communications*. Springer US, 12(1), pp. 1–18. doi: 10.1038/s41467-021-23224-7.

Avossa, D. *et al.* (2006) 'Early signs of motoneuron vulnerability in a disease model system: Characterization of transverse slice cultures of spinal cord isolated from embryonic ALS mice', *Neuroscience*, 138(4), pp. 1179–1194. doi: 10.1016/j.neuroscience.2005.12.009.

Bączyk, M. *et al.* (2020) 'Synaptic restoration by cAMP/PKA drives activity-dependent neuroprotection to motoneurons in ALS', *Journal of Experimental Medicine*, 217(8). doi: 10.1084/jem.20191734.

Barber, S. C. and Shaw, P. J. (2010) 'Oxidative stress in ALS: key role in motor neuron injury and therapeutic target.', *Free radical biology & medicine*. United States, 48(5), pp. 629–641. doi: 10.1016/j.freeradbiomed.2009.11.018.

Bayliss, D. A. *et al.* (1994) 'Characteristics and postnatal development of a hyperpolarization-activated inward current in rat hypoglossal motoneurons in vitro', *Journal of Neurophysiology*, 71(1), pp. 119–128. doi: 10.1152/jn.1994.71.1.119.

Beal, M. F. *et al.* (1997) 'Increased 3-nitrotyrosine in both sporadic and familial amyotrophic lateral sclerosis.', *Annals of neurology*. United States, 42(4), pp. 644–654. doi: 10.1002/ana.410420416.

Beckman, J. S. *et al.* (2001) 'Superoxide dismutase and the death of motoneurons in ALS.', *Trends in neurosciences*. England, 24(11 Suppl), pp. S15-20. doi: 10.1016/s0166-2236(00)01981-0.

Bendotti, C. *et al.* (2004) 'Activated p38MAPK Is a Novel Component of the Intracellular Inclusions Found in Human Amyotrophic Lateral Sclerosis and Mutant SOD1 Transgenic Mice', *Journal of Neuropathology and Experimental Neurology*, 63(2), pp. 113–119. doi: 10.1093/jnen/63.2.113.

Bensimon, G., Lacomblez, L. and Meininger, V. (1994) 'A controlled trial of riluzole in amyotrophic lateral sclerosis. ALS/Riluzole Study Group.', *The New England journal of medicine*. United States, 330(9), pp. 585–591. doi: 10.1056/NEJM199403033300901.

Bento, C. F. *et al.* (2016) 'Mammalian Autophagy: How Does It Work?', *Annual Review of Biochemistry*, 85, pp. 685–713. doi: 10.1146/annurev-biochem-060815-014556.

Binder, M. D., Heckman, C. J. and Powers, R. K. (1993) 'How different afferent inputs control motoneuron discharge and the output of the motoneuron pool.', *Current opinion in neurobiology*. England, 3(6), pp. 1028–1034. doi: 10.1016/0959-4388(93)90177-z.

Black, M. M. (2016) 'Axonal transport: The orderly motion of axonal structures.', *Methods in cell biology*. United States, 131, pp. 1–19. doi: 10.1016/bs.mcb.2015.06.001.

Bories, C. *et al.* (2007) 'Early electrophysiological abnormalities in lumbar motoneurons in a transgenic mouse model of amyotrophic lateral sclerosis', *European Journal of Neuroscience*, 25(2), pp. 451–459. doi: 10.1111/j.1460-9568.2007.05306.x.

Bostock, H. *et al.* (1995) 'Axonal ion channel dysfunction in amyotrophic lateral sclerosis', pp. 217–225.

Brännström, T. (1993) 'Quantitative synaptology of functionally different types of cat medial gastrocnemius α-motoneurons', *Journal of Comparative Neurology*, 330(3), pp. 439–454. doi: 10.1002/cne.903300311.

Broadhead, M. J. *et al.* (2020) 'Nanostructural Diversity of Synapses in the Mammalian Spinal Cord', *Scientific Reports*. Springer US, 10(1), pp. 1–18. doi: 10.1038/s41598-020-64874-9.

Broadhead, M. J. *et al.* (2022) 'Selective vulnerability of tripartite synapses in amyotrophic lateral sclerosis', *Acta Neuropathologica*. Springer Berlin Heidelberg, 143(4), pp. 471–486. doi: 10.1007/s00401-022-02412-9.

Brown, R. H. and Al-Chalabi, A. (2017) 'Amyotrophic lateral sclerosis', *New England Journal of Medicine*, 377(2), pp. 162–172. doi: 10.1056/NEJMra1603471.

Brownstone, R. M. and Bui, T. V. (2010) 'Spinal interneurons providing input to the final common path during locomotion', *Progress in Brain Research*, 187(C), pp. 81–95. doi: 10.1016/B978-0-444-53613-6.00006-X.

Buskila, Y. *et al.* (2019) 'Dynamic interplay between H-current and M-current controls motoneuron hyperexcitability in amyotrophic lateral sclerosis', *Cell Death and Disease*. Springer US, 10(4). doi: 10.1038/s41419-019-1538-9.

Cacabelos, D. *et al.* (2016) 'Early and gender-specific differences in spinal cord mitochondrial function and oxidative stress markers in a mouse model of ALS', *Acta neuropathologica communications*. Acta Neuropathologica Communications, 4, p. 3. doi: 10.1186/s40478-015-0271-6.

Castillo, K. *et al.* (2013) 'Trehalose delays the progression of amyotrophic lateral sclerosis by enhancing autophagy in motoneurons', *Autophagy*, 9(9), pp. 1308–1320. doi: 10.4161/auto.25188.

Cavarsan, C. F. *et al.* (2022) 'Inhibitory interneurons show early dysfunction in a SOD1 mouse model of amyotrophic lateral sclerosis', *Journal of Physiology*, 3, pp. 647–667. doi: 10.1113/JP284192.

Chalif, J. I. and Mentis, G. Z. (2022) 'Normal Development and Pathology of Motoneurons: Anatomy, Electrophysiological Properties, Firing Patterns and Circuit Connectivity.', *Advances in neurobiology*. United States, 28, pp. 63–85. doi: 10.1007/978-3-031-07167-6_3.

Chang, Q. and Martin, L. J. (2009) 'Glycinergic innervation of motoneurons is deficient in amyotrophic lateral sclerosis mice: A quantitative confocal analysis', *American Journal of Pathology*. American Society for Investigative Pathology, 174(2), pp. 574–585. doi: 10.2353/ajpath.2009.080557.

Chang, Q. and Martin, L. J. (2011) 'Glycine receptor channels in spinal motoneurons are abnormal in a transgenic mouse model of amyotrophic lateral sclerosis', *Journal of Neuroscience*, 31(8), pp. 2815–2827. doi: 10.1523/JNEUROSCI.2475-10.2011.

Chang, X. *et al.* (2019) 'Hyperpolarization-activated cyclic nucleotide-gated channels: An emerging role in neurodegenerative diseases', *Frontiers in Molecular Neuroscience*, 12(June), pp. 1–14. doi: 10.3389/fnmol.2019.00141.

Choi, S. and Lovinger, D. M. (1997) 'Decreased frequency but not amplitude of quantal synaptic responses associated with expression of corticostriatal long-term depression', *Journal of Neuroscience*, 17(21), pp. 8613–8620. doi: 10.1523/jneurosci.17-21-08613.1997.

Cleveland, D. W. and Rothstein, J. D. (2001) 'From Charcot to Lou Gehrig: deciphering selective motor neuron death in ALS.', *Nature reviews. Neuroscience*. England, 2(11), pp. 806–819. doi: 10.1038/35097565.

Conradi, S. *et al.* (1979) 'Electron microscopic studies of serially sectioned cat spinal-motoneurons', *J. Comp. Neur.*, 184, pp. 769–782.

Corbo, M. and Hays, A. P. (1992) 'Peripherin and neurofilament protein coexist in spinal spheroids of motor neuron disease.', *Journal of neuropathology and experimental neurology*. England, 51(5), pp. 531–537. doi: 10.1097/00005072-199209000-00008.

Corona, J. C. and Tapia, R. (2004) 'AMPA receptor activation, but not the accumulation of endogenous extracellular glutamate, induces paralysis and motor neuron death in rat spinal cord in vivo', *Journal of Neurochemistry*, 89(4), pp. 988–997. doi: 10.1111/j.1471-4159.2004.02383.x.

Corona, J. C. and Tapia, R. (2007) 'Ca2+-permeable AMPA receptors and intracellular Ca2+ determine motoneuron vulnerability in rat spinal cord in vivo', *Neuropharmacology*. Elsevier Ltd, 52(5), pp. 1219–1228. doi: 10.1016/j.neuropharm.2006.12.008.

Couratier, P. *et al.* (1993) 'Cell culture evidence for neuronal degeneration in amyotrophic lateral

sclerosis being linked to glutamate AMPA/kainate receptors.', *Lancet (London, England)*. England, 341(8840), pp. 265–268. doi: 10.1016/0140-6736(93)92615-z.

Crosby, Kevin C. *et al.* (2019) 'Nanoscale Subsynaptic Domains Underlie the Organization of the Inhibitory Synapse', *Cell Reports*. ElsevierCompany., 26(12), pp. 3284-3297.e3. doi: 10.1016/j.celrep.2019.02.070.

Crosby, Kevin C *et al.* (2019) 'the Inhibitory Synapse', 26(12), pp. 3284–3297. doi: 10.1016/j.celrep.2019.02.070.Nanoscale.

Delestrée, N. *et al.* (2014) 'Adult spinal motoneurones are not hyperexcitable in a mouse model of inherited amyotrophic lateral sclerosis', *Journal of Physiology*, 592(7), pp. 1687–1703. doi: 10.1113/jphysiol.2013.265843.

Demmerle, J. *et al.* (2015) 'Assessing resolution in super-resolution imaging', *Methods*. Elsevier Inc., 88(2015), pp. 3–10. doi: 10.1016/j.ymeth.2015.07.001.

Doble, A. (1999) 'The role of excitotoxicity in neurodegenerative disease: Implications for therapy', *Pharmacology and Therapeutics*, 81(3), pp. 163–221. doi: 10.1016/S0163-7258(98)00042-4.

Eccles, B. J. C., Fatt, P. and Koketsu, K. (1954) 'Sherrington, 1931; Forbes, Smith', pp. 524–562.

ElBasiouny, S. M., Schuster, J. E. and Heckman, C. J. (2010) 'Persistent inward currents in spinal motoneurons: Important for normal function but potentially harmful after spinal cord injury and in amyotrophic lateral sclerosis', *Clinical Neurophysiology*, 121(10), pp. 1669–1679. doi: 10.1016/j.clinph.2009.12.041.

Engbers, J. D. T. *et al.* (2011) 'Distinct roles for I T and I H in controlling the frequency and timing of rebound spike responses', *Journal of Physiology*, 589(22), pp. 5391–5413. doi: 10.1113/jphysiol.2011.215632.

Este, G. *et al.* (2012) 'Mitochondrial Dynamics and Bioenergetic Dysfunction Is Associated with Synaptic Alterations in Mutant SOD1 Motor Neurons', 32(1), pp. 229–242. doi: 10.1523/JNEUROSCI.1233-11.2012.

Filipchuk, A. *et al.* (2021) 'Early Hypoexcitability in a Subgroup of Spinal Motoneurons in Superoxide Dismutase 1 Transgenic Mice, a Model of Amyotrophic Lateral Sclerosis', *Neuroscience*, 463, pp. 337–353. doi: 10.1016/j.neuroscience.2021.01.039.

Fogarty, M. J. *et al.* (2017) 'Motor Areas Show Altered Dendritic Structure in an Amyotrophic Lateral Sclerosis Mouse Model', 11(November), pp. 1–16. doi: 10.3389/fnins.2017.00609.

Foran, E. and Trotti, D. (2009) 'Glutamate transporters and the excitotoxic path to motor neuron degeneration in amyotrophic lateral sclerosis', *Antioxidants and Redox Signaling*, 11(7), pp. 1587–1602.

doi: 10.1089/ars.2009.2444.
Frey, D. *et al.* (2000) 'Early and selective loss of neuromuscular synapse subtypes with low sprouting competence in motoneuron diseases', *Journal of Neuroscience*, 20(7), pp. 2534–2542. doi: 10.1523/jneurosci.20-07-02534.2000.
Genç, B. *et al.* (2017) 'Apical dendrite degeneration, a novel cellular pathology for Betz cells in ALS', *Scientific Reports*. Nature Publishing Group, 7, pp. 1–10. doi: 10.1038/srep41765.
Gibbs, K. L., Greensmith, L. and Schiavo, G. (2015) 'Regulation of Axonal Transport by Protein Kinases', *Trends in Biochemical Sciences*. Elsevier Ltd, 40(10), pp. 597–610. doi: 10.1016/j.tibs.2015.08.003.
Goulding, M. (2009) 'Circuits controlling vertebrate locomotion: moving in a new direction.', *Nature reviews. Neuroscience*. England, 10(7), pp. 507–518. doi: 10.1038/nrn2608.
Gurney, M. E. *et al.* (1994) 'Motor neuron degeneration in mice that express a human Cu,Zn superoxide dismutase mutation', *Science*, 264(5166), pp. 1772–1775. doi: 10.1126/science.8209258.
Hadano, S. *et al.* (2006) 'Mice deficient in the Rab5 guanine nucleotide exchange factor ALS2 / alsin exhibit age-dependent neurological deficits and altered endosome trafficking', 15(2), pp. 233–250. doi: 10.1093/hmg/ddi440.
Hardiman, O. *et al.* (2017) 'Amyotrophic lateral sclerosis', *Nature Reviews Disease Primers*, 3(1), p. 17071. doi: 10.1038/nrdp.2017.71.
Harris, K. M. and Weinberg, R. J. (2012) 'Ultrastructure of synapses in the mammalian brain', *Cold Spring Harbor Perspectives in Biology*, 4(5), p. 7. doi: 10.1101/cshperspect.a005587.
Heckman, C. J. *et al.* (2008) 'Persistent inward currents in spinal motoneurons and their influence on human motoneuron firing patterns', *Neuroscientist*, 14(3), pp. 264–275. doi: 10.1177/1073858408314986.
Henstridge, C. M. *et al.* (2018) 'Synapse loss in the prefrontal cortex is associated with cognitive decline in amyotrophic lateral sclerosis', *Acta Neuropathologica*. Springer Berlin Heidelberg, 135(2), pp. 213–226. doi: 10.1007/s00401-017-1797-4.
Hetz, C. *et al.* (2009) 'XBP-1 deficiency in the nervous system protects against amyotrophic lateral sclerosis by increasing autophagy', *Genes and Development*, 23(19), pp. 2294–2306. doi: 10.1101/gad.1830709.
Hetz, C. (2012) 'The unfolded protein response: Controlling cell fate decisions under ER stress and beyond', *Nature Reviews Molecular Cell Biology*. Nature Publishing Group, 13(2), pp. 89–102. doi: 10.1038/nrm3270.
Hetz, C. and Mollereau, B. (2014) 'Disturbance of endoplasmic reticulum proteostasis in

neurodegenerative diseases', *Nature Reviews Neuroscience*. Nature Publishing Group, 15(4), pp. 233–249. doi: 10.1038/nrn3689.

Higgins, C. M. J., Jung, C. and Xu, Z. (2003) 'ALS-associated mutant SODIG93A causes mitochondrial vacuolation by expansion of the intermembrane space by involvement of SODI aggregation and peroxisomes', *BMC Neuroscience*, 4, pp. 1–14. doi: 10.1186/1471-2202-4-16.

Hirata, A. *et al.* (1997) 'AMPA receptor-mediated slow neuronal death in the rat spinal cord induced by long-term blockade of glutamate transporters with THA', *Brain Research*, 771(1), pp. 37–44. doi: 10.1016/S0006-8993(97)00709-9.

Hirokawa, N., Niwa, S. and Tanaka, Y. (2010) 'Molecular motors in neurons: transport mechanisms and roles in brain function, development, and disease.', *Neuron*. United States, 68(4), pp. 610–638. doi: 10.1016/j.neuron.2010.09.039.

Hossaini, M. *et al.* (2011) 'Spinal inhibitory interneuron pathology follows motor neuron degeneration independent of glial mutant superoxide dismutase 1 expression in SOD1-ALS mice', *Journal of Neuropathology and Experimental Neurology*, 70(8), pp. 662–677. doi: 10.1097/NEN.0b013e31822581ac.

Howland, D. S. *et al.* (2002) 'Focal loss of the glutamate transporter EAAT2 in a transgenic rat model of SOD1 mutant-mediated amyotrophic lateral sclerosis (ALS).', *Proceedings of the National Academy of Sciences of the United States of America*. United States, 99(3), pp. 1604–1609. doi: 10.1073/pnas.032539299.

Huh, S., Heckman, Charles J. and Manuel, M. (2021) 'Time course of alterations in adult spinal motoneuron properties in the sod1(G93a) mouse model of als', *eNeuro*, 8(2), pp. 1–16. doi: 10.1523/ENEURO.0378-20.2021.

Huh, S., Heckman, Charles J and Manuel, M. (2021) 'Time Course of Alterations in Adult Spinal Motoneuron Properties in the SOD1 (G93A) Mouse Model of ALS', 1(April), pp. 1–16.

Jensen, D. B. *et al.* (2020) 'Spinal motoneurones are intrinsically more responsive in the adult G93A SOD1 mouse model of amyotrophic lateral sclerosis', 19, pp. 4385–4403. doi: 10.1113/JP280097.

Jiang, M. C. *et al.* (2017) 'Hyperexcitability in synaptic and firing activities of spinal motoneurons in an adult mouse model of amyotrophic lateral sclerosis', *Neuroscience*. IBRO, 362, pp. 33–46. doi: 10.1016/j.neuroscience.2017.08.041.

Kassa, R. M. *et al.* (2018) 'The role of mutated SOD1 gene in synaptic stripping and MHC class I expression following nerve axotomy in ALS murine model', *European Journal of Histochemistry*, 62(2), pp. 158–165. doi: 10.4081/ejh.2018.2904.

Kawasaki, H. *et al.* (1997) 'Activation and involvement of p38 mitogen-activated protein kinase in glutamate-induced apoptosis in rat cerebellar granule cells', *Journal of Biological Chemistry*. Â© 1997 ASBMB. Currently published by Elsevier Inc; originally published by American Society for Biochemistry and Molecular Biology., 272(30), pp. 18518–18521. doi: 10.1074/jbc.272.30.18518.

Kernell, D. (1966) 'Input resistance, electrical excitability, and size of ventral horn cells in cat spinal cord.', *Science (New York, N.Y.)*. United States, 152(3729), pp. 1637–1640. doi: 10.1126/science.152.3729.1637.

Kiehn, O. *et al.* (2000) 'Contributions of intrinsic motor neuron properties to the production of rhythmic motor output in the mammalian spinal cord', *Brain Research Bulletin*, 53(5), pp. 649–659. doi: 10.1016/S0361-9230(00)00398-1.

Kieran, D. *et al.* (2005) 'A mutation in dynein rescues axonal transport defects and extends the life span of ALS mice', *Journal of Cell Biology*, 169(4), pp. 561–567. doi: 10.1083/jcb.200501085.

Kim, K. *et al.* (2011) 'Role of Excitatory Amino Acid Transporter-2 (EAAT2) and glutamate in neurodegeneration: Opportunities for developing novel therapeutics', *Journal of Cellular Physiology*, 226(10), pp. 2484–2493. doi: 10.1002/jcp.22609.

Kishore, S. and Fetcho, J. R. (2013) 'Homeostatic regulation of dendritic dynamics in a motor map in vivo', *Nature Communications*. Nature Publishing Group, 4(May), pp. 1–8. doi: 10.1038/ncomms3086.

Klinman, E. and Holzbaur, E. L. F. (2015) 'Stress-Induced CDK5 Activation Disrupts Axonal Transport via Lis1/Ndel1/Dynein', *Cell Reports*. The Authors, 12(3), pp. 462–473. doi: 10.1016/j.celrep.2015.06.032.

Kostera, A. *et al.* (2002) 'Motor unit hyperexcitability in amyotrophic lateral sclerosis vs amino acids acting as neurotransmitters', pp. 34–38.

Krueger-Burg, D., Papadopoulos, T. and Brose, N. (2017) 'Organizers of inhibitory synapses come of age', *Current Opinion in Neurobiology*. Elsevier Ltd, 45, pp. 66–77. doi: 10.1016/j.conb.2017.04.003.

Kuo, J. J. *et al.* (2004) 'Hyperexcitability of Cultured Spinal Motoneurons from Presymptomatic ALS Mice', *Journal of Neurophysiology*, 91(1), pp. 571–575. doi: 10.1152/jn.00665.2003.

Kuo, J. J. *et al.* (2005) 'Increased persistent Na+ current and its effect on excitability in motoneurones cultured from mutant SOD1 mice', *Journal of Physiology*, 563(3), pp. 843–854. doi: 10.1113/jphysiol.2004.074138.

Lalancette-Hebert, M. *et al.* (2016) 'Gamma motor neurons survive and exacerbate alpha motor neuron degeneration in ALS', *Proceedings of the National Academy of Sciences of the United States of America*, 113(51), pp. E8316–E8325. doi: 10.1073/pnas.1605210113.

Lambo, M. E. and Turrigiano, G. G. (2013) 'Synaptic and intrinsic homeostatic mechanisms cooperate to

increase L2/3 pyramidal neuron excitability during a late phase of critical period plasticity', *Journal of Neuroscience*, 33(20), pp. 8810–8819. doi: 10.1523/JNEUROSCI.4502-12.2013.
Leroy, F. *et al.* (2014) 'Early intrinsic hyperexcitability does not contribute to motoneuron degeneration in amyotrophic lateral sclerosis', *eLife*, 3(2007), pp. 1–25. doi: 10.7554/eLife.04046.
Lévi, S. *et al.* (2004) 'Gephyrin Is Critical for Glycine Receptor Clustering but Not for the Formation of Functional GABAergic Synapses in Hippocampal Neurons', *Journal of Neuroscience*, 24(1), pp. 207–217. doi: 10.1523/JNEUROSCI.1661-03.2004.
Ligon, L. A. *et al.* (2005) 'Mutant superoxide dismutase disrupts cytoplasmic dynein in motor neurons.', *Neuroreport*. England, 16(6), pp. 533–536. doi: 10.1097/00001756-200504250-00002.
Lum, J. S. and Yerbury, J. J. (2022) 'Misfolding at the synapse: A role in amyotrophic lateral sclerosis pathogenesis?', *Frontiers in Molecular Neuroscience*, 15(September), pp. 1–8. doi: 10.3389/fnmol.2022.997661.
Lushnikova, I. *et al.* (2011) 'Excitatory synaptic activity is associated with a rapid structural plasticity of inhibitory synapses on hippocampal CA1 pyramidal cells', *Neuropharmacology*. Elsevier Ltd, 60(5), pp. 757–764. doi: 10.1016/j.neuropharm.2010.12.014.
Lutz, C. (2018) 'Mouse models of ALS: Past, present and future', *Brain Research*. Elsevier B.V., 1693, pp. 1–10. doi: 10.1016/j.brainres.2018.03.024.
MacGillavry, H. D. *et al.* (2013) 'Nanoscale scaffolding domains within the postsynaptic density concentrate synaptic ampa receptors', *Neuron*. Elsevier, 78(4), pp. 615–622. doi: 10.1016/j.neuron.2013.03.009.
MacLean, J. N. *et al.* (2003) 'Activity-independent homeostasis in rhythmically active neurons', *Neuron*, 37(1), pp. 109–120. doi: 10.1016/S0896-6273(02)01104-2.
Magrané, J. *et al.* (2014) 'Abnormal mitochondrial transport and morphology are common pathological denominators in SOD1 and TDP43 ALS mouse models', *Human Molecular Genetics*, 23(6), pp. 1413–1424. doi: 10.1093/hmg/ddt528.
Martin, E. *et al.* (2013a) 'Embryonic alteration of motoneuronal morphology induces hyperexcitability in the mouse model of amyotrophic lateral sclerosis', *Neurobiology of Disease*. Elsevier B.V., 54, pp. 116–126. doi: 10.1016/j.nbd.2013.02.011.
Martin, E. *et al.* (2013b) 'Embryonic alteration of motoneuronal morphology induces hyperexcitability in the mouse model of amyotrophic lateral sclerosis', *Neurobiology of Disease*. Elsevier B.V., 54, pp. 116–126. doi: 10.1016/j.nbd.2013.02.011.
Martínez-Silva, M. de L. *et al.* (2018) 'Hypoexcitability precedes denervation in the large fast-contracting

motor units in two unrelated mouse models of ALS', *eLife*, 7(2007), pp. 1–26. doi: 10.7554/eLife.30955.
Le Masson, G., Przedborski, S. and Abbott, L. F. (2014) 'A computational model of motor neuron degeneration.', *Neuron*. United States, 83(4), pp. 975–988. doi: 10.1016/j.neuron.2014.07.001.
Mehta, P. *et al.* (2016) 'Prevalence of Amyotrophic Lateral Sclerosis - United States, 2012-2013.', *Morbidity and mortality weekly report. Surveillance summaries (Washington, D.C. : 2002)*. United States, 65(8), pp. 1–12. doi: 10.15585/mmwr.ss6508a1.
Menon, P. *et al.* (2020) 'Cortical hyperexcitability evolves with disease progression in ALS', *Annals of Clinical and Translational Neurology*, pp. 1–9. doi: 10.1002/acn3.51039.
Millecamps, S. and Julien, J. P. (2013) 'Axonal transport deficits and neurodegenerative diseases', *Nature Reviews Neuroscience*. Nature Publishing Group, 14(3), pp. 161–176. doi: 10.1038/nrn3380.
Milligan, C. J., Edwards, I. J. and Deuchars, J. (2006) 'HCN1 ion channel immunoreactivity in spinal cord and medulla oblongata', *Brain Research*, 1081(1), pp. 79–91. doi: 10.1016/j.brainres.2006.01.019.
Morgan, S. and Orrell, R. W. (2016) 'Pathogenesis of amyotrophic lateral sclerosis.', *British medical bulletin*. England, 119(1), pp. 87–98. doi: 10.1093/bmb/ldw026.
Morrice, J. R., Gregory-Evans, C. Y. and Shaw, C. A. (2018) 'Animal models of amyotrophic lateral sclerosis: A comparison of model validity', *Neural Regeneration Research*, 13(12), pp. 2050–2054. doi: 10.4103/1673-5374.241445.
Nair, D. *et al.* (2013) 'Super-resolution imaging reveals that AMPA receptors inside synapses are dynamically organized in nanodomains regulated by PSD95', *Journal of Neuroscience*, 33(32), pp. 13204–13224. doi: 10.1523/JNEUROSCI.2381-12.2013.
Nakamura, R. *et al.* (1997) 'Concentration-dependent changes in motor behavior produced by continuous intrathecal infusion of excitatory amino acids in the rat spinal cord', *Brain Research Protocols*, 1(4), pp. 385–390. doi: 10.1016/S1385-299X(97)00015-9.
Nakata, M. *et al.* (2006) 'Distal excitability changes in motor axons in amyotrophic lateral sclerosis', 117, pp. 1444–1448. doi: 10.1016/j.clinph.2006.04.005.
Naujock, M. *et al.* (2016) '4-Aminopyridine Induced Activity Rescues Hypoexcitable Motor Neurons from Amyotrophic Lateral Sclerosis Patient-Derived Induced Pluripotent Stem Cells.', *Stem cells (Dayton, Ohio)*. England, 34(6), pp. 1563–1575. doi: 10.1002/stem.2354.
Nguyen, M. D., Larivière, R. C. and Julien, J. P. (2001) 'Deregulation of Cdk5 in a mouse model of ALS: Toxicity alleviated by perikaryal neurofilament inclusions', *Neuron*, 30(1), pp. 135–148. doi: 10.1016/S0896-6273(01)00268-9.
Niessen, H. G. *et al.* (2007) 'Metabolic progression markers of neurodegeneration in the transgenic

G93A-SOD1 mouse model of amyotrophic lateral sclerosis', *European Journal of Neuroscience*, 25(6), pp. 1669–1677. doi: 10.1111/j.1460-9568.2007.05415.x.
Nishitoh, H. *et al.* (2008) 'ALS-linked mutant SOD1 induces ER stress- and ASK1-dependent motor neuron death by targeting Derlin-1', *Genes and Development*, 22(11), pp. 1451–1464. doi: 10.1101/gad.1640108.
Nusser, Z., Cull-Candy, S. and Farrant, M. (1997) 'Differences in synaptic GABA(A) receptor number underlie variation in GABA mini amplitude', *Neuron*, 19(3), pp. 697–709. doi: 10.1016/S0896-6273(00)80382-7.
O, R. J. *et al.* (1998) 'Activity-Dependent Modulation of Synaptic AMPA Receptor Accumulation death due to the induction of local circuit epileptiform activity. We have previously reported that blockade of excit', *Neuron*, 21(1989), pp. 1067–1078.
Okamoto, K., Mizuno, Y. and Fujita, Y. (2008) 'Bunina bodies in amyotrophic lateral sclerosis', *Neuropathology*, 28(2), pp. 109–115. doi: 10.1111/j.1440-1789.2007.00873.x.
Olney, J. W. (1969) 'Brain lesions, obesity, and other disturbances in mice treated with monosodium glutamate', *Science*, 164(3880), pp. 719–721. doi: 10.1126/science.164.3880.719.
Orr, B. O. *et al.* (2020) 'Presynaptic Homeostasis Opposes Disease Progression in Mouse Models of ALS-Like Degeneration: Evidence for Homeostatic Neuroprotection', *Neuron*. Elsevier Inc., 107(1), pp. 95-111.e6. doi: 10.1016/j.neuron.2020.04.009.
Orsini, M. *et al.* (2015) 'Amyotrophic Lateral Sclerosis: New Perpectives and Update.', *Neurology international*. Switzerland, 7(2), p. 5885. doi: 10.4081/ni.2015.5885.
Özyurt, M. G. *et al.* (2020) 'Amyotrophic lateral sclerosis weakens spinal recurrent inhibition and post-activation depression', *Clinical Neurophysiology*, 131(12), pp. 2875–2886. doi: 10.1016/j.clinph.2020.09.021.
Pambo-Pambo, A., Durand, J. and Gueritaud, J. P. (2009) 'Early excitability changes in lumbar motoneurons of transgenic SOD1 G85R and SOD1G93A-Low mice', *Journal of Neurophysiology*, 102(6), pp. 3627–3642. doi: 10.1152/jn.00482.2009.
Pardo, A. C. *et al.* (2006) 'Loss of the astrocyte glutamate transporter GLT1 modifies disease in SOD1G93A mice', *Experimental Neurology*, 201(1), pp. 120–130. doi: 10.1016/j.expneurol.2006.03.028.
Petri, S. *et al.* (2003) 'Distribution of GABAA receptor mRNa in the motor cortex of ALS patients', *Journal of Neuropathology and Experimental Neurology*, 62(10), pp. 1041–1051. doi: 10.1093/jnen/62.10.1041.
Petri, S. *et al.* (2005) 'The cellular mRNA expression of GABA and glutamate receptors in spinal motor neurons of SOD1 mice', *Journal of the Neurological Sciences*, 238(1–2), pp. 25–30. doi:

10.1016/j.jns.2005.06.005.
Picton, L. D., Zhang, H. and Sillar, K. T. (2017) 'Sodium pump regulation of locomotor control circuits', *Journal of Neurophysiology*, 118(2), pp. 1070–1081. doi: 10.1152/jn.00066.2017.
Pieri, M. (2003) 'Altered excitability of motor neurons in a transgenic mouse model of familial amyotrophic lateral sclerosis', *Neuroscience Letters*, 351, pp. 153–156. doi: 10.1016/s0304-3940(03)00945-5.
Piotrkiewicz, M., Kudina, L. and Mierzejewska, J. (2008) 'Analysis of Double Discharges in Amyotrophic', (July), pp. 845–854. doi: 10.1002/mus.20997.
Pun, S. *et al.* (2006) 'Selective vulnerability and pruning of phasic motoneuron axons in motoneuron disease alleviated by CNTF', *Nature Neuroscience*, 9(3), pp. 408–419. doi: 10.1038/nn1653.
Quinlan, K. A. *et al.* (2011a) 'Altered postnatal maturation of electrical properties in spinal motoneurons in a mouse model of amyotrophic lateral sclerosis', *Journal of Physiology*, 589(9), pp. 2245–2260. doi: 10.1113/jphysiol.2010.200659.
Quinlan, K. A. *et al.* (2011b) 'Altered postnatal maturation of electrical properties in spinal motoneurons in a mouse model of amyotrophic lateral sclerosis', *Journal of Physiology*, 589(9), pp. 2245–2260. doi: 10.1113/jphysiol.2010.200659.
Ramírez-Jarquín, U. N. and Tapia, R. (2018) 'Excitatory and Inhibitory Neuronal Circuits in the Spinal Cord and Their Role in the Control of Motor Neuron Function and Degeneration', *ACS Chemical Neuroscience*, 9(2), pp. 211–216. doi: 10.1021/acschemneuro.7b00503.
Rao, S. D., Yin, H. Z. and Weiss, J. H. (2003) 'Disruption of glial glutamate transport by reactive oxygen species produced in motor neurons', *Journal of Neuroscience*, 23(7), pp. 2627–2633. doi: 10.1523/jneurosci.23-07-02627.2003.
Reaume, A. G. *et al.* (1996) 'Motor neurons in Cu/Zn superoxide dismutase-deficient mice develop normally but exhibit enhanced cell death after axonal injury.', *Nature genetics*. United States, 13(1), pp. 43–47. doi: 10.1038/ng0596-43.
Rosen, D. R. *et al.* (1993) 'lateral sclerosis', 362(March), pp. 59–62.
Rossignol, S., Dubuc, R. and Gossard, J. P. (2006) 'Dynamic sensorimotor interactions in locomotion', *Physiological Reviews*, 86(1), pp. 89–154. doi: 10.1152/physrev.00028.2005.
Rothstein, J. D. *et al.* (1990) 'Abnormal excitatory amino acid metabolism in amyotrophic lateral sclerosis.', *Annals of neurology*. United States, 28(1), pp. 18–25. doi: 10.1002/ana.410280106.
Rothstein, J. D. *et al.* (1995) 'Selective loss of glial glutamate transporter GLT-1 in amyotrophic lateral sclerosis.', *Annals of neurology*. United States, 38(1), pp. 73–84. doi: 10.1002/ana.410380114.

Ruegsegger, C. *et al.* (2016) 'Aberrant association of misfolded SOD1 with Na+/K+ATPase-α3 impairs its activity and contributes to motor neuron vulnerability in ALS', *Acta Neuropathologica*. Springer Berlin Heidelberg, 131(3), pp. 427–451. doi: 10.1007/s00401-015-1510-4.

Saito, K. *et al.* (2010) 'The physiological roles of vesicular GABA transporter during embryonic development: A study using knockout mice', *Molecular Brain*, 3(1), pp. 1–13. doi: 10.1186/1756-6606-3-40.

Santoro, B. *et al.* (2000) 'Molecular and functional heterogeneity of hyperpolarization-activated pacemaker channels in the mouse CNS', *Journal of Neuroscience*, 20(14), pp. 5264–5275. doi: 10.1523/jneurosci.20-14-05264.2000.

Sasaki, S. (2011) 'Autophagy in spinal cord motor neurons in sporadic amyotrophic lateral sclerosis', *Journal of Neuropathology and Experimental Neurology*, 70(5), pp. 349–359. doi: 10.1097/NEN.0b013e3182160690.

Sasaki, S. and Iwata, M. (2007) 'Mitochondrial alterations in the spinal cord of patients with sporadic amyotrophic lateral sclerosis', *Journal of Neuropathology and Experimental Neurology*, 66(1), pp. 10–16. doi: 10.1097/nen.0b013e31802c396b.

Saxena, S., Cabuy, E. and Caroni, P. (2009) 'A role for motoneuron subtype-selective ER stress in disease manifestations of FALS mice', *Nature Neuroscience*, 12(5), pp. 627–636. doi: 10.1038/nn.2297.

Schütz, B. (2005) 'Imbalanced excitatory to inhibitory synaptic input precedes motor neuron degeneration in an animal model of amyotrophic lateral sclerosis', *Neurobiology of Disease*, 20(1), pp. 131–140. doi: 10.1016/j.nbd.2005.02.006.

Seki, S. *et al.* (2019) 'Circuit-Specific early impairment of proprioceptive sensory neurons in the SOD1G93A Mouse Model for ALS', *Journal of Neuroscience*, 39(44), pp. 8798–8815. doi: 10.1523/JNEUROSCI.1214-19.2019.

Shao, C. Y. *et al.* (2011) 'Postsynaptic degeneration as revealed by PSD-95 reduction occurs after advanced Aβ and tau pathology in transgenic mouse models of Alzheimer's disease', *Acta Neuropathologica*, 122(3), pp. 285–292. doi: 10.1007/s00401-011-0843-x.

Sharples, S. A. and Miles, G. B. (2021) 'Maturation of persistent and hyperpolarization-activated inward currents shapes the differential activation of motoneuron subtypes during postnatal development', *eLife*, 10, pp. 1–30. doi: 10.7554/eLife.71385.

Smith, C. C. and Brownstone, R. M. (2022) 'Electrical Properties of Adult Mammalian Motoneurons.', *Advances in neurobiology*. United States, 28, pp. 191–232. doi: 10.1007/978-3-031-07167-6_9.

Specht, C. G. *et al.* (2013) 'Quantitative nanoscopy of inhibitory synapses: Counting gephyrin molecules

and receptor binding sites', *Neuron*. Elsevier Inc., 79(2), pp. 308–321. doi: 10.1016/j.neuron.2013.05.013.

Spreux-Varoquaux, O. *et al.* (2002) 'Glutamate levels in cerebrospinal fluid in amyotrophic lateral sclerosis: a reappraisal using a new HPLC method with coulometric detection in a large cohort of patients.', *Journal of the neurological sciences*. Netherlands, 193(2), pp. 73–78. doi: 10.1016/s0022-510x(01)00661-x.

Stephens, B. *et al.* (2006) 'Widespread loss of neuronal populations in the spinal ventral horn in sporadic motor neuron disease. A morphometric study', *Journal of the Neurological Sciences*, 244(1–2), pp. 41–58. doi: 10.1016/j.jns.2005.12.003.

Sultana, R., Banks, W. A. and Butterfield, D. A. (2010) 'Decreased levels of PSD95 and two associated proteins and increased levels of BCl2 and caspase 3 in hippocampus from subjects with amnestic mild cognitive impairment: Insights into their potential roles for loss of synapses and memory, accumulation of Aβ', *Journal of Neuroscience Research*, 88(3), pp. 469–477. doi: 10.1002/jnr.22227.

Sunico, C. R. *et al.* (2011) 'Reduction in the motoneuron inhibitory/excitatory synaptic ratio in an early-symptomatic mouse model of amyotrophic lateral sclerosis', *Brain Pathology*, 21(1), pp. 1–15. doi: 10.1111/j.1750-3639.2010.00417.x.

Tang, D. *et al.* (2020) 'Cryo-EM structure of C9ORF72–SMCR8–WDR41 reveals the role as a GAP for Rab8a and Rab11a', *Proceedings of the National Academy of Sciences*. National Academy of Sciences, 117(18), pp. 9876–9883. doi: 10.1073/PNAS.2002110117.

Taylor, J. P., Brown, R. H. and Cleveland, D. W. (2016) 'Decoding ALS: From genes to mechanism', *Nature*, 539(7628), pp. 197–206. doi: 10.1038/nature20413.

Trotti, D., Danbolt, N. C. and Volterra, A. (1998) 'Glutamate transporters are oxidant-vulnerable: a molecular link between oxidative and excitotoxic neurodegeneration?', *Trends in pharmacological sciences*. England, 19(8), pp. 328–334. doi: 10.1016/s0165-6147(98)01230-9.

Tsay, D., Dudman, J. T. and Siegelbaum, S. A. (2007) 'HCN1 Channels Constrain Synaptically Evoked Ca2+ Spikes in Distal Dendrites of CA1 Pyramidal Neurons', *Neuron*, 56(6), pp. 1076–1089. doi: 10.1016/j.neuron.2007.11.015.

Turrigiano, G. G. and Nelson, S. B. (2004) 'HOMEOSTATIC PLASTICITY IN THE DEVELOPING NERVOUS SYSTEM'. doi: 10.1038/nrn1327.

Vaughan, S. K. *et al.* (2015) 'Degeneration of proprioceptive sensory nerve endings in mice harboring amyotrophic lateral sclerosis-causing mutations', *Journal of Comparative Neurology*, 523(17), pp. 2477–2494. doi: 10.1002/cne.23848.

Verkhratsky, A. and Kirchhoff, F. (2007) 'Glutamate-mediated neuronal-glial transmission', *Journal of Anatomy*, 210(6), pp. 651–660. doi: 10.1111/j.1469-7580.2007.00734.x.

Viana, F., Bayliss, D. A. and Berger, A. J. (1993) 'Multiple potassium conductances and their role in action potential repolarization and repetitive firing behavior of neonatal rat hypoglossal motoneurons', *Journal of Neurophysiology*, 69(6), pp. 2150–2163. doi: 10.1152/jn.1993.69.6.2150.

De vos, K. J. *et al.* (2007) 'Familial amyotrophic lateral sclerosis-linked SOD1 mutants perturb fast axonal transport to reduce axonal mitochondria content', *Human Molecular Genetics*, 16(22), pp. 2720–2728. doi: 10.1093/hmg/ddm226.

Vucic, S., Nicholson, G. A. and Kiernan, M. C. (2008) 'Cortical hyperexcitability may precede the onset of familial amyotrophic lateral sclerosis', *Brain*, 131(6), pp. 1540–1550. doi: 10.1093/brain/awn071.

Wainger, B. J. *et al.* (2014) 'NIH Public Access', 7(1), pp. 1–11. doi: :10.1016/j.celrep.2014.03.019.

Warita, H., Itoyama, Y. and Abe, K. (1999) 'Selective impairment of fast anterograde axonal transport in the peripheral nerves of asymptomatic transgenic mice with a G93A mutant SOD1 gene', *Brain Research*, 819(1–2), pp. 120–131. doi: 10.1016/S0006-8993(98)01351-1.

Webster, C. P. *et al.* (2017) 'Protein homeostasis in amyotrophic lateral sclerosis: Therapeutic opportunities?', *Frontiers in Molecular Neuroscience*, 10(May), pp. 1–22. doi: 10.3389/fnmol.2017.00123.

Wijesekera, L. C. and Leigh, P. N. (2009) 'Amyotrophic lateral sclerosis', *Orphanet Journal of Rare Diseases*, 4(1), pp. 1–22. doi: 10.1186/1750-1172-4-3.

Wootz, H., FitzSimons-Kantamneni, E., *et al.* (2013) 'Alterations in the motor neuron-renshaw cell circuit in the Sod1 G93A mouse model', *Journal of Comparative Neurology*, 521(7), pp. 1449–1469. doi: 10.1002/cne.23266.

Wootz, H., Fitzsimons-Kantamneni, E., *et al.* (2013) 'Alterations in the motor neuron-renshaw cell circuit in the Sod1G93A mouse model', *Journal of Comparative Neurology*, 521(7), pp. 1449–1469. doi: 10.1002/cne.23266.

Yoshino, H. and Kimura, A. (2006) 'Investigation of the therapeutic effects of edaravone, a free radical scavenger, on amyotrophic lateral sclerosis (Phase II study).', *Amyotrophic lateral sclerosis : official publication of the World Federation of Neurology Research Group on Motor Neuron Diseases*. England, 7(4), pp. 241–245. doi: 10.1080/17482960600881870.

Zang, D. W., Lopes, E. C. and Cheema, S. S. (2005) 'Loss of synaptophysin-positive boutons on lumbar motor neurons innervating the medial gastrocnemius muscle of the SOD1G93A G1H transgenic mouse model of ALS', *Journal of Neuroscience Research*, 79(5), pp. 694–699. doi: 10.1002/jnr.20379.

Van Zundert, B. *et al.* (2008) 'Neonatal neuronal circuitry shows hyperexcitable disturbance in a mouse model of the adult-onset neurodegenerative disease amyotrophic lateral sclerosis', *Journal of Neuroscience*, 28(43), pp. 10864–10874. doi: 10.1016.